DOE/BC/14899-28
Distribution Category UC-122

Supri Heavy Oil Research Program

Annual Report for the Period
February 8, 1994 to February 7, 1995

By
W. Brigham

July 1995

Work Performed Under Contract No. DE-FG22-93BC14899

Prepared for
U.S. Department of Energy
Assistant Secretary for Fossil Energy

Thomas Reid, Project Manager
Bartlesville Project Office
P.O. Box 1398
Bartlesville, OK 74005

Prepared by
Stanford University
Petroleum Research Institute
Stanford, CA 94305

DISCLAIMER

TABLE OF CONTENTS

LIST OF FIGURES

SUMMARY

The goal of the Stanford University Petroleum Research Institute is to conduct research directed toward increasing the recovery of heavy oils. Presently, SUPRI is working in five main directions:

1. FLOW PROPERTIES STUDIES - To assess the influence of different reservoir conditions (temperature and pressure) on the absolute and relative permeability to oil and water and on capillary pressure.

2. IN-SITU COMBUSTION - To evaluate the effect of different reservoir parameters on the *in-situ* combustion process. This project includes the study of the kinetics of the reactions.

3. STEAM WITH ADDITIVES - To develop and understand the mechanisms of the process using commercially available surfactants for reduction of gravity override and channeling of steam.

4. FORMATION EVALUATION - To develop and improve techniques of formation evaluation such as tracer tests and pressure transient tests.

5. FIELD SUPPORT SERVICES - To provide technical support for design and monitoring of DOE sponsored or industry initiated field projects.

PROJECT 1: FLOW PROPERTY STUDIES

To assess the influence of different reservoir conditions (temperature and pressure) on the absolute and relative permeability to oil and water and on capillary pressure.

1.1 AN ERROR ANALYSIS OF RELATIVE PERMEABILITIES CALCULATED USING CONVENTIONAL TECHNIQUES

(Suhail Qadeer, K. Aziz, J. Fayers, L.M. Castanier, and W.E. Brigham)

1.1.1 SUMMARY

A complete technical report on this topic is in the draft stage. The paper presented at the International Energy Symposium in Bergen, Norway, August 28-31,1994, is a short summary of this work.

AN ERROR ANALYSIS OF RELATIVE PERMEABILITIES CALCULATED USING CONVENTIONAL TECHNIQUES

by

S. Qadeer, K. Aziz, J. Fayers, L.M. Castanier and W.E. Brigham

ABSTRACT

Conventionally, either the Johnson, Bossler and Neumann (JBN) method, or some kind of history matching technique, is used to calculate the relative permeabilities from unsteady state displacement experiments. In the JBN method, it is assumed that the capillary forces are negligible, the saturation changes monotonically through the core, and the flow is linear throughout the core. In the numerical technique, so far only linear models have been used for history matching. Capillary forces can be accounted for in the numerical model. There has been some work done to show that errors are introduced in the calculated relative permeability curves by assumptions in the JBN method. The studies conducted so far have not shown the severity of errors caused by the nonmonotonic changes in saturation, and the nonlinear flow near the core faces. In this study we have used a 2D radial coordinate numerical simulator. The data from the numerical model and from displacement experiments show that the flow near the core faces is hemispherical. It is also shown, both from in-situ measurements of saturations and simulations, that in strongly water wet systems there are strong saturation gradients at the end of drainage displacements even at high rates. This results in nonmonotonic changes in saturation during subsequent imbibition displacements.

The pressure drop and recovery data generated from numerical experiments was used to study the errors introduced in the calculated relative permeability curves by both the JBN and history matching techniques. The results indicate that, because of the initial saturation gradient in the core, the relative permeability curves obtained from imbibition displacements have large errors at low water saturation. As the saturation gradient later diminishes the errors also decrease.

Similar errors were observed during the drainage displacements, but now the errors increase toward the end of the displacement process. For the cases studied, the error is greater during imbibition than in drainage. The errors in both oil and water relative permeabilities in the lower water saturation range can be greater than 100%.

An Error Analysis of Relative Permeabilities Calculated using Conventional Techniques

by
S. Qadeer, K. Aziz, L.M. Castanier, F.J. Fayers, and W.E. Brigham
Stanford University

INTRODUCTION

Conventionally either the Johnson, Bossler and Neumann[1] (JBN) method, or some kind of history matching technique, is used to calculate the relative permeabilities from unsteady state displacement experiments. In the JBN method, it is assumed that the capillary forces are negligible, the saturations change monotonicaly through the core, and the flow is linear throughout the core. In the numerical technique the capillary forces can be accounted for, but typically, only linear models have been used for history matching.

It is generally assumed that, if the flow rate is high enough during the displacement process, the capillary forces and associated end effects can be neglected, and the JBN analysis can be used to calculate relative permeabilities with negligible errors. Rappaport and Leas[2] have suggested that if the value of the term, $Lv\mu_w$, is greater than from about 1 to 3 cm^2cp/min, the capillary forces can be neglected. Bentson[3] in his study has reported that if the value of the Capillary Number, N_c, defined by $\sigma A k_w / qL\mu_w$ is less than about 0.1, Buckley Leverett theory, and hence the JBN analysis, is valid. Capillary Number, N_c, as defined by Bentson is obtained by inverting Rappaport and Leas' Number, N_{rl}, and multiplying by $\sigma k_w/60$, to make it dimensionless.

In this study we have used 2-D numerical simulations and experimental data to show that there are strong saturation gradients in the core after drainage displacements, even at high flow rates. We also show from simulations that the flow near the core faces is not linear, but nearly hemispherical. The saturation gradients resulting from drainage displacements cause large errors in the relative permeabilities calculated by the JBN method, both from drainage and subsequent imbibition displacements.

THE JBN METHOD

Johnson et.al.[1] presented a method for calculating the relative permeabilities from data obtained during displacement experiments. Their method is based upon the earlier work of Welge[4]. The basic assumptions in their method are: (a) the flow is linear and incompressible, and (b) the flow rate is high enough that the capillary forces can be neglected. Although not mentioned in their paper, an important requirement for the method to work is that the saturations should change monotonicaly during the displacement process.

The data required for calculating the relative permeabilities from displacement experiments is the pressure drop, Δp, across the core and the cumulative recovery, V_p, of the displaced phase as a function of the total fluid injected, V_i. The cumulative recovery is used to calculate the average saturation, $\overline{S}_w$, in the core and the fractional flow of oil, f_{o2}, at the outlet face by:

$$\overline{S}_w = S_{wi} + V_p \tag{1}$$

and:

$$f_{o2} = \frac{d\overline{S}_w}{dV_i} \tag{2}$$

The water saturation at the oultlet face, S_{w2}, is given by Welge[4]:

$$S_{w2} = \overline{S}_w - f_{o2} V_i \tag{3}$$

To calculate individual relative permeabilities the relative injectivity, I_r, is calculated from the pressure drop, Δp, and flow rate, q, by:

$$I_r = \frac{(q/\Delta P)}{(q/\Delta P)_i} \tag{4}$$

where the subscript, i, indicates the base (initial) conditions used to calculate the relative permeability. The relative permeability to oil, k_{ro}, is then given by:

$$k_{ro} = f_{o2} d\left(\frac{1}{V_i}\right) \Big/ d\left(\frac{1}{V_i I_r}\right) \tag{5}$$

The relative permeability to water, k_{rw}, can now be calculated by:

$$k_{rw} = \frac{(1 - f_{o2})}{f_{o2}} \frac{\mu_w}{\mu_o} k_{ro} \qquad (6)$$

where μ_w and μ_o are the viscosities of water and oil.

All of these calculations are based on the measurement of pressure drop across the core and the cumulative productions of oil and water. The individual k_r's are calculated from the k_r ratios which in turn are directly related to the fractional flow at the outlet end. Both the pressure drops and the recoveries strongly depend on the saturation distributions in the core. In particular, it is necessary for the initial water saturation to be connate and uniform. Experiments and numerical simulations were conducted to understand how the saturations will change during displacements.

Some authors (for example, Batycky et al.[5]) have recommended that both relative permeabilities and the capillary pressure can be inferred numerically from indirect one dimensional inversion to match low rate core tests. It is easy to show that obtaining both sets of curves simultaneously is a badly ill-conditioned problem. Other authors (for example, Sigmund and McCaffery[6]) have shown how relative permeabilities can be inferred when an independent measurement of the capillary pressure is available. Unfortunately, the only established method for obtaining imbibition capillary pressures is by the porous plate method, which is very time consuming and often impractical. This is why high rate displacement, coupled with JBN-analysis, remains an industry standard procedure.

EXPERIMENTS

The displacement experiments were conducted on two inch diameter, ten inch long Berea sandstone cores. The cores were fired at 400°C for eight hours to deactivate the clays. The fluids used are 8% sodium bromide brine as the wetting phase and cylco-hexane as the non-wetting phase. Sodium bromide was used rather than sodium chloride to improve the CT scan contrast between the oil and the brine. Both of these

fluids have a viscosity of about 1.0 cp. at room temperature. The experimental setup is shown in Fig. 1. The core was placed horizontaly in the X-ray CT scanner[7]. The core holder was designed so that the core could be scanned during the displacement experiments to determine saturation distributions. The core was initially saturated with brine and a sequence of drainage and imbibition displacements were conducted. The displacements were stopped after 24 hours when there was virtually no more production of the displaced phase and the saturations as measured by the CT scanner didn't change over a period of several hours. The flow rates ranged from 1.0 to 8.0 cc/min. These correspond to Darcy velocities of 0.5 to 4.0 cm/min (23.6 to 189.0 ft/day), which would normaly be considered high enough for capillary forces and end effects to be negligible in a relative permeability experiment.

SIMULATIONS

In this study we have used a commercial black oil simulator, ECLIPSE, from INTERA[8]. The simulator was used to study the flow geometry within the core, and also to obtain pressure drop and recovery predictions from known relative permeability and capillary pressure data. Preliminary studies were conducted to determine the effect of gravity. It was found that the flow rates are large enough to allow the gravity forces to be neglected in this study. The grid used is schematically shown in Fig. 2. It is a 2-D, r-z coordinate system. The z-axis runs through the axis of the core. After doing a sensitivity study it was decided to use 16 grid blocks in the r direction and 60 blocks in the z direction. As it is much more convenient in the simulations to use a verticle z-axis, and the effects of gravity are negligible in the experiments, it was decided to use 2-D, r-z simulations, with a vertical z-axis. To completely eliminate the effects of gravity in this configuration, the specific gravity of both oil and brine was set to 1.0.

To study the effects of flow geometry on the results it is important to include the geometry of the end plugs in the simulations. The configuration of the distribution grooves in the end plugs used in the experiments is shown in Fig. 3. The fluids enter the end plate through a hole in the center, and distribute over the core face through the conducting radial and concentric grooves. This geometry is often used in relative

permeability and other displacement experiments. These grooves were represented, at both ends of the core, by one layer of grid blocks with very high permeability, zero capillary pressure and straight line relative permeabilities. It should be realized that not all of the core face is open to flow. To take this into account, the transmissivity distribution in the first and last rows of blocks were set proportional to the surface areas of each groove, and not to the area of the face of the grid block representing that grove. The appropriate portions of the radial lines in the "spider web" were also lumped into the transmissivity of the corresponding grid block.

The relative permeability and capillary pressure data used in these simulations are shown in Fig. 4. The relative permeability data were selected on a judgemental basis using representative end points for Berea sandstone. Note that the water relative permeability is around 0.15 at irreducible oil saturation of 0.2, which is appropriate to a strongly water wet system. The capillary pressure curve was obtained by measuring the drainage capillary pressure for the high water saturations and by extrapolating some early information on the apparent connate water saturation from the displacement experiments. The simulations were conducted for 24 hours (same as experiments) for each displacement run. It was noted that both the calculated and experimental pressure drops and fractional flows had stabilized by that time. The saturation maps generated by these simulations helped us to understand the flow geometry. The simulated recovery and pressure drop data were used in JBN analyses to determine the errors in the calculated relative permeabilities caused by the assumptions made in the JBN analysis method.

RESULTS FROM EXPERIMENTS

The displacements were conducted at three different rates. The sequence of the runs is shown in Table 1. The experiments begin with the core fully saturated with brine. The first displacement is the primary drainage at 8.0 cc/min, followed by imbibition-drainage cycles at differening rates. These rates give Rappaport and Leas Numbers, N_{rl}, ranging from 1.9 to 9.8 cm^2cp/min. The corresponding Capillary Numbers, N_c, defined by $\sigma A k_w / qL\mu_w$ for imbibition, and $\sigma A k_o / qL\mu_o$ for drainage displacements, are in the range of 0.019 to 0.243. The average saturation profiles at the

end of the drainage displacements are shown in Fig 5, while those at the end of imbibition are shown in Fig 6. For drainage displacements, the average saturation near the inlet end changes from a low of 0.30 for the 8.0 cc/min displacement, to a high of 0.45 at a rate of 1.0 cc /min. The individual saturation profiles show a scatter of about ± 2.0 %. This scatter is caused by the random changes in the X-rays generated by the CT scanner.

Table 1. Sequence of Displacement Experiments

Displacement		Flow Rate (cc/min.)
Primary Drainage	(DP)	8.0
Imbibition-1	(I1)	8.0
Drainage-1	(D1)	8.0
Imbibition-2	(I2)	4.0
Drainage-2	(D2)	4.0
Imbibition-3	(I3)	1.0
Drainage-3	(D3)	1.0

The effect of rate is smaller in the imbibition displacements (Fig. 6). The average saturation at the end of the 8.0 cc/min displacement is 0.70, whereas for both the 4.0 cc/min and 1.0 cc/min displacements it is 0.67, with the same scatter of about ± 2.0 %.

It is obvious from Fig 5 that, at the end of all drainage displacements, there were strong saturation gradients near the outlet end of the core. These gradients are caused by the wetting phase buildup near the outlet due to the capillary discontinuity. Thus the requirement of a uniform initial connate water saturation at the start of the imbibition was not achievable in these experiments. The profiles show no gradients after imbibition displacements (Fig. 6).

RESULTS FROM SIMULATIONS

The rates and the sequence of displacements simulated were the same as in the experiments (Table 1). The simulations give us insight at a much finer scale than the experiments. The saturation contours plotted at two different times for Imbibition-1 (8.0 cc/min.) are shown in Fig. 7. The core inlet is at the bottom and the outlet is at the top of the figure. The left edge is the center of the core. Comparing the positions of the 65% and 70% saturation contours in the two plots, it is obvious that the shapes of the contours change as they move through the core. This clearly shows that the flow pattern is not linear inside the core. The plots also show that the flow lines are almost hemispherical near the faces of the core.

The average saturation profiles from the same simulation at various times are shown in Fig. 8. The extreme data points at the ends of the core in this figure and in Figs. 10 to 12 correspond to the end plugs. These show sharp jumps in saturations due to capillary discontinuities. Note that the saturation distribution in Fig. 8 at the start of the imbibition (the end of drainage), is similar in shape to the experimental drainage data in Fig. 5. Also notice that the saturation distribution at 0.03 hr in Fig. 8 shows the severity of the non-monotonic changes in the saturation in the core during displacement. The wetting phase saturation is decreasing through the first half of the core and then it increases in the other half. This violates the assumption of monotonic changes in saturation required by JBN analysis.

The calculated saturation maps from the 8.0 cc/min. drainage simulation are shown in Fig. 9. Again the curvature of the saturation contours is quite obvious. The corresponding average saturation profiles are shown in Fig. 10. Similar behavior was observed during the other displacement simulations, for both imbibition and drainage.

The average saturation profiles from two imbibition simulations at 1.0 cc/min and 4.0 cc/min are shown in Fig 11. As the two displacements start from different initial conditions, the breakthrough for the lower rate imbibition is earlier than that of the higher rate. Simulations were also run with an oil to water viscosity ratio of 5.0, with results similar to those for unit viscosity ratio.

Figure 12 shows the comparison between the experimental and simulated saturation profiles for the 8.0 cc/min imbibition and drainage displacements. The results show that, although the saturations differ by about 10-15%, the shapes of the saturation profiles are similar. The choice of $S_{or} = 0.2$ in the input relative permeabilities appears to be too small, and $S_{wc} = 0.4$ is too large.

ERROR ANALYSIS OF JBN METHOD

The pressure drop and recovery data obtained from the simulations was used in JBN analysis to calculate the apparent relative permeabilities. As we start with known relative permeabilities it is easy to quantify the errors introduced by the assumptions made in the JBN method. The saturation maps and the average saturation profiles have shown that the assumption regarding linear flow and monotonic saturation changes are violated even at high rates.

The original and the calculated relative permeabilities, from the 8.0 cc/min imbibition simulation are compared in Fig 13. In this and all subsequent figures, the relative permeabilities used in the simulations are shown as solid lines, while the results calculated by JBN analysis are shown as crosses and stars. It is observed that, at the beginning of the displacement, when the water saturation is low and there are large saturation gradients, the errors are quite large. The errors decrease as the water saturation increases and the capillary effects are reduced. However throughout the experiments, the calculated k_{rO} values were much smaller than the input data. Fig 14 shows the comparison for the 1.0 cc/min. displacement simulation. The results obtained are similar to those at 8.0 cc/min, except for the points soon after breakthrough.

The results from the Drainage-1 and 3 displacement simulations are shown in Figs. 15 and 16 at rates of 8.0 and 1.0 cc/min. The errors in the oil relative permeability curves, though still significant are smaller than they were for imbibition. At lower water saturations, where both imbibition and drainage relative permeabilities can be obtained, the errors in the water relative permeabilities are smaller, but at higher saturations they are similar to the errors in the imbibition curves. It can be seen from Figs 8 and 10 that, in both imbibition and drainage, high water saturations occur near the outlet of the core at

times near breakthrough. These cause large pressure gradients due to the capillary end effect, which, from Eq. 5, results in the low values calculated for k_{ro}.

The results from higher viscosity ratio of 5.0 for 8.0 cc/min are presented in Figs. 17 and 18. Contrary to our expectations, the imbibition errors for both relative permeability curves were not much different from those at unit viscosity ratio. In the drainage displacements, the errors are similar at low water saturations, but at higher water saturations the data show double curvature, the calculated oil curve is concave downward at lower saturations and upward at higher saturations.

One limitation of the JBN method is that, in the case of imbibition, no information can normally be obtained when the water saturation is less than the Buckley Leverett cut-off value, S_{BL}, the point of first tangency to the fractional flow curve. For our input relative permeabilities, S_{BL} is 0.71 for a viscosity ratio of 1.0, and is 0.67 for a viscosity ratio of 5.0. Because capillary pressures smooth out the Buckley-Leverett front, it is apparently possible to infer relative permeabilities for S_w less than S_{BL}. Such results will always be invalid, for in this range the data violates the assumptions in the JBN equation.

CONCLUSIONS

These experiments were conducted on Berea sandstone cores, which are strongly water wet. Most reservoirs are known to be of intermediate wettability and similar analyses should be conducted on such systems. From the experimental and calculated results of this system we can draw the following conclusions.

1. There are large saturation gradients in the core, even at high flow rates.
2. In homogeneous cores, the flow near the ends is 2-D in nature, being nearly hemispherical.
3. The basic assumptions of linear flow and monotonic saturation changes, required for JBN analysis, are violated in the displacement experiments.
4. Nonlinear flow, saturation gradients, and capillary end effects cause large errors in the relative permeability curves calculated by the JBN method.
5. Contrary to our expectations, displacements at a viscosity ratio of five did not produce more accurate results than those at unit viscosity ratio.

ACKNOWLEDGMENT

The authors gratefully acknowledge the support provided by the SUPRI-A Industrial Associates, and by the DOE through contract No. DE-PG 22-90 BC 14600.

REFERENCES

1. Johnson, E.F., Bossler, D.P., and Neumann, V.O. : "Calculation of Relative Permeability from Displacement Experiments", *Trans. AIME* (1959) **216,** 370-372
2. Rappaport, L.A., and Leas, W.J. : "Properties of Linear Water Floods", *Trans. AIME* (1953), **198,** 139-148
3. Bentson, R.G.: "Conditions under which the capillary term may be neglected", *JCPT* (Oct.-Dec. 1978), 25-30
4. Welge, H.J. : "A Simplified Method for Computing Oil Recovery by Gas or Water Drive", *Trans. AIME* (1952), **195,** 91-98
5. Batycky, J.P., McCaffery, F.G., Hodgins, P.K., and Fisher, D.B.: "Interpreting Relative Permeability and Wettability From Unsteady-State Displacement Measurements", *SPEJ*, (Jun. 1981), 296-308.
6. Sigmund, P.M. and McCaffery, F.G.: "An improved Unsteady-State Procedure for Determining Relative Permeability Characteristics of Heterogeneous Porous Media", *SPEJ*, (Feb. 1979), 15-28.
7. Aziz, K. Ramey, H.J., and Brigham, W.E.: "SUPRI Heavy Oil Research Program", 14th Annual Report, Oct. 1, 1990- Sep. 30, 1991, Department of Petroleum Eng., Stanford Universty, California.
8. "ECLIPSE-100 Reference Manual version 88-09", Intera Information Technologies Limited, Oxfordshire, England (Sep. 1988).

NOMENCLATURE

f_{o2} fractional flow

I_r relative injectivity

k_r relative permeability

N_C Capillary Number

N_{rl} Rappaport and Leas Number (cm^2cp/min)

Δp pressure drop across the core (atm)

q flow rate(cm^3/s)

S_{BL} Buckley Leverett cut off saturation (fraction)

S_{or} residual oil saturation (fraction)

S_w water saturation (fraction)

S_{wc} connate water saturation (fraction)

$\overline{S}_w$ average water saturation (fraction)

V dimensionless volume (pore volumes)

μ viscosity(cp)

Subscripts

i initial or injected

o oil

p produced

w water

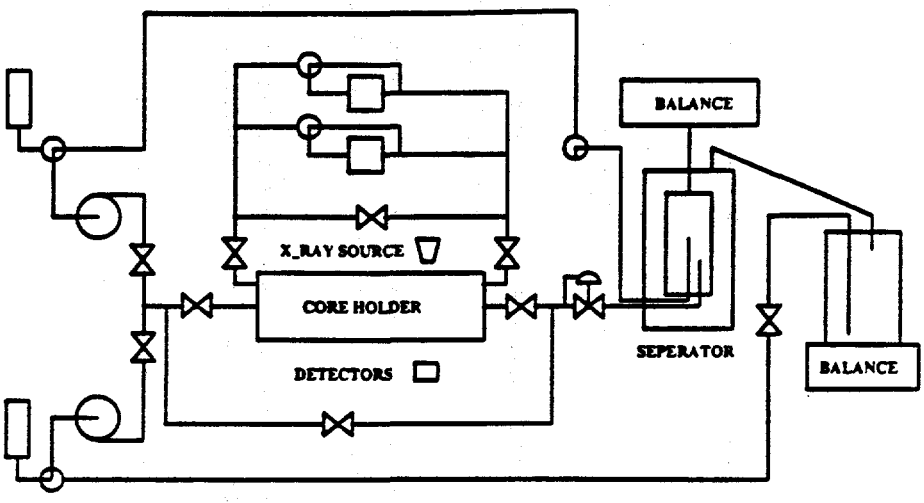

Figure 1: The Experimental System.

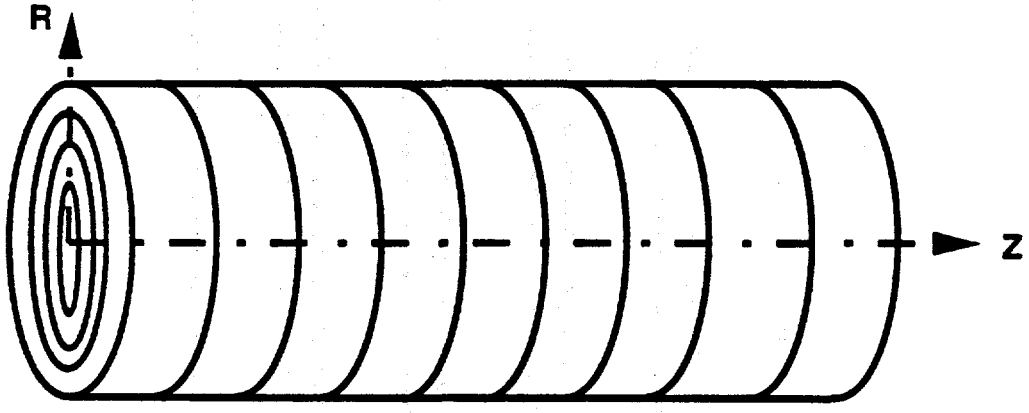

Figure 2 Schematic of 2-D, r-z Griding for Simulations

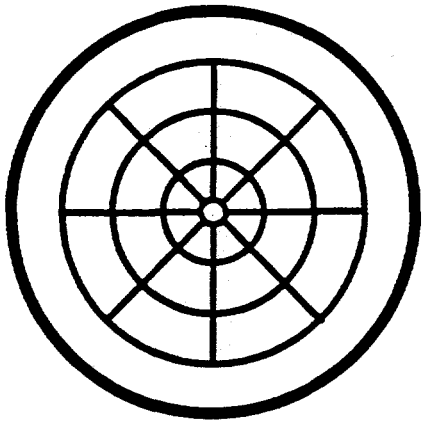

Figure 3: Configuration of Distribution Grooves in End Plugs.

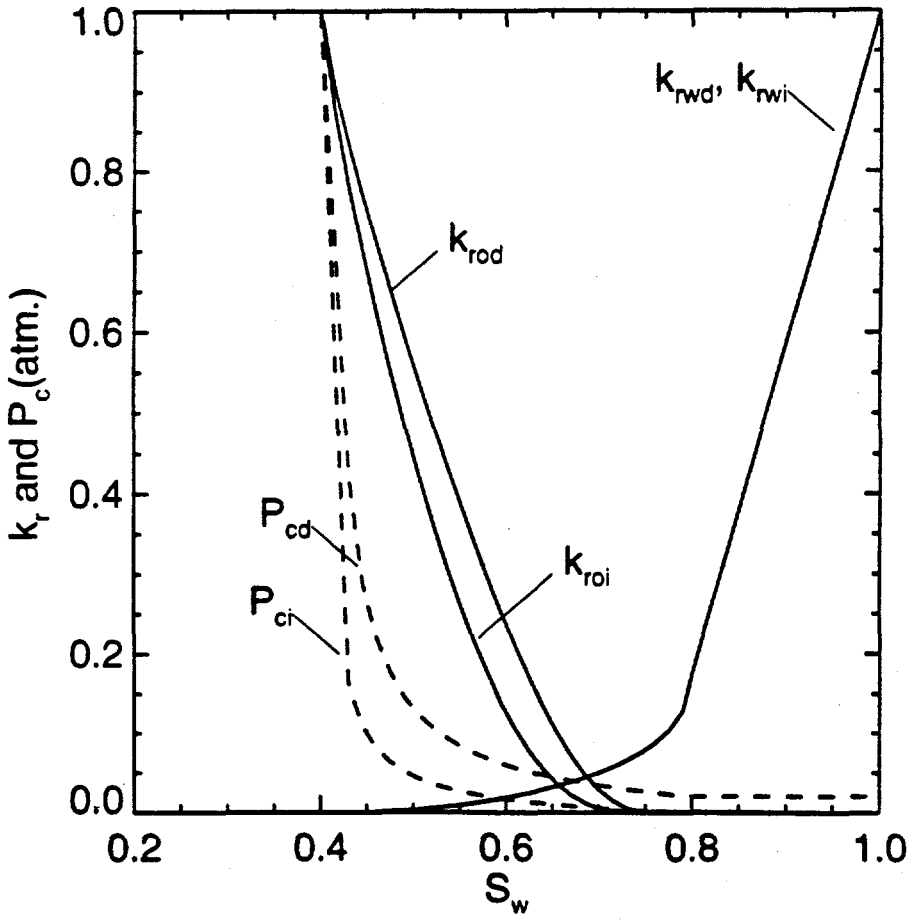

Figure 4: Capillary Pressures and Relative Permeability Curves Used in Simulations.

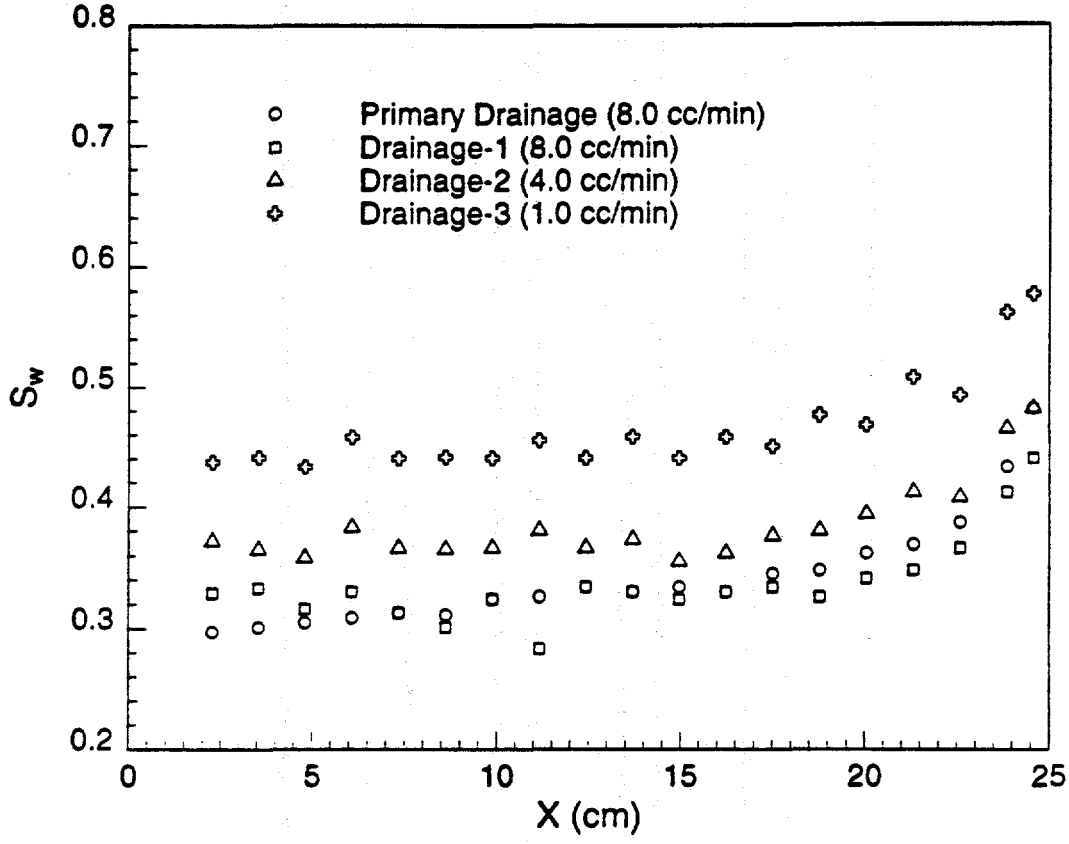

Figure 5: Saturation Profiles at the End of Drainage Displacements.

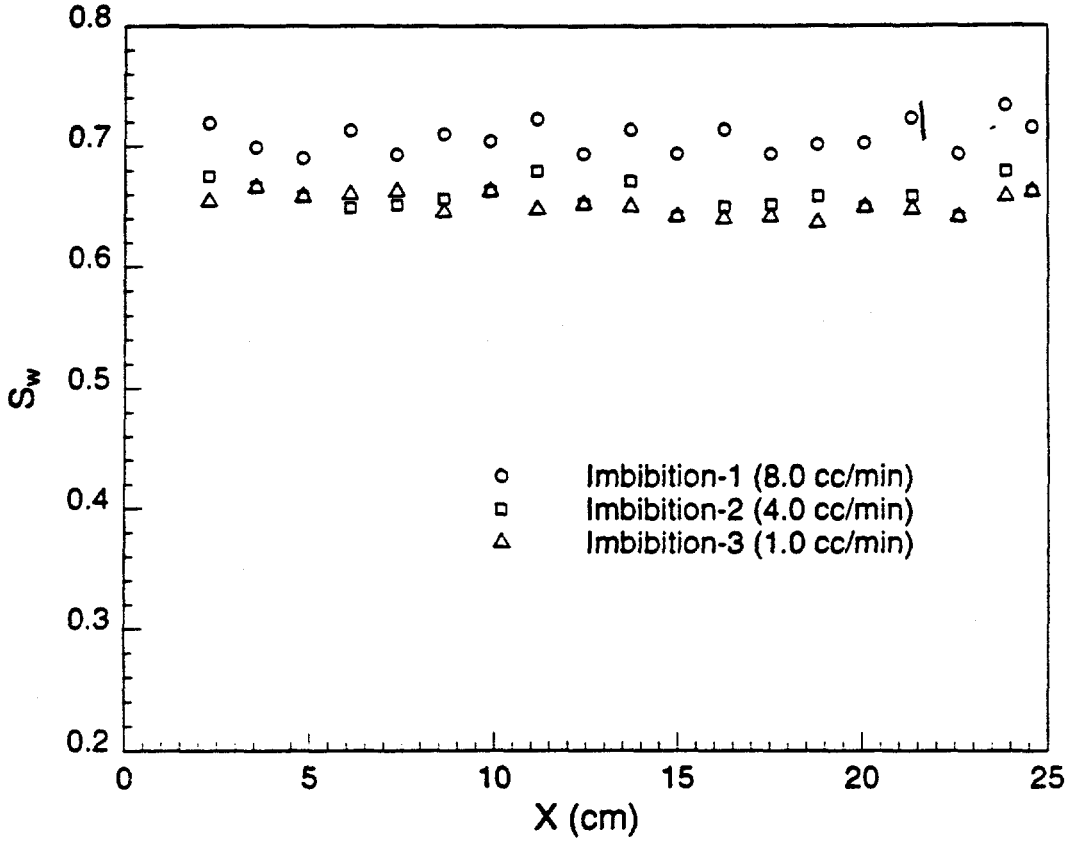

Figure 6: Saturation Profiles at the End of Imbibition Displacements.

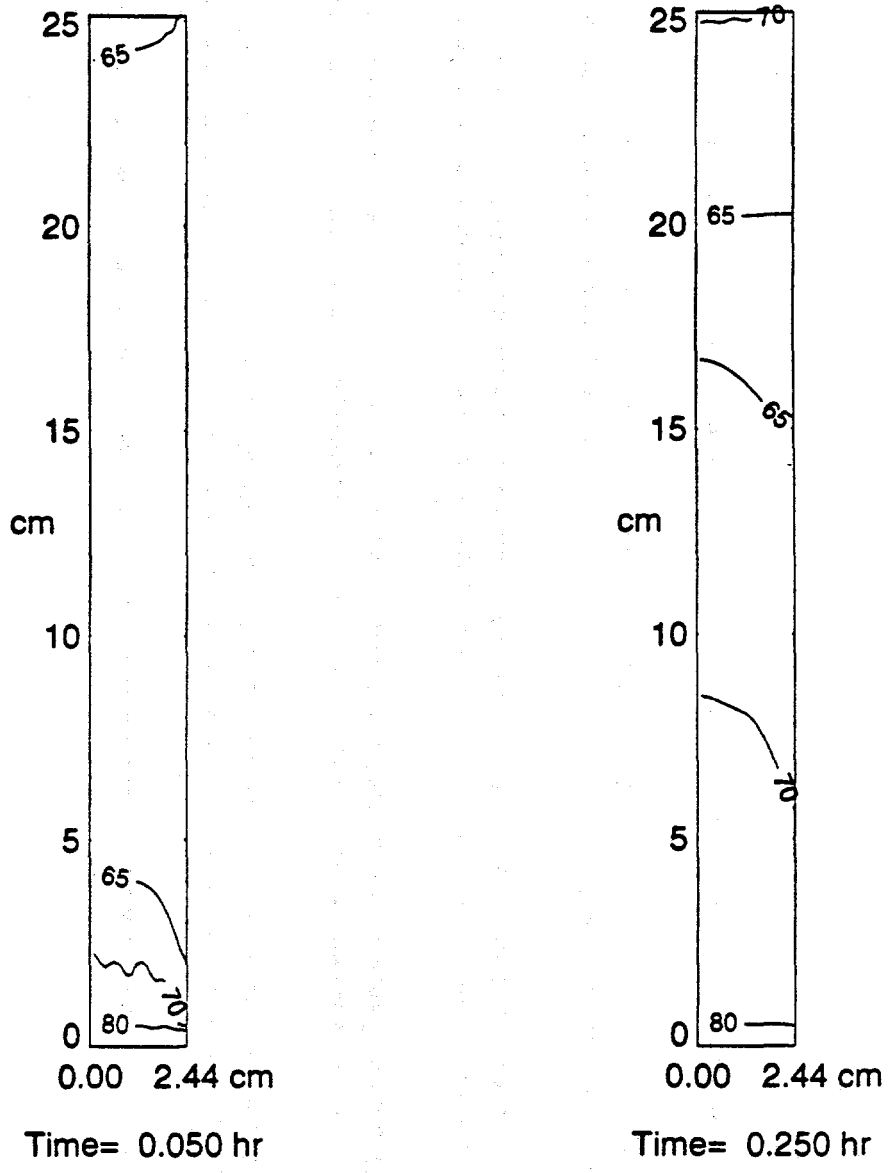

Figure 7: Saturation Maps from Simulated Imbibitions (8.0 cc/min)

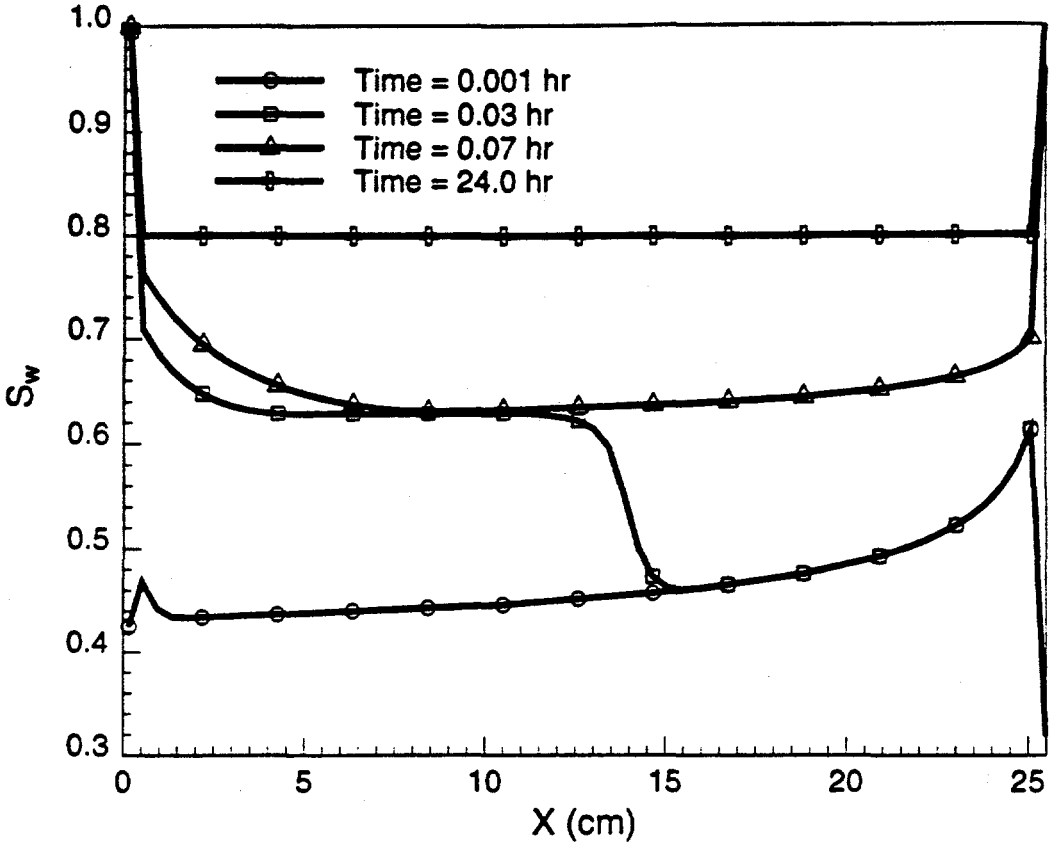

Figure 8: Average Simulated Saturation Profiles at Different Times, Imbibition (8.0 cc/min)

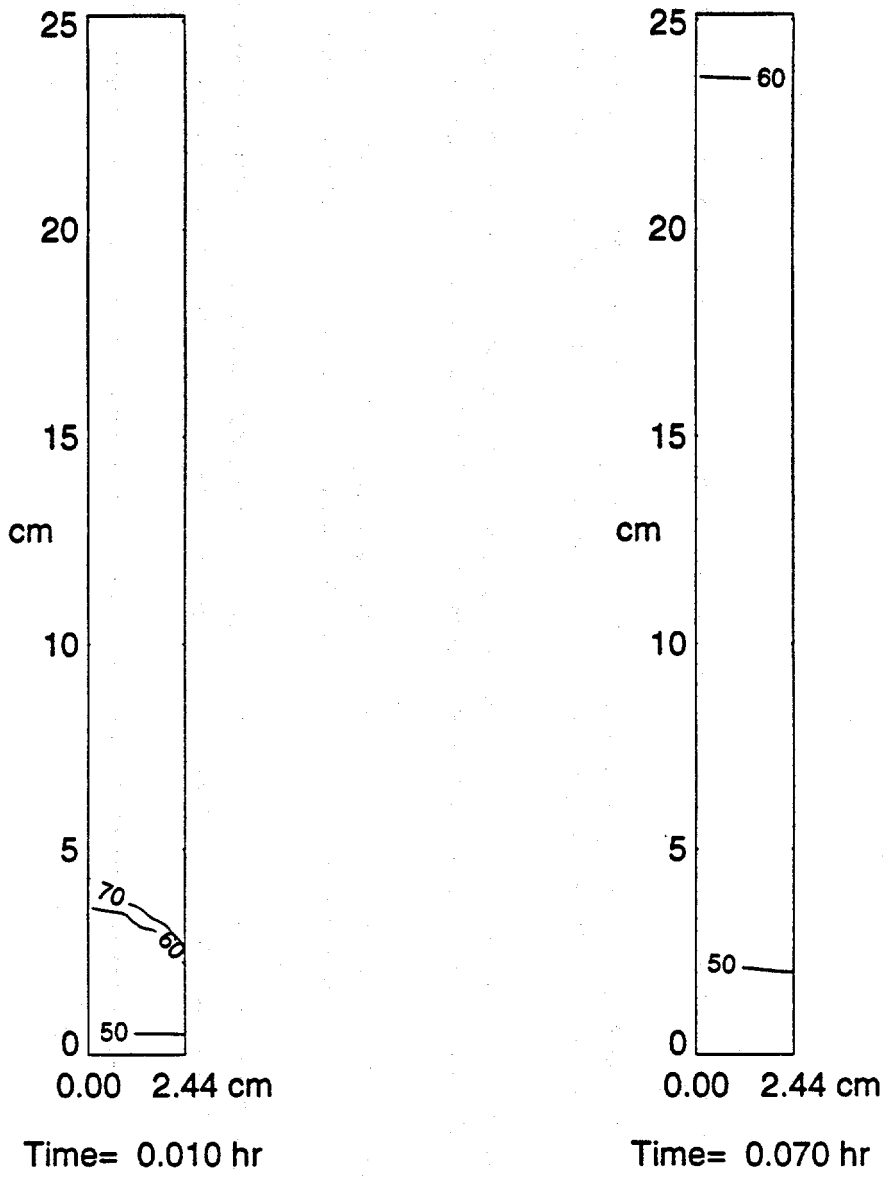

Figure 9: Saturation Maps from Simulated Drainage Data (8.0 cc/min).

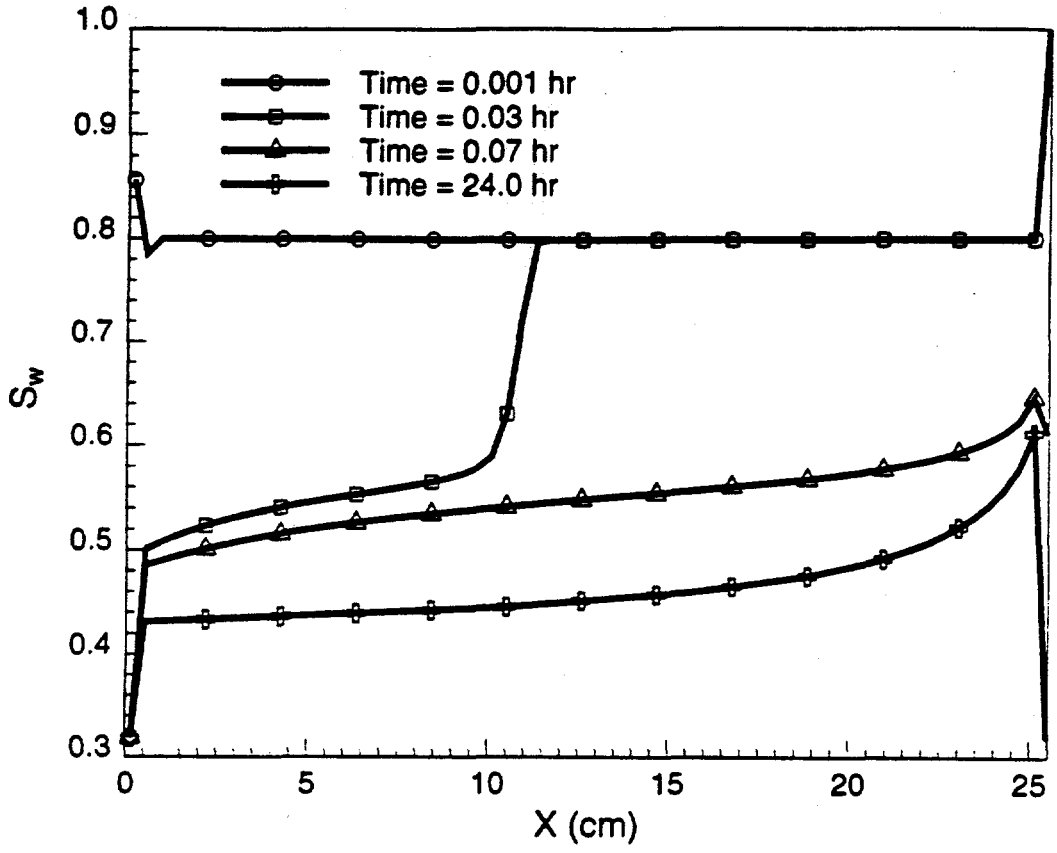

Figure 10: Average Simulated Saturation Profiles at Different Times, Drainage (8.0 cc/min).

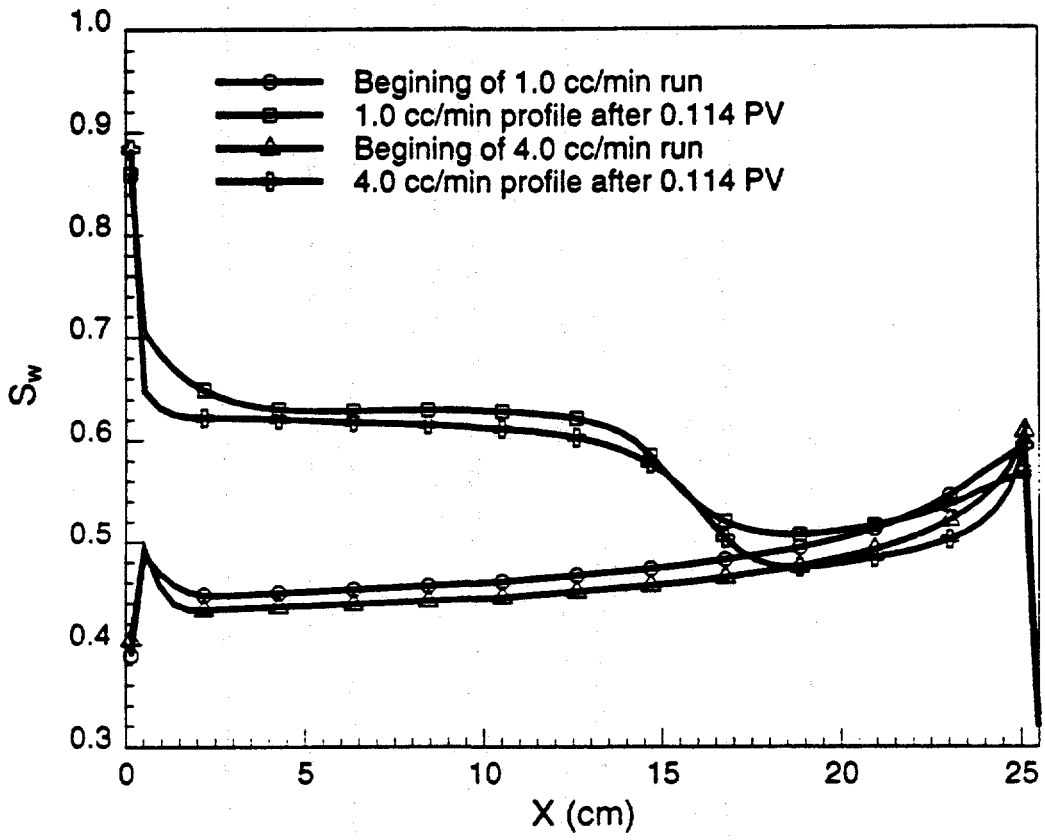

Figure 11: Comparison of Simulated Saturation Profiles, Imbibition, (1.0 and 4.0 cc/min).

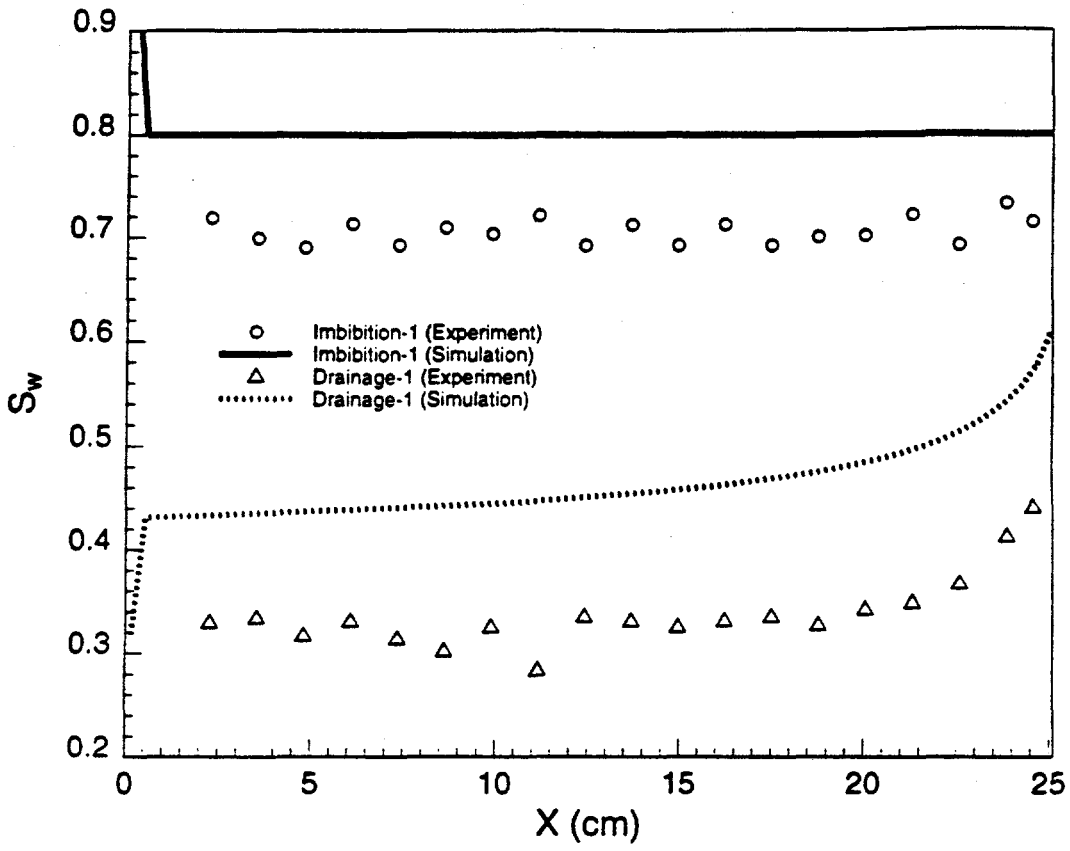

Figure 12: Comparison of experimental and simulated saturation profiles.

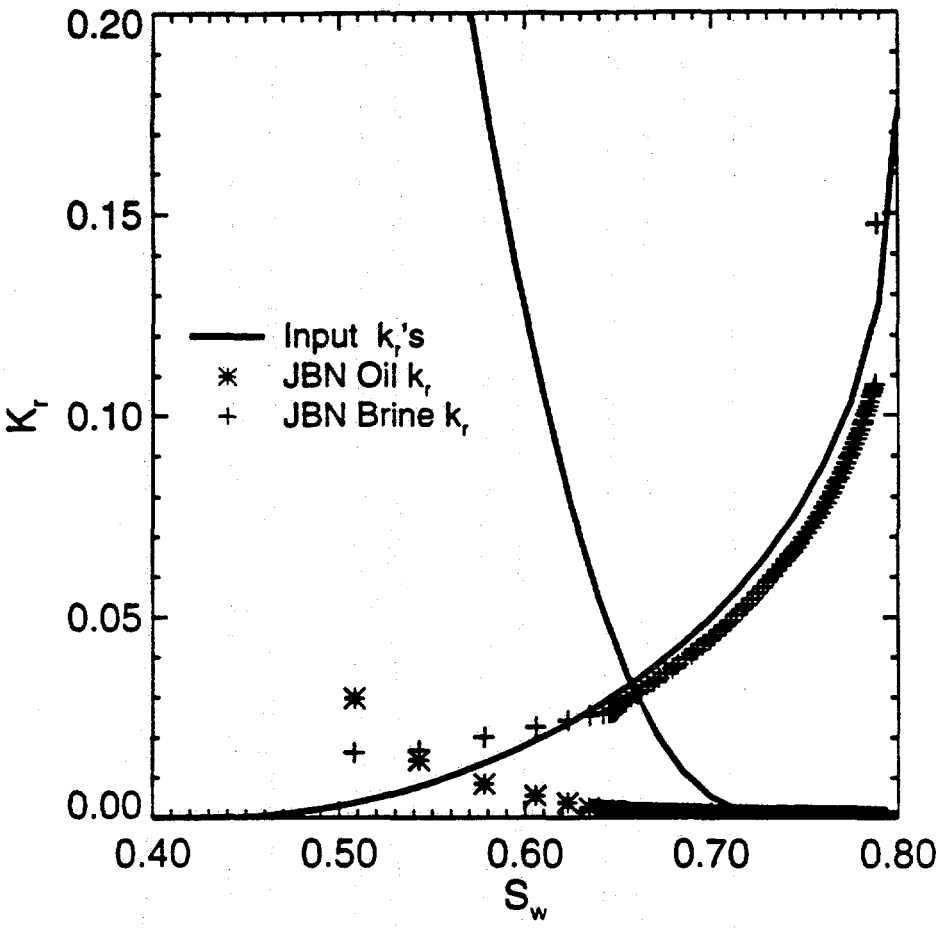

Figure 13: JBN Relative Permeabilities (Imbibition Rate=8.0 cc/min, μ_o/μ_w = 1.0)

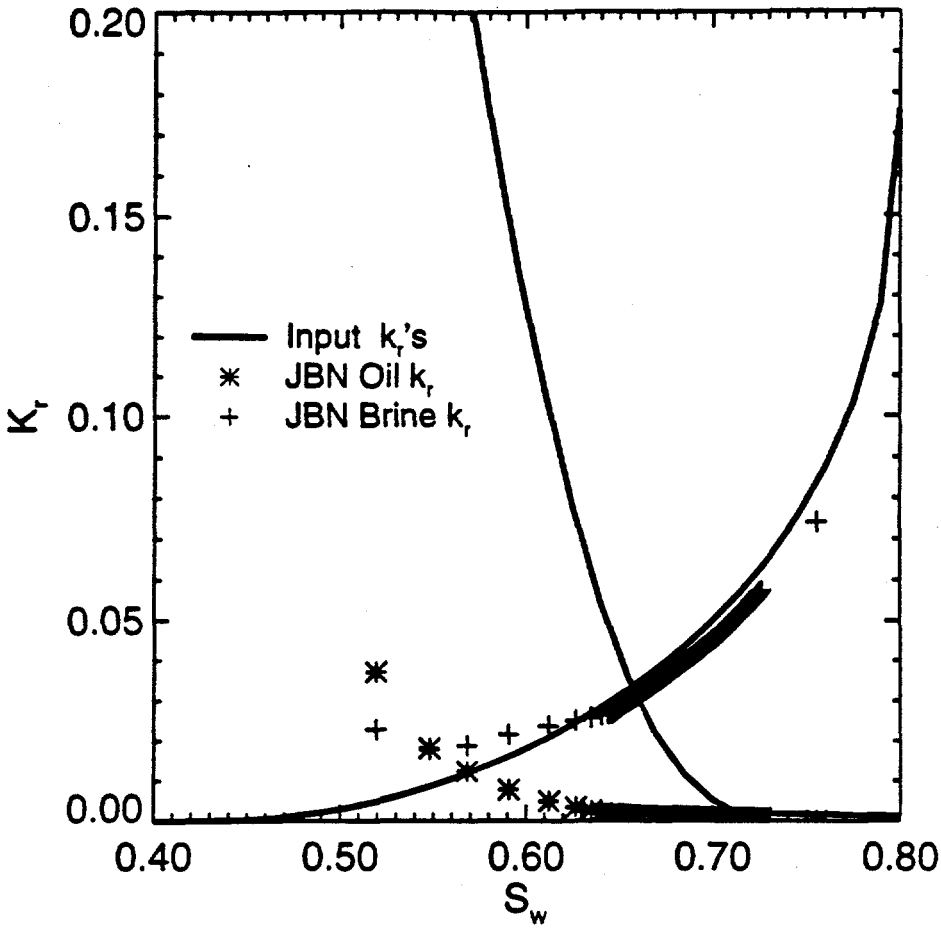

Figure 14: JBN Relative Permeabilities (Imbibition Rate=1.0 cc/min, μ_O/μ_W = 1.0)

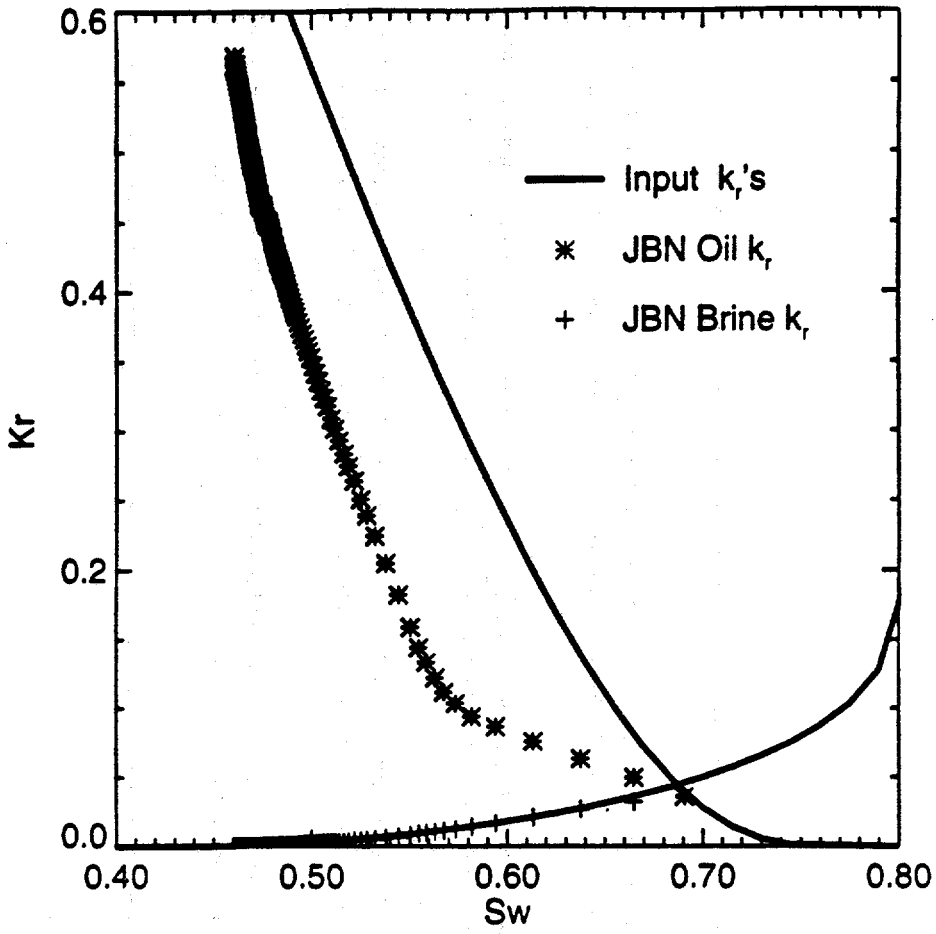

Figure 15: JBN Relative Permeabilities (Drainage Rate=8.0 cc/min, μ_O/μ_W = 1.0)

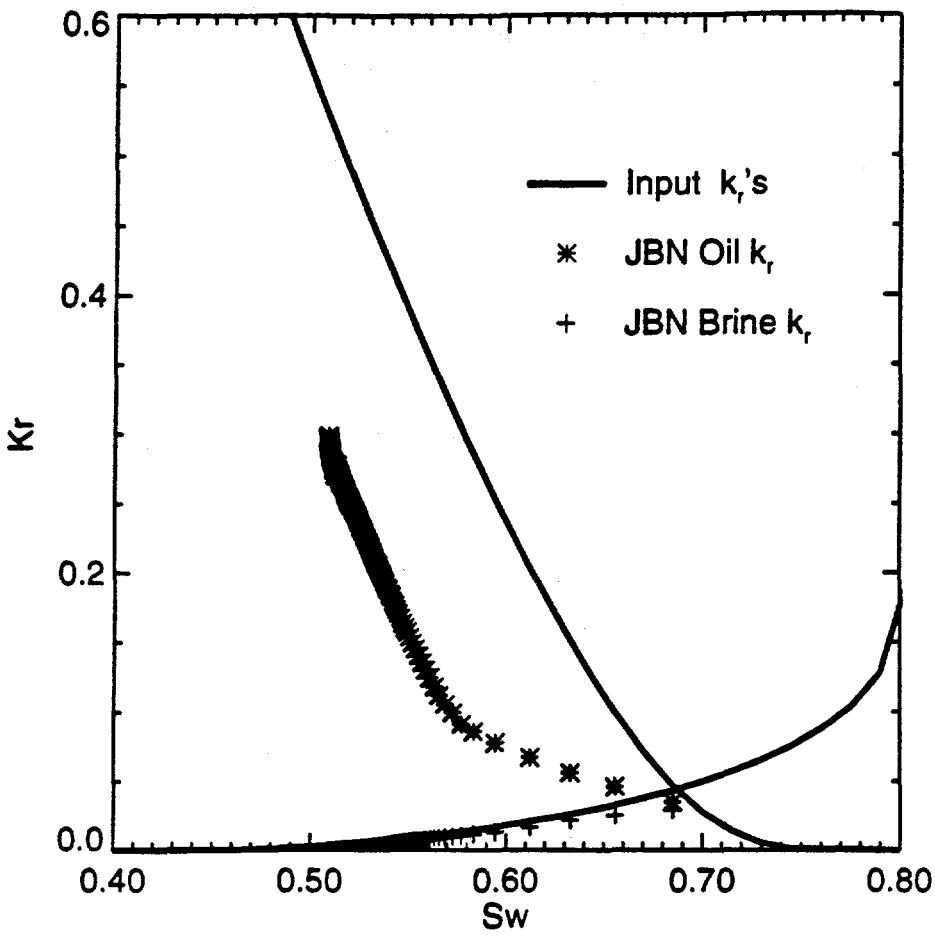

Figure 16: JBN Relative Permeabilities (Drainage Rate=1.0 cc/min, $\mu_O/\mu_W = 1.0$)

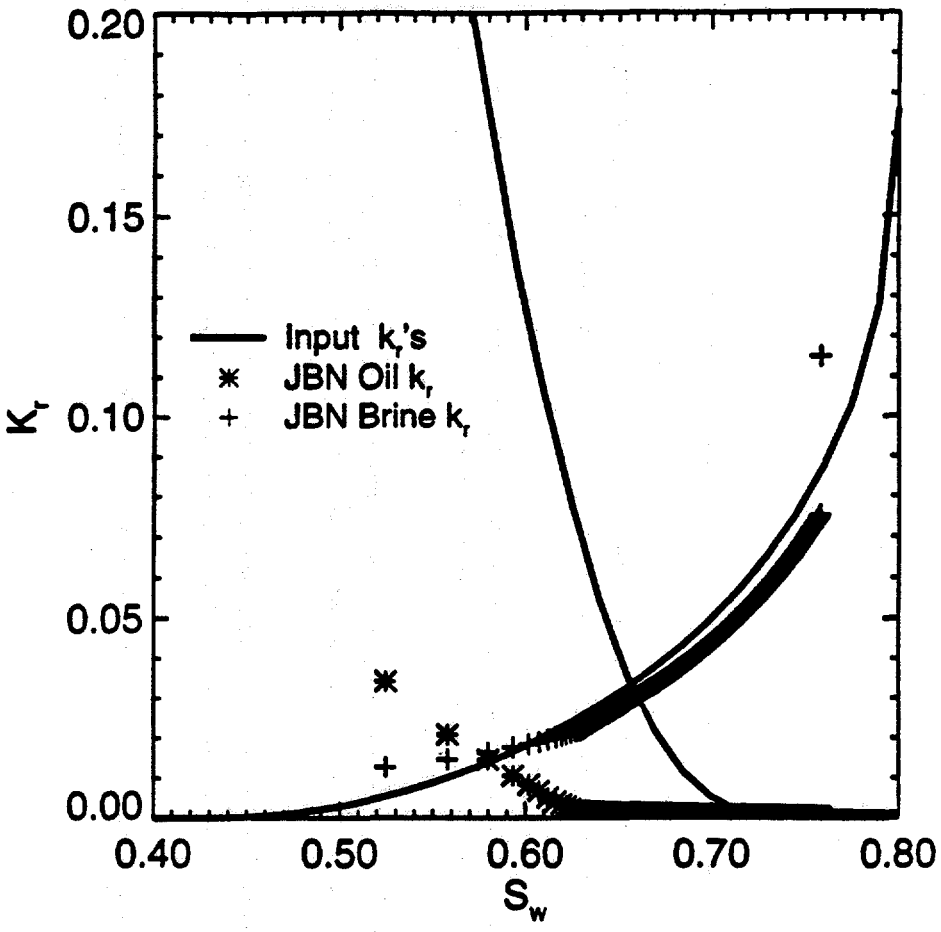

Figure 17: JBN Relative Permeabilities (Imbibition Rate=8.0 cc/min, $\mu_o/\mu_w = 5.0$)

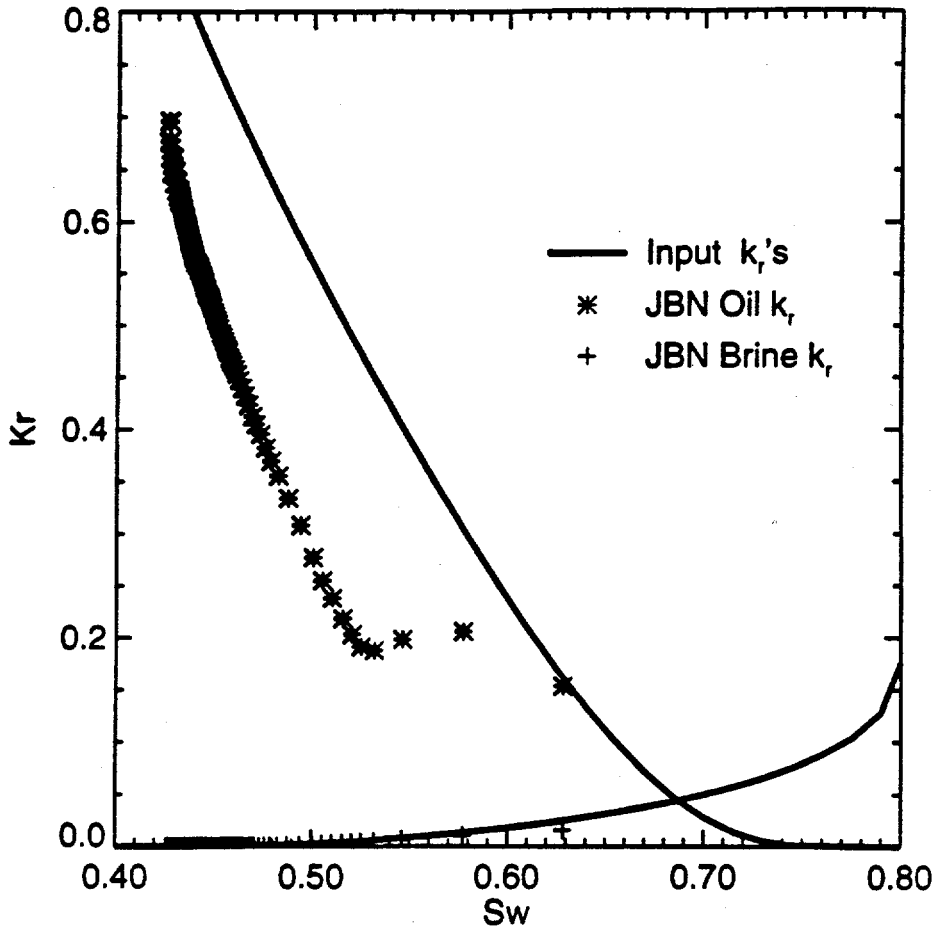

Figure 18: JBN Relative Permeabilities (Drainage Rate=8.0 cc/min, $\mu_o/\mu_w = 5.0$)

1.2 STEAM-WATER RELATIVE PERMEABILITY
(Mark Meeks)

Steam-water relative permeability is a topic of practical importance for modeling multiphase flow in enhanced oil recovery and geothermal projects. However, it is not a well-understood phenomenon. To gather background information on theory as well as published experimental and history-matching data a literature review was conducted by searching the following data bases: EI Compendex; Enviro/Energy Line; Geo Ref; and Math Sci. These data bases yielded information primarily on studies appearing since 1987. To locate earlier studies a secondary bibliography was compiled from references listed in the primary works. This proved to be a fruitful approach, locating many pertinent works not located by the computer-assisted search.

1.2.1 LITERATURE REVIEW

The literature review showed that although preliminary studies in this area began as early as the 1950's, there still remains fundamental disagreement about the values for relative permeability curves as functions of water saturation and about the physical processes of fluid movement and heat transfer. The lack of agreement between experimentally determined values has led to the widespread usage of estimated values in computer simulation studies. A large part of the controversy stems from the difficulties arising in obtaining reliable saturation profiles in heterogeneous media. We hope that the acquisition of a new CT scanner capable of producing high-resolution images will enable us to establish accurate, reliable saturation profiles ultimately which will lead to more reliable multiphase flow models.

One of the first key studies to appear was by Arihara (1974), who was unable to determine saturations. Instead, he measured the temperature profile through the boiling region of a synthetic sandstone core to obtain fluid properties, enthalpy, and pressure throughout the two-phase region. Then he utilized equations for steady, single-component, two-phase, nonisothermal adiabatic flow together with a calculated relative permeability ratio and a water-oil permeability vs. water saturation curve to derive a water saturation for each steam or water relative permeability. A disadvantage to his approach is that the water-oil permeability ratio may not necessarily be transferable to a steam-water system.

Trimble and Menzie (1975) developed relative permeability curves for Boise and Berea sandstone cores. However, their assumption that liquid and vapor velocities were identical would have skewed the results when they calculated water saturation from steam quality. Chen (1976) scored a major advance by directly measuring water saturation with a capacitance probe for a synthetic consolidated sandstone core, assuming a nearly linear relationship between the capacitance probe signal and water content. His results, which showed nonzero values of relative permeability to water only for water saturation values above 0.75, contrasted markedly with the results of Trimble and Menzie, who gave positive values for relative permeability to water corresponding to water saturation values between zero and 0.2.

Several interesting attempts to circumvent the issue of saturation profiles followed. Instead of focusing on core samples, attention was shifted to the macroscopic level of geothermal field data from the Wairakei field of New Zealand. Grant (1977) calculated permeability reduction factors by making the assumption that the driving pressure gradient and temperature were not affected by a change in the producing enthalpy. After correlating liquid/water flow rates with discharge enthalpy he was able to conclude, with an admitted

degree of uncertainty, that steam-water flow in a fractured medium differed from flow in a porous medium. Further, he theorized that steam-water flow in a fractured rock does not involve the interference between the two phases as occurs in a porous rock.

Horne (1978) continued research in this area by examining wellhead pressure change with time and by utilizing actual downhole temperatures in lieu of mean temperatures and fluid properties. He was able to derive a relative permeability curve based on values for flowing water saturation while ignoring the immobilized water in the field. Thus, his curves were not relative permeability curves in the conventional sense. His flowing water saturations were really flowing liquid mass fractions, not resident volumetric water saturation. Despite further refinements by Shinohara (1978) these attempts to conduct analysis on the macrolevel did not produce satisfactory permeability curves.

Counsil (1979) employed Chen's technique of measuring water saturation with a capacitance probe to obtain steam-water relative permeabilities from steady-state two-phase, nonisothermal bench-scale flow experiments. Additionally, he obtained nitrogen-water relative permeabilities for a synthetic sandstone core under transient conditions. He concluded that, for high water saturation, the isothermal external gas drive (nitrogen-water) gas relative permeabilities were lower than those of the nonisothermal boiling internal gas drive (steam-water) system. This may have been due to the different positions occupied by nitrogen and steam in the porous media.

Monsalve *et al.* (1984) investigated the effects of surfactants upon steam-water systems, noting that the residual steam saturation increases with increasing surfactant concentration. Accordingly, on a graph of relative permeabilities to steam versus water saturation the curves retain their general shape while shifting to the left as more surfactant is added. They concluded that, contrary to previous studies on gas-liquid systems, the relative permeability to water increased with increasing surfactant concentration rather than holding constant.

Sanchez *et al.* (1987) argued that errors in the measurement of steam quality by Monsalve *et al.* prevented exact comparisons with gas-water systems. Furthermore, Sanchez *et al.* maintained that the large differences between Counsil's steam-water and gas-water relative permeabilities were due to vaporization from pressure drop along the core and to problems with the calculation of heat transfer. Their experiment, carefully designed to minimize heat losses with adiabatic two-phase flow in an unconsolidated Ottawa sand pack, concluded that steam permeability can be accurately represented by gas permeability for two-phase flow. Instead of relying on a simple mass balance, numerical integration was used to calculate mean residence time of the an NaCl-36 tracer, which together with the volumetric flow rate permitted calculation of water saturations.

To address the issue of whether steam-water permeabilities should be viewed in terms of a noncondensable gas-water model or a condensing phase model, Parlar and Yortsos (1987) drew upon percolation theory to describe capillary condensation and evaporation processes obtained in previous studies. They concluded that primary imbibition curves behave in accordance with the flow patterns of immiscible fluids, while the primary drainage curve by comparison begins at zero residual vapor saturation with the corresponding liquid relative permeability remaining normal for a wetting phase in immiscible flow. Capillary pressure curves were obtained with the standard features of immiscible fluids except that residual saturations became very small for both liquid and gas phases and for primary drainage and imbibition processes. Apart from these considerations, their results generally supported the idea that steam-water relative permeability could be approximated by studying immiscible gas-liquid flow regimes.

Closmann and Vinegar (1988) addressed the need to find a more accurate way of measuring liquid saturation by making CT scans of liquid saturation of natural cores at each equilibrium point. This approach allowed them to measure steam-water relative permeabilities for cores at steam-drive oil residual saturation under *in-situ* conditions. New techniques were introduced for calculating steam permeability from pressure data and from inlet and outlet temperatures. Following the last steam flow test and the last total liquid saturation measurement methylene chloride solution was used to extract and measure the residual oil saturation. Next, the core was flooded with methanol and then air-dried to remove any water. After CT scanning in this dry state the core was saturated with distilled water, scanned once again, and the absolute permeability was measured at 100% water saturation. These absolute values were used in calculating relative permeabilities. By monitoring inlet and outlet temperatures it was possible to estimate heat losses. Final analysis revealed steam relative permeabilities close to values in the literature for gas flow through porous media. Water relative permeabilities were somewhat below values in the literature.

Sedgwick and Miles-Dixon (1988) developed three X-ray imaging methods for investigating multiphase flow through oil sands: (1) a single beam technique to directly measure bitumen and water saturation; (2) X-ray xeroradiography (a qualitative technique developed to visualize encased field cores and coreflood experiments), producing high-contrast two-dimensional images of internal core structure and fluid distributions; and (3) computerized tomography with a complete three-dimensional imaging capability. The first and third methods yielded similar relative permeability curves for water and bitumen comparing favorably with data obtained by conventional steady state methods as found in the literature. Xeroradiography was useful in obtaining high-contrast images; however, actual saturation data could not be determined by this method.

Oak *et al.* (1990) performed X-ray scans of two- and three-phase flow in fired Berea sandstone in a steady-state regime for two primary saturation histories: (1) DDI (decreasing, decreasing, increasing); and (2) IID (increasing, increasing, decreasing). For the DDI case oil and gas three-phase relative permeabilities were functions of water, oil, and gas saturations. For the IID case oil and gas relative permeabilities were functions of oil and gas, respectively. In both instances, water relative permeability was primarily a function of water saturation.

In summarizing the results of the literature search we can see two main approaches to the study of steam-water relative permeability:

(1) a model based on adiabatic "boiling" flow with water as the sole chemical component moving in liquid and vapor phases; and
(2) isothermal immiscible "gas-drive" flow using nitrogen and water.

The more-recent studies have suggested that, when heat losses are properly controlled, the two approaches can yield roughly equivalent relative permeability data. If these studies are correct, then gas-drive flow models with no mass transfer could possibly provide reliable data which can be substituted in the absence of data on steam-water relative permeability.

1.2.2 FUTURE WORK

We hope to obtain reliable permeability curves useful in resolving this issue. Optimal size, flow rates, and heat properties are being determined by the Computer Modeling Group's Steam and Additive Reservoir Simulator (STARS, Version 4.0.1). Key

factors which we wish to be conscious of include heat loss effects, gravity segregation, pressure drop, temperature profiles, slippage and Klinkenberg effects, scaling factors, heat pipe effects, stratification, capillary end effects, salinity of water, and steam quality. Optimal design parameters for steam/water flow through a cylindrical sandstone core have been obtained from preliminary simulation studies. Results indicate that the dip factor is of minor importance, allowing for either horizontal or vertical flow. To minimize heat losses it is best to operate at a lower temperature, shorten the length of the cylinder, increase its radius, and increase the time of flow. Initial results indicate that a 2×8 in. cylindrical sandstone core can be used to optimize all parameters including minimal heat loss. Heat losses per unit of area, time, and mass flow rate can also be reduced by increasing the flow rate (see Fig. 1.2.1); however, the pressure increase needed to accomplish this has the undesirable effect of inducing condensation at a lower temperature. Currently, the experimental monitoring equipment and coreholder are being built.

Acculam G7 plastic was chosen as the material for the coreholder because of its low thermal conductivity and temperature resistance up to 450°F. A series of experiments is being designed with the assistance of STARS simulation studies. The thrust of our approach is to obtain saturation profile data from CT scanning which can be used in history matching to generate reliable relative permeability curves using simulation techniques. The first experiments will be performed at ambient temperatures with a noncondensible nitrogen-water system to check out the accuracy of the data gathering and history matching processes. The next phase will be to begin measurements of water-steam systems.

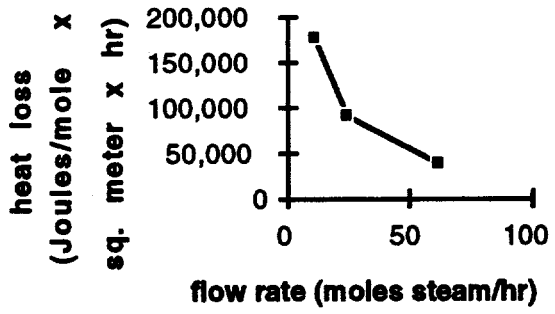

Figure 1.2.1 Heat loss versus flow rate.

1.3 CT IMAGING OF TWO-PHASE (OIL/WATER) FLOW IN FRACTURED POROUS MEDIA

(Richard Hughes)

1.3.1 INTRODUCTION

The purpose of this study is to investigate the physics of isothermal two-phase flow. Boise sandstone has been chosen as the porous medium and three cores have been prepared. The first core is a $3 \times 3 \times 11$ in. compact core. The second and third cores each consist of two $1.5 \times 3 \times 11$ in. blocks. The second has a 1 millimeter spacer to provide a separation between the blocks to simulate a fracture. The third core has no spacer between the blocks. Mineral Oil and 8% NaBr solution have been chosen as the oil and water phases for the experiments.

1.3.2 EXPERIMENTAL RESULTS

A core holder similar to the original design by Guzman (1993) has been developed for each of the cores. It consists of an epoxy resin (Tap Plastics Marine Grade Resin #314 with Tap Plastics #143 Hardener) surrounding the core with Plexiglas endplates. The original design had six pressure taps all on the top of the core holder. The new design has two pressure taps on the top and two on the bottom as shown in Fig. 1.3.1. This will allow us to clean the core while obtaining necessary data. Plexiglas rods hold the endplates in place. In addition, a Plexiglas plate that was glued to the top surface of the core was removed in the new design. The plate was found to be unnecessary and a potential source for leaks.

Several different epoxies were tested. Among these were Tap Plastics "One to One" General Purpose Epoxy, Tap Plastics "Super Hard" Four to One Epoxy and Evercoat Laminating Resin. All of these epoxies were extremely exothermic when reacting to become solid. The Tap Plastics Marine Grade Epoxy system that we chose uses the #314 resin in combination with various hardeners to provide different cure times with similar chemical resistances and strengths. The #143 Hardener was chosen because it provides a slower cure yet retains its chemical resistance properties. This system is slightly less viscous so penetration is a bit deeper into the core than it was for some of the other systems we observed; however for this experiment the added control the slow cure time provided was deemed to be a more important issue than penetration depth. In addition to using a slower curing epoxy system, an aluminum mold was constructed to allow better heat dissipation. The mold was built so that there would be a 1/2 inch border of epoxy around the bottom and sides of the core. It has an open top and the sides are six inches taller than the estimated top of the core holder. This seemed to allow the heat to radiate out of the mold and prevent cracking of the epoxy.

1.3.3 CORE HOLDER CONSTRUCTION

Plexiglas endplates were attached with GE White RTV 102 Silicon Rubber Adhesive Sealant and held in place with clamps. Epoxy was layered on with a paintbrush and allowed to sit for one hour. The core was then placed into the mold. The mold was tilted at a 45° angle while pouring the epoxy resin to reduce the number of air bubbles formed along the bottom of the core. Once the liquid resin covered the core, the mold was returned to level and additional resin was added to reach the desired height. During the construction of the first core holder, heat expansion of the air inside the core caused bubbles to form and rise at one of the ends. For the two subsequent cores, holes were drilled in the Plexiglas end plates, and this action alleviated the problem. The cores were removed from the mold and taken to a local monument shop where the

ends were trimmed to provide the 11-in. length. Plexiglas end plates were constructed for the core holders with a piece of 3/8 in.Viton acting as a gasket surrounding the core and held in place with automotive gasket material as shown in Fig. 1.3.2.

1.3.4 ONGOING EXPERIMENTAL WORK

The flow system from the dynamic relative permeability study (Qadeer, 1995) is being modified for use in this study. Modifications are being made to the injection system and to the fluid measurement system. In addition, preliminary CT scans on the dry cores are being performed. During initial training on the new scanner, several 1 millimeter vugs were discovered. As seen in Fig. 1.3.3, some of these vugs will not effect the study dramatically since they are in a remote portion of the core. Others may have direct effects and the responses will need to be observed carefully. The preliminary CT scans are an attempt to determine the location of as many of the vugs as possible.

1.3.5 SIMULATION STUDIES

Evaluations of the simulation runs performed in the initial study confirmed that most of the information gained from those runs could be transferred to the new experimental configuration. Specifically the capillary pressure curves used in the original study were examined. It was found that the capillary pressure curves used were for a mineral-oil/ brine system similar to the one proposed in this study.

One aspect that did not seem to be adequately evaluated was how to clean the cores for use in other experiments. Simulation runs using the Eclipse simulator were made to determine a satisfactory configuration for data collection and for cleaning. From these evaluations the pressures at the measuring points seem to be very small. To simplify the design and to aid in the cleaning of the models it was decided that the original design of six pressure measurements along the top of the models could be replaced by two measurements on the top and two on the bottom of the models. Figure 1.3.4 presents the average oil saturation as a function of time for a configuration where injection is in the inlet port and the top two ports and production is from the exit port and the bottom two ports. The average oil saturation in the model was reduced to an average of 1.6% after 25 hours of isopropyl alcohol injection. This is in contrast to the result in the original design where oil saturation remained at 19% throughout the 25 hour period.

1.3.6 FUTURE PLANS

Once construction of the system is complete, several displacements with 100% water cut will be performed to make comparisons to similar previous studies (Mattax and Kyte, 1962; Kleppe and Morse, 1974; Kazemi and Merrill, 1979; and Babadagli, 1994). These displacements will be followed by variations in the injected water cuts in an attempt to determine potential fracture relative permeability effects.

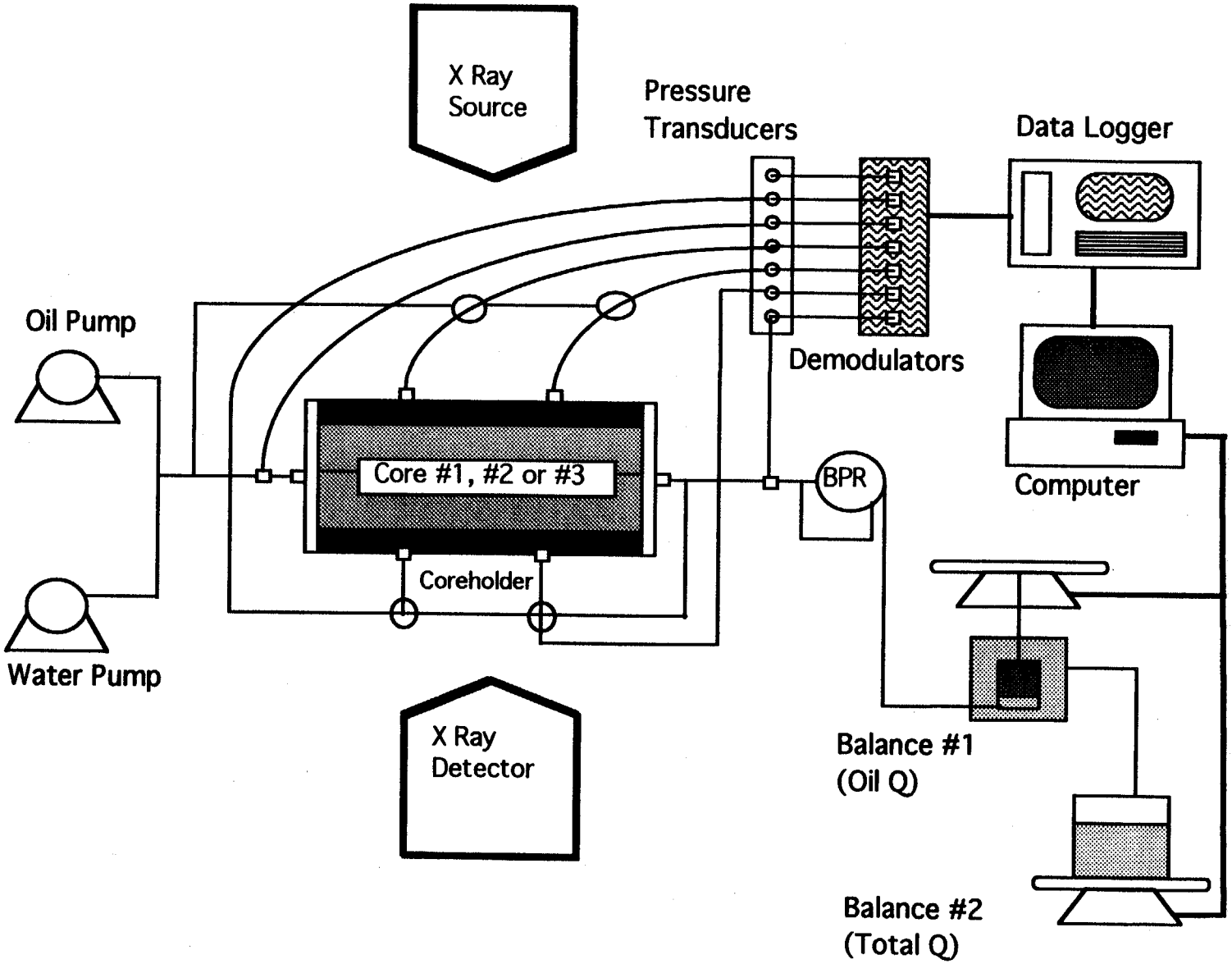

Figure 1.3.1 Experiment setup.

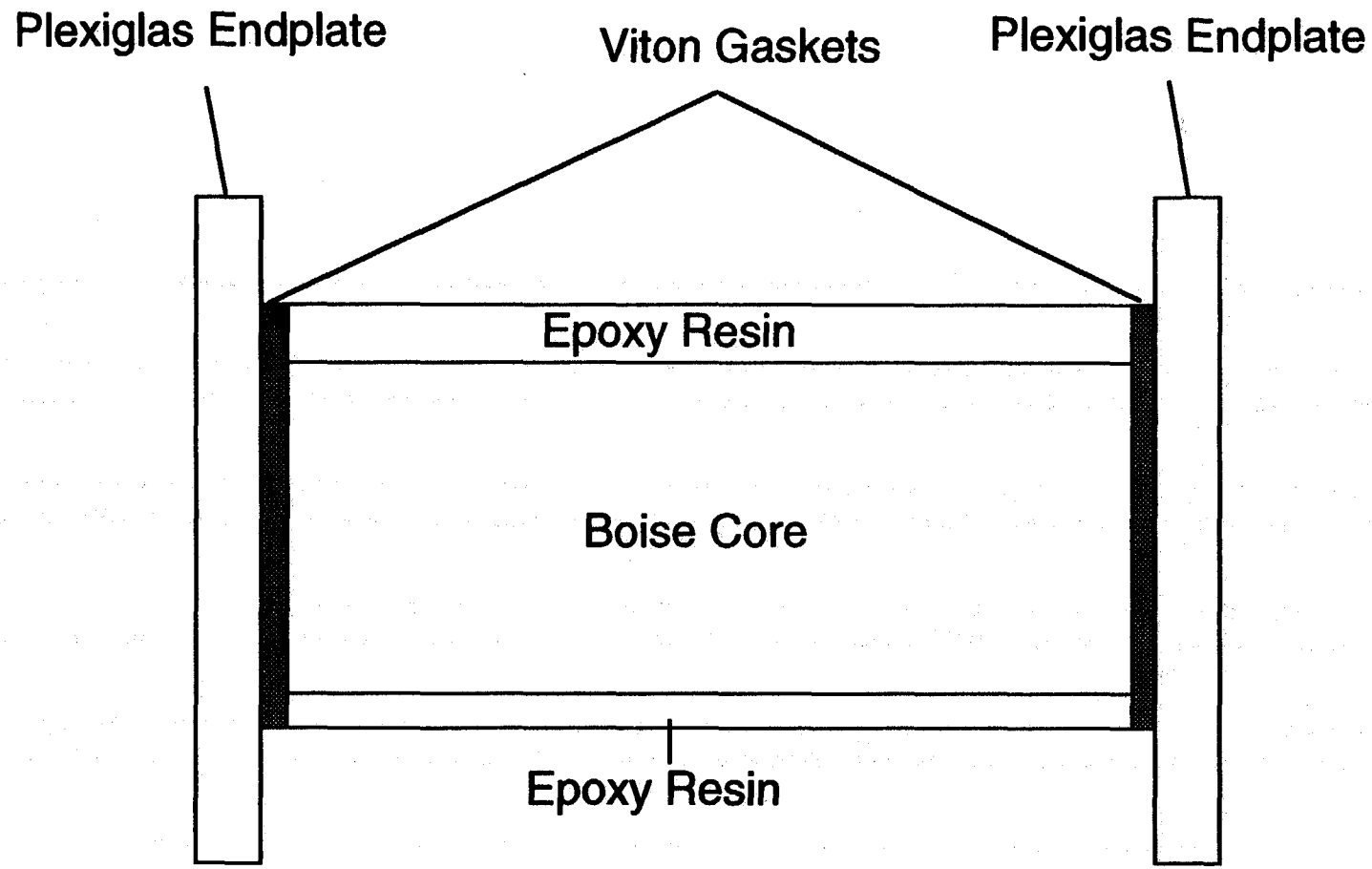

Figure 1.3.2 Coreholder design

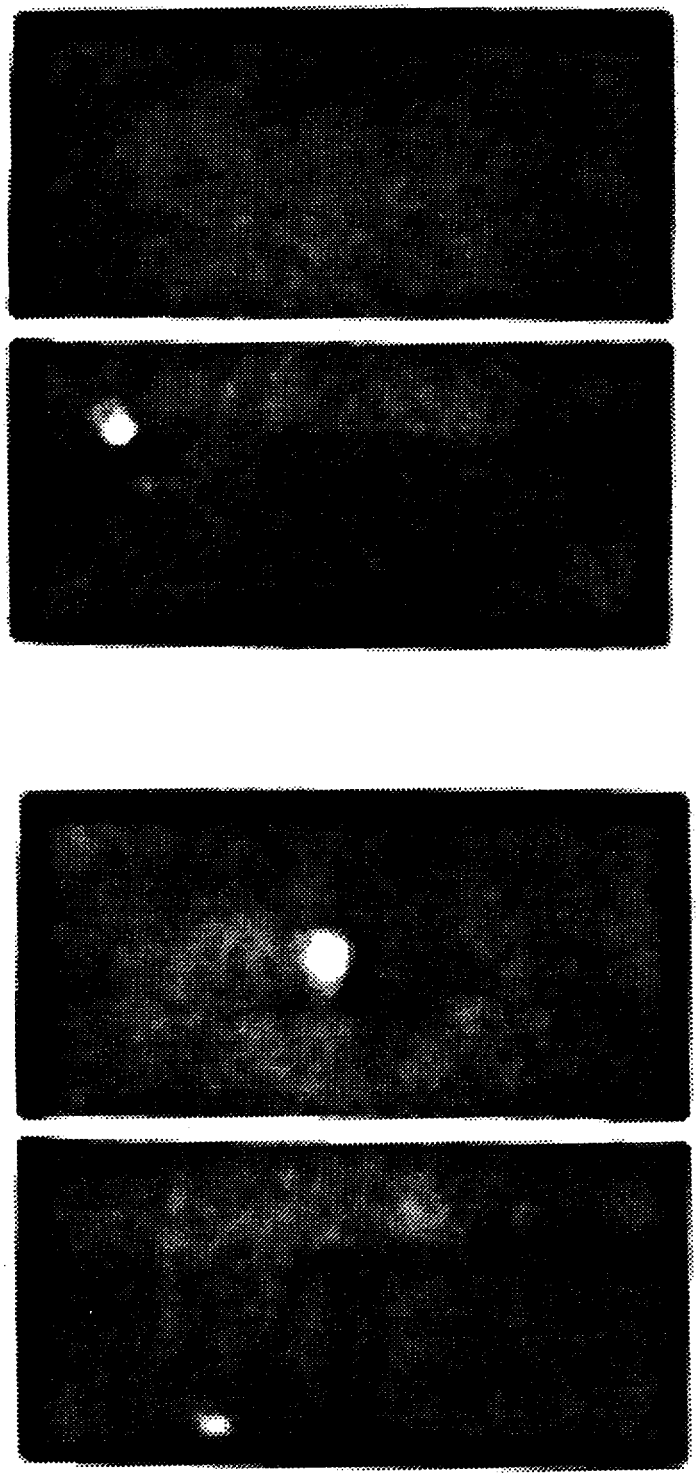

Figure 1.3.3 Two CT scans showing vugs in the core.

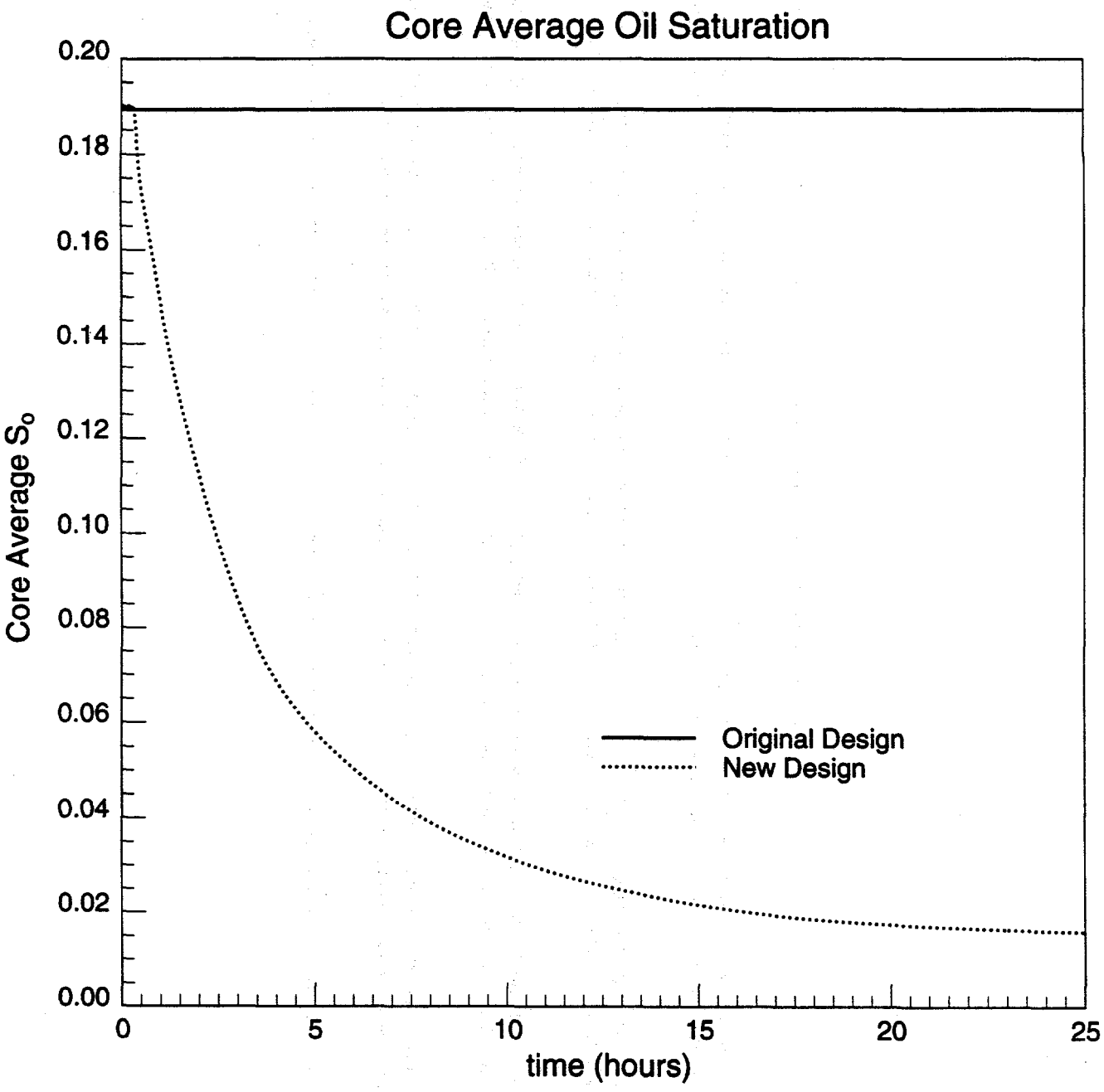

Figure 1.3.4 Cleaning run with top ports injecting.

1.4 CT FACILITY STATUS AND PROJECTS
(Louis M. Castanier)

The Petroleum Engineering Department has purchased a new X ray CT scanner located in the Earth Sciences Green Research Building. SUPRI A is one of the major financial contributors to this project, its operator and one of the main users. The purpose of this summary is to briefly describe the facility, to give some examples of its usage not specifically related to SUPRI A projects and to review the status of the software and hardware.

1.4.1 DESCRIPTION OF THE FACILITY

The scanner is a modified Pickers 1200SX X-ray machine. The choice of this type of equipment was made because of price, availability, cost of maintenance and unique possibility of vertical positioning modifications. The main features of the hardware are described below.

(a) The scanner: It is a fourth generation scanner where the X-ray tube assembly rotates inside a circle of 1200 detectors. This allows rapid collection of the data (one slice takes 2.3 seconds versus nearly one minute for our older EMI 5005 second generation system). It also improves the spatial definition by a factor of 25 over the older machine allowing measurements of 0.5 by 0.5 by 1 mm volume elements (voxels). Processing time and quality is also improved by the presence of a Perkin Elmer 3200 computer which processes data on a 512 by 512 matrix format.

The X-ray tube is a rotating anode system which give adequate monochromaticity of the X-ray beam while increasing the available intensity thus reducing statistical and beam hardening errors. It also is adequate for multi-energy level scanning, a feature indispensable for proper three-phase saturation measurements.

(b) Special modifications: The gantry was modified to allow scans on an axis varying from +20 degrees to -90 degrees from horizontal. The purpose of this modification is to improve measurements of systems where gravity plays an important role; for example, multiphase flow of fluids with large density differences such as gas and liquids. To our knowledge, no other fourth generation scanner, allowing vertical and horizontal scanning, exists in the oil industry.

The interface between the X-ray generator and the console was modified to allow automatic selection of nonstandard X-ray voltages ranging from 80 keV to 140 keV. A computer attached to the system controls automatic scanning of preprogrammed sequences such as rapid dual energy scans of the same slice. This feature should greatly improve the accuracy of three-phase saturation determination.

Better archiving of the data is made possible by addition of an optical disk to replace the conventional medical tape drive. This change increases storage space and speed and allows storage of the raw CT data in addition to the normal picture files. The data can then be retrieved for further processing using the previously developed interpretation software packages.

The positioning table was modified to reproduce the exact position of slices as accurately as possible. A pilot feature allows quick selection of the slices of interest.

1.4.2 SOFTWARE STATUS

For medical applications, a picture is often adequate. Voxel by voxel processing of the CT data is necessary to obtain quantitative information for parameters such as density, porosity or saturation distributions. Special software needs to be developed and tested for data transfer and display and for quantitative interpretation of the results.

As the data coming out of the CT computers are in a proprietary format not given by the manufacturer of the scanner, we needed to find a program reformatting the data into a usable format for display and processing. After some detective work, a PC based formatting routine was written and tested. This program transforms the raw data obtained from the scanner computer into TIFF files, TEXT files and CT number files.

The TEXT files contain information such as date, slice number and comments on the experiment. The TIFF files are image files that can be immediately displayed and processed on a Macintosh computer, for example. The CT files contain the CT numbers for each voxel of the slice considered. They can be accessed by spreadsheet utilities, such as EXCEL, or can be transferred to the SUN SPARK workstation for further processing.

Our existing software, CATSOFT and GENCODE, is being adapted to handle the new CT files formats. It is able to process the data on a voxel by voxel basis to obtain the needed quantitative values of the desired parameters relevant for a given process. This software was tested on data obtained by our old EMI 5005 scanner but has not yet been modified for use on the data obtained from the new PICKERS machine. A preliminary test of the software has been initiated.

Phantoms of sandstone containing known amounts of water, gas and oil have been built. They will be used to verify the software accuracy in describing porosity and saturation distribution in a core similar to most of the cores used for flow experiments.

1.4.3 STUDIES COMPLETED AND IN PROGRESS

In addition to the work presented elsewhere in this report, several projects dealing with various problems of fluid flow in porous media problems have been initiated in collaboration with researchers from other departments and other universities. The CT scanner is proving to be a useful tool in better understanding porous media.

(a) University of California at Santa Cruz Project. Cores were collected from the ocean floor by a team of researchers from the University of California at Santa Cruz. Some of these cores will be used to measure sonic propagation data for seismic survey calibration. The CT scanner was used to examine 48 cores. About half of the cores showed cracks, fractures or major heterogeneities and proved unsuitable for the type of measurements planned by the UCSC team. The CT scanner helped improve quality control and saved time for those experiments (Figs. 1.4.1 and 1.4.2).

(b) University of California at Berkeley Environmental Project. The Mechanical Engineering Department of the University of California at Berkeley has a research project studying the flow of hydrocarbon contaminants in water saturated porous media. We are performing preliminary experiments aimed at the observation of such systems in Berea cores. This project could be the beginning of cooperative

efforts between Berkeley and Stanford on a variety of problems dealing with flow through porous media.

(c) Fractured Media Characterization. A long term study of flow through fractured media is continuing in collaboration with the Civil Engineering Department at Stanford University. The first results have been published (Johns *et al.*,1993). This project is now aimed at better characterization of fractures and insight on flow characteristics of naturally fractured non-sedimentary rocks (Figs. 1.4.3 and 1.4.4).

(d) Miscible flooding and Geothermal Projects. In our own Petroleum Engineering department, other research programs are benefiting from the CT facility. Observation of miscible or near miscible floods in long cores is in progress and CT determination of adsorbed water in geothermal rocks will be attempted soon. Other projects are planned in enhanced oil recovery research and basic studies of multiphase flow through porous media.

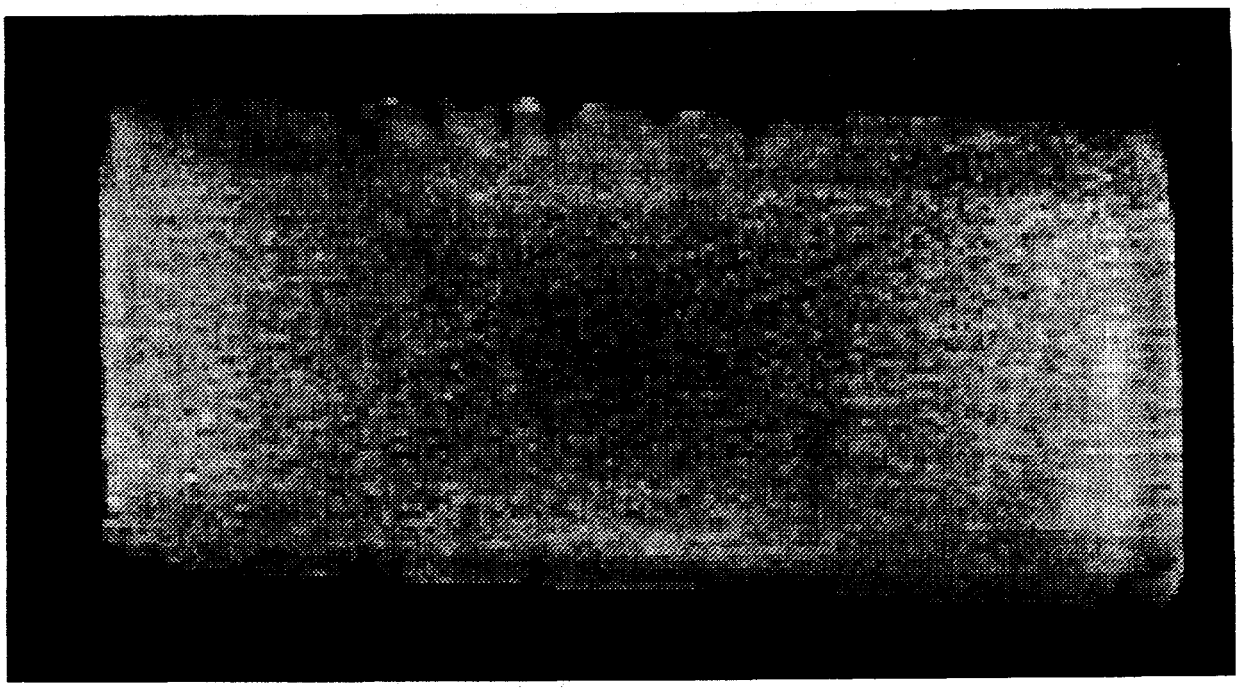

Figure 1.4.1 Ocean floor core for seismic calculation.

Figure 1.4.2 Ocean floor core improper for seismic calibration.

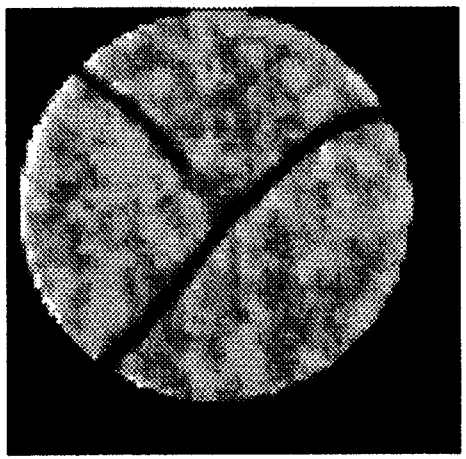

FRACTURE

APERTURE

MEASUREMENTS

Figure 1.4.3 Fracture aperture measurements.

BEFORE

AFTER

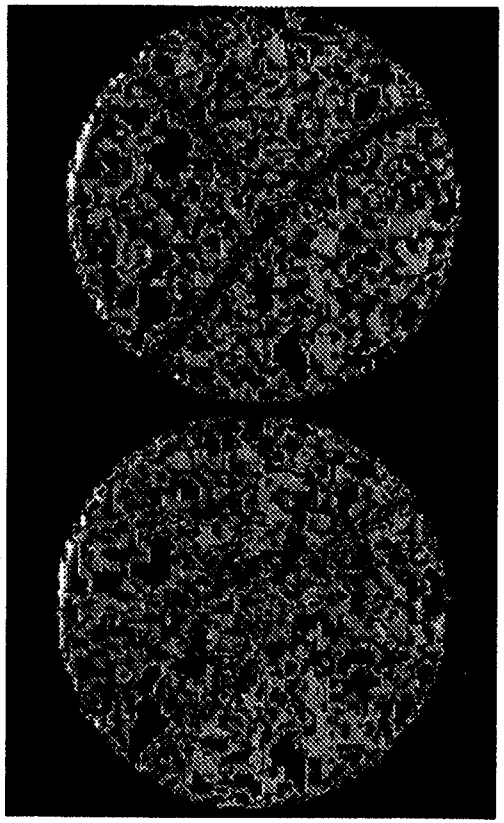

STUDY OF FLOW THROUGH NATURALLY FRACTURED ROCKS

Figure 1.4.4 Flow through naturally fractured granite.

PROJECT 2: IN-SITU COMBUSTION

To evaluate the effect of different reservoir parameters on the in-situ combustion process. This project includes the study of the kinetics of the reactions.

2.1 A STUDY OF IN-SITU COMBUSTION ON SAUDI TAR

(Vivek K. Agrawal)

2.1.1 ABSTRACT

In-situ combustion is classed among the most energy efficient improved oil recovery methods available today. However, a chief constraint limiting practical application of in-situ combustion is the amount of fuel formed in the reservoir matrix ahead of the combustion front. If sufficient fuel is not deposited, as in the case of high gravity oils the combustion front will not sustain itself. Conversely, if fuel deposition is in excess as in the case of low gravity oils, the rate of advance of the front tends to be slow and there is a high demand of air to sustain combustion.

It is desired to find substances which have a catalytic effect on the kinetics of oxidation processes in in-situ combustion. There are many factors affecting the catalysis of such reactions among which are primarily the composition and concentration of the catalyst, surface area of the catalyst available for combustion reactions and the temperature. Therefore, if the amount of fuel deposition ahead of the combustion zone can be controlled by the addition of a suitable quantity of catalyst, we can make this method of thermal recovery practically feasible over a broader range of oil properties.

The kinetics of crude oil oxidation reactions involved in in-situ combustion has been heavily investigated. Measurements of kinetic parameters have been achieved by oxidizing crude oil in packed beds under a programmed heating schedule and by subsequently analyzing the effluent gases (Bousaid and Ramey, 1968; Weijdema, 1968; Burger and Sahuquet, 1972; Dabbous and Fulton, 1974; Thomas *et. al.*, 1979; Fassihi, 1981; Mamora, 1993). All these studies indicate that the overall oxidation mechanism of crude oils in porous media is the result of an overlap of several reactions that occur at different temperature ranges. These different reactions can be broadly classified in three categories :

1. Low-temperature oxidation reactions. These are heterogeneous and produce no carbon oxides.

2. Medium-temperature (fuel deposition) reactions, which are homogeneous and involve the oxidation of the products of distillation and pyrolysis.

3. High-temperature fuel combustion reactions, which are heterogeneous in nature, where oxygen reacts with the heavy coke-like residue deposited at lower temperatures.

A new oxidation reaction model (Mamora,1993) includes two partially overlapping reactions; low-temperature oxidation followed by high-temperature oxidation. The new model includes the effects of grain size and the hydrogen-carbon (H/C) and oxygen-carbon (O/C) ratios of the fuel.

Previous studies (Shallcross, *et al.* 1991), reported results from kinetic runs performed on crude samples from Hamaca, Venezuela and Huntington Beach, California using aqueous solutions of metallic salts. It was discovered that the presence of nickel,

copper and cadmium had little or no effect; however, iron, zinc, tin and aluminum increased the fuel concentrations in the Huntington Beach oil.

Although all these studies have provided qualitative information about the effects of soluble metallic additives on the kinetics of combustion reactions, we still need field related quantitative parameters such as the amount of air needed to burn a unit volume of the reservoir or the fuel concentration .The objective of this study is to observe the variation of various combustion parameters like with changes in concentrations of aqueous solutions of iron nitrate added to the sand pack as part of the water saturation.

2.1.2 LITERATURE REVIEW

The amount of fuel deposited and the velocity of the combustion front are affected by the kinetics of the oxidation and pyrolysis reactions occurring in the porous reservoir matrix. A desirable catalyst, when introduced during in-situ combustion will modify the amount of fuel deposited and also can alter the fuel composition. If such catalysts can be identified and their effects on the combustion process quantified, then in-situ combustion would be feasible for a broader range of crudes and different reservoir matrices. The first study was carried out by Racz (1985). Subsequent work done at Stanford University by Shallcross *et. al.* (1991) and Baena *et al.* (1990) indicated that the addition of water soluble metallic salts can change the kinetics of the combustion reactions. The kinetics studies conducted by Holt, 1992, describes combustion runs done using two types of Californian oil, Cymric light and Cymric heavy, the metallic additives tested were iron, tin and zinc and were observed to improve combustion efficiency in each case. The front velocities were also seen to increase by the addition of metallic salts. Holt also observed changes in H/C ratio of the fuel, heat of combustion, air requirements and density of the produced crude. One of the interesting effects of metallic additives was observed in light Californian oil , the control run indicated that the combustion could not be propagated due to a lack of adequate fuel deposition, however the addition of iron caused a dramatic difference. The front was sustained and propagated. The existing literature has so far not addressed the quantitative determination of the influence of metallic additives and their impacts on combustion parameters. As can be seen from the literature there is also a need to find suitable additives that reduce the amount of fuel deposition which would be desirable in heavy crudes which require an uneconomically high volume of air to sustain combustion.

2.1.3 EXPERIMENTAL APPARATUS

The experimental apparatus has been rebuilt and organized in the new Green Earth Sciences Research Building, it continues to be the same for the most part, some minor modifications have been incorporated. Following are the main features of the apparatus, details are available in the paper by Mamora *et al.*(1993)

The combustion tube is a 1 m long and 7.6 cm O.D. tube made out of 316 stainless steel with 0.041 cm wall thickness. A thermowell is placed along the axis, allowing the temperature measurements to be made anywhere along the axis of the tube. Two electrical heaters located at 10 cm from the top of the tube are used as igniters. the tube is placed vertically in a thermally insulated pressurized chamber which is externally insulated to reduce heat loss to the surroundings. Air injection is controlled by a mass flow meter. The produced fluids are collected via a separator and condenser. The gases are continuously monitored for the amount of oxygen, carbon monoxide and carbon dioxide produced. All the measurements, data logging and analysis are controlled by a microcomputer interfaced

with the apparatus. Software routines were developed by Mamora, 1993 to facilitate data logging and analysis on the microcomputer.

A mix of approximately 6400 g sand,350 g fire clay, 450 g oil and 300 g water containing a known concentration of metallic additive is packed into a 90 cm long tube. The tube is then preheated to about 60°C to simulate reservoir temperatures by using external heaters, nitrogen is injected and the igniter is turned on. When the temperature of the igniter reaches about 315°C, air injection at 3 SLPM is started and nitrogen shut off. The pressure in the system is maintained at 100 psig. The start of combustion is indicated by the gas composition at the outlet. The igniter is shut off when the combustion becomes stable and the front begins to propagate downwards as indicated by the temperature profiles. At the end of the run, the combustion is quenched by returning to nitrogen injection and the air supply is shut off. This is typically done at 90 cm from the top to avoid damage to the bottom flange.

2.1.4 MOTIVATION

A series of six combustion tube runs were conducted to study the effects of iron nitrate on the combustion of Saudi tar. The motivation for this study stems from the fact that most Saudi reservoirs have a zone of low gravity tar which isolates the reservoir from pressure support of the underlying aquifer. It is an attempt to mobilize this tar zone that combustion studies were done.

2.1.5 RESULTS AND DISCUSSION

Combustion studies were conducted on different packings with varying concentrations of metallic additive, iron nitrate which was added in concentrations of 0, 5, 10, 20 mass % in the water saturation of the simulated cores. The first run was a control run without any additive. A sustained combustion could not be achieved despite efforts to start up secondary heaters. It was then decided that we would go with small concentrations of the additive, only 1%; but this run also failed. Our next attempt was to increase the oil saturation; however, this also failed to give a sustained combustion although this run lasted a little longer than the former runs. This was probably because it took longer for the system to achieve a steady state behavior due to the increased oil saturation. The results of the study show that a self propagating combustion front is barely attained with a 5% concentration, this was evident from the gas analysis data which showed considerable fluctuation at this concentration. In the case of 10% and 20% iron nitrate, a self sustained combustion was achieved and the concentration of effluent gases was fairly uniform over the entire period of the runs.

Iron nitrate is seen to have a profound effect on combustion performance of Saudi tar. Small quantities of the additive also affect the reaction performance. This process could have significant practical applications if an injected slug of additive could help sustain combustion.This is an idea that needs experimentation. Our future research would focus on experimenting with additive slugs and observing the adsorption of iron nitrate on the core matrix.

PROJECT 3: STEAM WITH ADDITIVES

To develop and understand the mechanisms of the process using commercially available surfactants for reduction of gravity override and channeling of steam.

3.1 STUDY OF STEAM INJECTION IN FRACTURED SYSTEMS
(M. Deniz Sumnu-Dindoruk)

3.1.1 INTRODUCTION

This report is a summary of the progress in the research project, "Study of Steam Injection in Fractures Systems" in 1994. The objective of this study is to develop a matrix-fracture transfer function for nonisothermal processes like steam injection. During this period continuous steam injection experiments were performed on the fractured model. In addition to the temperature, pressure and heat flux measurements, two-phase steam-water saturationswere measured by using a Cat scanner. The analysis of the experimental results by numerical simulations andone-dimensional heat loss calculations were started.

The first part of the report consists of some experimental results, the second part summarizes the numerical simulations and one-dimensional heat loss calculations. Finally, the report concludes with a summary of results seen so far and planned future work.

3.1.2 EXPERIMENTAL ACCOMPLISHMENTS

The detailed description of the experimental setup and thecore holder used in this study is given in detail in last year's annual report, Brigham and Castanier (1994). The preliminary experiments performed on this model were used to test the setup and the core holder and aided in the determination of the steam injection rates that allowed the development of a steam zone within a reasonable injection time.

Later, for the next sets of experiments, the experimental setup was moved to the CT scanning room and the core holder was assembled on the scanner table with the help of a mounting system. The electrical connections and the plumbing of the model were completed and tested. Considering all the metallic objects around the core holder, like thermocouple and tubing, two appropriate scanning locations were selected. With the aid of the CT positioning table the locations of the two scanning slices were determined accurately to assure consistency of all the scans. Figure 3.1.1 shows the locations of the two scan slices. Slice 1 is the slice at the front closer to the injector and Slice 2 is at the back close to the producer. The thermocouples and the pressure taps are located at the middle plane allowing us to scan at both sides of the thermocouples.

After determining the two scan locations, the model was scanned while dry. Different settings were used on the scanner to determine the settings for the best possible image. Two different energy levels, 100kV and 140kV were used. Figures 3.1.2 and 3.1.3 show the CT number maps for Slices 1 and 2 at the two different energy levels. The darker colored regions in CT maps show denser areas (higher CT number). The fracture is characterized by negative CT numbers, close to the CT number for air.

After the dry scans, the model was evacuated followed by carbon dioxide injection. The evacuation and carbon dioxide injection cycles were repeated several times. Then deionized water was allowed to saturate the model by gravity, and under vacuum. Following the water saturation process, the model was scanned again at the same two energy levels. Figures 3.1.4 and 3.1.5 show the CT number maps for the water saturated core at two different energy levels. In these scans, since the fractures are filled with water, the CT numbers are different than the CT number for air, but are close to the CT number for deionized water. Water saturated core has higher CT numbers than the dry core. There were significant cross shaped artifacts in the 100 kV scans when the core was saturated

with water. As a result, we have decided to use 140 kV for the steam injection runs, with the hope of reducing the artifacts.

3.1.2.1 Porosity Calculations from CT Measurements

The porosity of the core was determined pixel by pixel by using the CT numbers. The porosity is given by,

$$\phi = \frac{CT_{wc} - CT_{dc}}{CT_w - CT_a} \tag{3.1.1}$$

where,

CT_{wc} = number for the core saturated with water

CT_{dc} = number for dry core

CT_w = number for pure deionized water

CT_a = number for air

CT processing software, CATSOFT, was used in these calculations (Brigham and Castanier, 1994).

Figure 3.1.6 shows the resulting porosity maps for the two core slices. The average porosity of the core was calculated to be 0.294 for Slice 1 and 0.291 for Slice 2. These porosity values agreed quite well with the previously measured porosity value of 0.307 by the saturation method.

3.1.2.2 Steam Injection Experiments

Different rates, back pressures and injection temperatures were used in the experiments. The procedure followed in these runs are as follows.

First, before each run the chromatography pump is calibrated and set at the desired injection rate. Then the temperature controller for the steam generator is set to the desired temperature and the water is pumped through the steam generator. The steam is diverted through a bypass line to a vent until it is at the desired injection temperature. In the meantime, the pressure transducers are calibrated. Once steam is observed in the bypass line outlet, back pressure is applied to the core outlet and the injection valve is opened to the model. Slightly superheated steam is injected to the system. This is done so that the enthalpy of the injected steam is known accurately. The injector is completed at the bottom, and the producer is completed at the top of the model. They are located at the two diagonal corners of the model.

Temperatures, pressures and heat losses from heat flux sensors are recorded by the data logger. CT scans of the model are taken every 15 minutes during the experiment. Once the steam injection run is finished cold water is continuously injected until the entire system is cooled down.

The effect of steam injection temperature is found to be insignificant on the temperature distribution and the steam zone development throughout the model. Figure 3.1.7 shows the temperature distributions at $t = 65$ minutes of steam injection. The two temperature maps are almost identical. The same behavior is also observed at a later time of $t = 180$ minutes (Fig. 3.1.8). This is to be expected since injection temperatures did not change much between the two runs. More runs are being planned to investigate the effect of steam injection temperature by using a wide range of injection temperatures.

The back pressure on the model affected the results significantly. At the earlier stages of the steamflood, the temperature inside the model increased faster for the low back pressure case. On the other hand, at the later stages, temperature observed in the high back pressure run was higher than the low back pressure run. The physical mechanisms behind this difference in behavior is being investigated now with the help of numerical simulations.

One important observation that is obtained from all of the steam injection runs performed at different pressures and rates is that steam saturation developed only in the fractures. The experiments show that steam flows only in the fractures, and the matrix is heated only only conduction. Figures 3.1.9, 3.1.10 and 3.1.11 show the temperature and steam saturation maps observed from the experiments at different times. The left-hand sides of the maps are closer to the injection corner and the right hand sides are closer to the production corner. In situ steam saturations are calculated from the CT numbers by using the CT image processing software, CATSOFT (Brigham and Castanier, 1994).

As can be observed from the temperature maps, temperature in the matrix increases with time even though there is no steam in the matrix. The nonzero steam saturations in the matrix shown in the maps are due to the artifacts and noise that are inherent in CT images. This behavior is also evident from the steam saturations calculated from the CT numbers at the beginning of the steam injection run (before any steam is injected into the system). Apparent nonzero steam saturations are calculated in portions of the system even at zero time (Fig. 3.1.12).

True steam saturations can be found by subtracting the image at zero time from the images at later times. The subtraction aids in the removal of most of the artifacts and the unrealistic steam saturations in the matrix (Figs. 3.1.13 and 3.1.14). However, nonzero steam saturations in the matrix are not eliminated completely. This is because of the noise present due to the nature of the CT-scanner measurements and the geometry of the core holder. The artifacts are not fully repeatable. An averaging method is used next to smooth the data and to get better steam saturation maps. First, the values that are greater than a threshold value are set equal to the threshold. Then, the domain is divided into specified number of submatrices. The pixel values are averaged inside each submatrix and the mean is assigned to the center of the submatrix. The effect of two-dimensional averaging of the data is evident from Figs. 3.1.15 and 3.1.16. The differences in steam saturation in matrix and fracture are more easily distinguished from the averaged data. More elaborate image processing methods should be used to eliminate and filter the noise, and also the artifacts due to the geometry of the model.

3.1.3 NUMERICAL SIMULATIONS

Computer Modeling Group's STARS (CMG, 1993) thermal simulator is used to analyze and history match the experimental results. The grid system used in the simulations is rectangular with fine grids to model the fracture and the areas close to the

fracture. The grids become coarser in size as we move away from fracture. Our aim is to be able to match the temperatures, steam saturations and the heat loss histories of the experiments.

Generally, when using numerical simulators, it is difficult to match and analyze the heat losses from the experimental models since heat loss models used in the simulations are designed for field scale steam injection processes. STARS has two different heat loss models.

1. Semi-analytical infinite overburden model.
2. Convective heat loss model.

The semi-analytical infinite overburden model (Vinsome and Westerveld, 1980) describes heat loss by conduction to overburden and underburden by using a fitting function for the resulting temperature profile. Since the overburden and underburden are considered to be infinite, the model is not realistic for a laboratory model with a finite layer of insulation around it.

In the convective heat loss model the heat loss from the system to the surroundings is given by,

$$q = h_{conv} * (T - T_{amb}) \qquad (3.1.2)$$

where,

q = rate of heat loss (convective) from the model

h_{conv} = overall convective heat transfer coefficient

T = temperature inside the model

T_{amb} = ambient temperature (air)

Both heat loss models were used in the simulations, and the results are compared with the experimental data recorded by heat flux sensors. Six heat flux sensors are used in the experiments. HF 1 is located at the top of the model closer to the injector, HF 2 is also located at the top and is closer to the producer. HF 3 and HF 4 are located at the bottom with similar locations. Finally, HF 5 and HF 6 are located at the injector and producer sides of the model.

Figure 3.1.17 shows the heat loss rates from the experiment and from the simulation using different heat loss models. The infinite overburden heat loss model predicts a declining heat loss curve. This is contrary to both the convective heat loss model and the experimental heat loss data. This result is expected due to the nature of the model. On the other hand the convective heat loss model first shows an increase in rate and then reaches the steady state like the experimental heat loss curves. This confirms the conclusion that when simulating heat losses from experimental models it is not realistic to use the infinite overburden heat loss model.

The transient portion of the convective heat loss curve however, is still considerably different from the experimental curve. This shows us that even the convective heat loss model of the simulator is not sufficient, by itself, to model the experimental heat losses.

Therefore, we decided to modify the grid system used in the simulations by incorporating the core holder into the grid system, with the hope that this would describe the heat loss process more realistically. Additional grid blocks with zero porosity and permeability were used to model the core holder, and the convective heat loss model was used outside these additional grid blocks.

Figure 3.1.18 shows the comparison between the experimental heat loss from the bottom of the model and the convective heat loss calculated from the simulation run with the modified grid system. The heat loss curve from the simulation run looks similar to the experimental heat loss curve. To produce this curve, no parameters were adjusted to help improve the fit. A sensitivity study on the overall heat transfer coefficient used in the simulations may help in more closely matching of the heat losses from the experiment. However, even these results are quite good compared to the earlier results of Fig. 3.1.17.

Up to now, described simulations were two-dimensional cross-sectional simulations. To see the effect of 3-D simulations on the results, the experiments were simulated with a 3-D grid system. Three-dimensional grids are taken in such a way that the x-z planes correspond to the temperature measurement and the scan locations in the physical model. The results from the 3-D simulation run showed temperatures and steam saturations that are closer to the experimental values than the results from 2-D runs. For history matching purposes 3-D simulations may show better matches with the experimental data.

One common observation from both the simulations and the experiments is that there is very little steam saturation development in the matrix due to the high conductivity fractures surrounding the system. In order to see if steam saturation could be developed in the matrix, simulation at different rates were run which covered a much longer time period than the actual experimental time. These runs showed that even when the injection time was increased considerably, there was still little steam saturation developed in the matrix.

We are now looking into the effect of lowering the back pressure on the model after the system is heated. Results from the preliminary simulations show that reducing the back pressure after a certain period of steam injection causes steam saturation to develop in the matrix. This in turn increases steam permeability in the matrix, allowing steam to enter it. This behavior is now being investigated in detail with simulation runs, to help plan future experiments.

3.1.4 ONE-DIMENSIONAL HEAT LOSS CALCULATIONS

To analyze the experimental heat losses, the one-dimensional transient conduction equation is solved analytically and also with the finite difference method. Solutions with different boundary conditions are analyzed. One heat flux sensor (Sensor 1) results will be used for comparison.

3.1.4.1 Analytical Solutions

(1) Case:1 1-layer, constant temperature inner and outer boundary conditions. The outer boundary condition is taken as air temperature and inner boundary condition as steam temperature.
(2) Case:2 1-layer, convective outer boundary condition and constant temperature inner boundary condition (steam temperature).

Figure 3.1.19 shows the comparison between the calculated and the experimental heat losses. The three curves reach steady state approximately at the same time. However, the calculated heat losses are all much higher than the measured heat losses. One reason is due to the assumption of a constant temperature inner boundary condition in the calculations. In reality this assumption is not correct. The temperature in fact changes with time. The heat losses calculated for Case 2 is lower than Case 1 since temperature changes are more gradual with a convective boundary condition. This is due to the extra resistance from the film layer in convective heat transfer.

(1) Case:3 2-layer composite solution with constant temperature outer and inner boundary conditions.
(2) Case:4 2-layer composite solution with convective inner and outer boundary conditions.

In the physical model, we have the polysulfone core holder as Layer 1 and on top of it, we have a layer of fiberfrax insulation. In Case 3, the one-dimensional transient conduction equation is solved for two layers to compare the heat losses. Figure 20 shows the heat losses from three different solutions. The two layer solution matches the early transient part of the experimental heat loss curve quite well, but at later times it is much higher than the experimental curve. It is closer to the 1-layer convective boundary solution (Case 2) at later times. Again the reason for getting higher heat losses from Case 3 compared to the experiment is the assumption of constant temperature at the inner boundary. When heat losses from Case 3 and Case 4 are compared, it is observed that the two layer solution with convective boundary conditions gives lower heat losses than the constant temperature boundary solution (Fig. 3.1.21).

All of the above solutions except Case 4 assume that temperature is constant at the inner boundary and is at the steam temperature. It is obvious from the thermocouple measurements that the temperature at the inner boundary changes with time. Figure 3.1.22 shows the temperature measurement for the thermocouple inside the fracture at the location closest to Sensor 1. It is clear from the measurements that the inner boundary condition should be variable with time to model the actual heat losses from the model.

The one-dimensional transient heat conduction equation was solved by Laplace transformation taking the inner boundary condition as variable. The temperature distribution at the boundary was modeled by fitting a polynomial to the temperature curve of Fig. 3.1.22 by using least squares curve fitting. We encountered some numerical problems while inverting the Laplace transform. This solution is being analyzed in detail to overcome the numerical problems and the same problem is now being solved analytically by separation of variables to compare the two solutions.

3.1.4.2 Numerical Calculations

Explicit finite difference solution has been used to solve the one-dimensional transient conduction equation with variable temperature inner boundary condition. Figure 3.1.23 shows three calculated heat loss curves compared with the measured heat loss. Only the polysulfone layer is considered for these solutions since the second layer of insulation is not in perfect contact with the core holder due to some physical restrictions. By changing the conductivity and diffusivity of the insulation, a good match is obtained with the measured heat loss. The conductivity and the diffusivity values that give the match are not the actual values for polysulfone ($k = 2.6e-3$ and $\alpha = 1.79e-3$). This may be due to using a one-dimensional solution to match the heat losses from a 3-D physical model.

These values may be considered as effective values. The finite difference solutions are now being repeated to model the heat losses from the remaining five heat flux sensors. Furthermore, the analyses will be extended to the remaining experimental runs to try to find a common effective conductivity and diffusivity for the model that can describe the heat losses for all the runs. Also analytical solutions are repeated now with convective outer boundary condition to see if a better match can be obtained by using the actual conductivity and diffusivity values for polysulfone.

3.1.5 CONCLUSIONS

1. Steam injection experiments were completed at different rates, injection temperatures and pressures.

2. The experiments showed that there was no steam saturation in the matrix, steam flowed only in the fractures and the matrix was heated by conduction.

3. Numerical simulations were used to analyze and history match the experimental results. Convective heat loss model in the simulations showed the best comparisons with the experimental heat losses.

4. Results from one-dimensional analytical solutions showed that 1-D analytical solution with a variable inner boundary condition should be used to model the heat losses from the experiment. The solution is being analyzed in detail to overcome the numerical problems in the inversion of the Laplace transform.

5. The one-dimensional finite difference solution with a variable boundary condition showed a good match to the experimental heat loss after adjusting the conductivity and diffusivity of the insulating layer (polysulfone core holder).

3.1.6 FUTURE WORK

One major conclusion that we obtained from the results of simulations and experiments, was that steam did not get into the matrix. The effect of lowering the back pressure on the model is now investigated by numerical simulations. Preliminary results showed that steam saturation developed in the matrix when the pressure is lowered. An experimental run is being planned to see the effect of lowering the back pressure. Furthermore, history matching of the steam injection experiments will be continued. Heat losses from the experiment will be continued to be analyzed by one-dimensional analytical and numerical solutions.

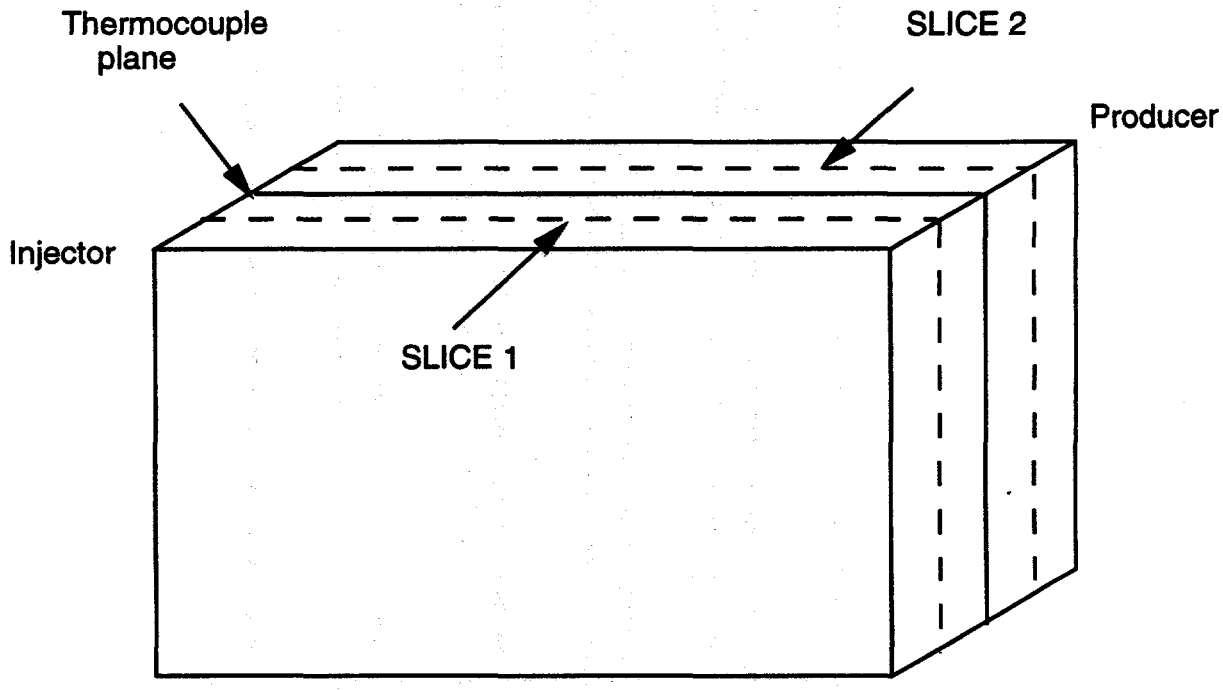

Figure 3.1.1 Scan locations.

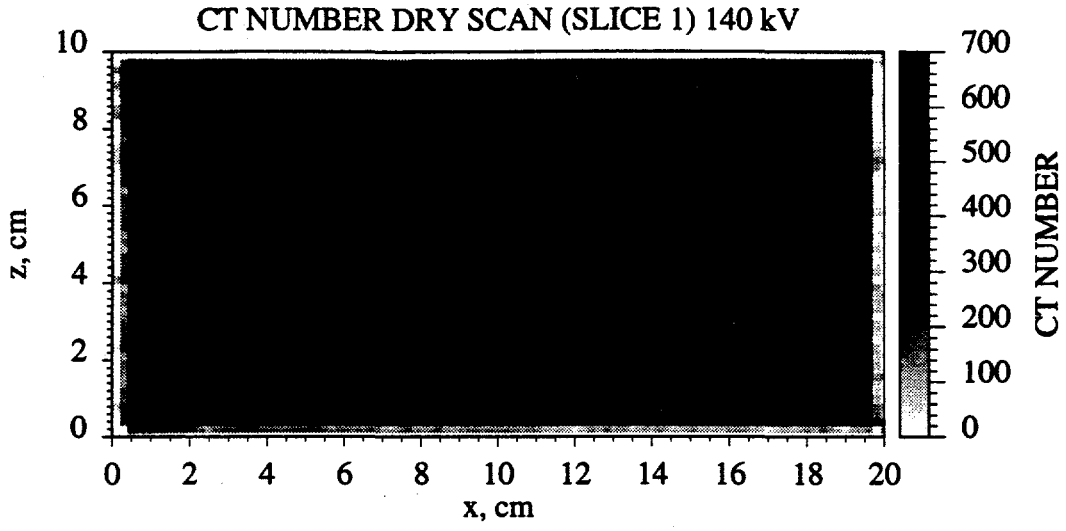

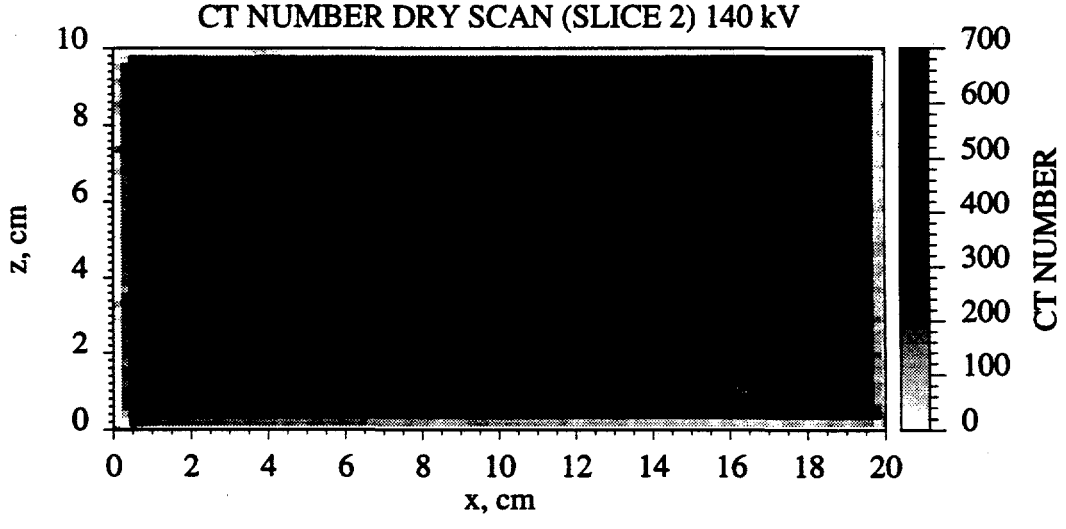

Figure 3.1.2 CT number maps for dry scans at 140 kV.

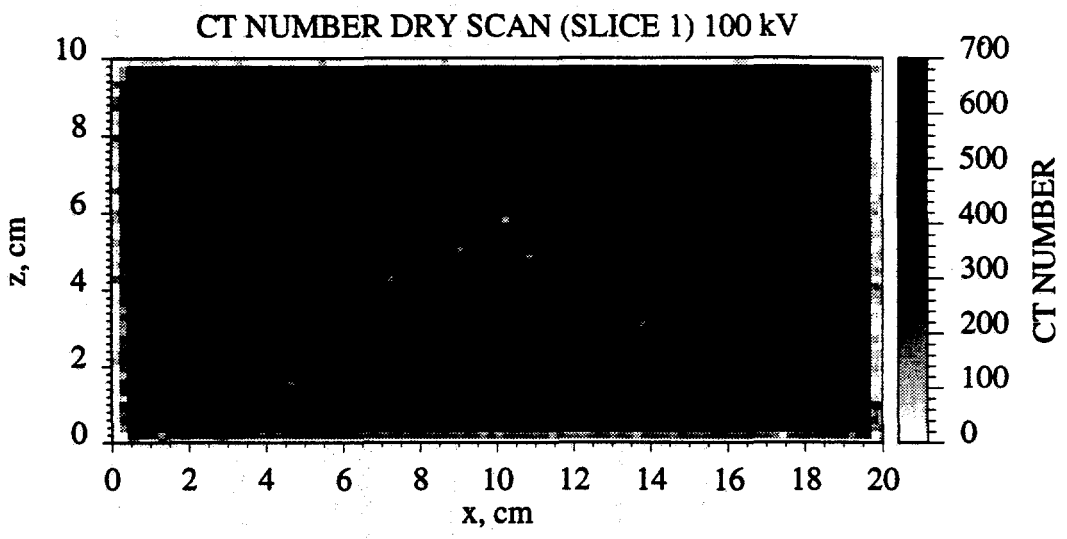

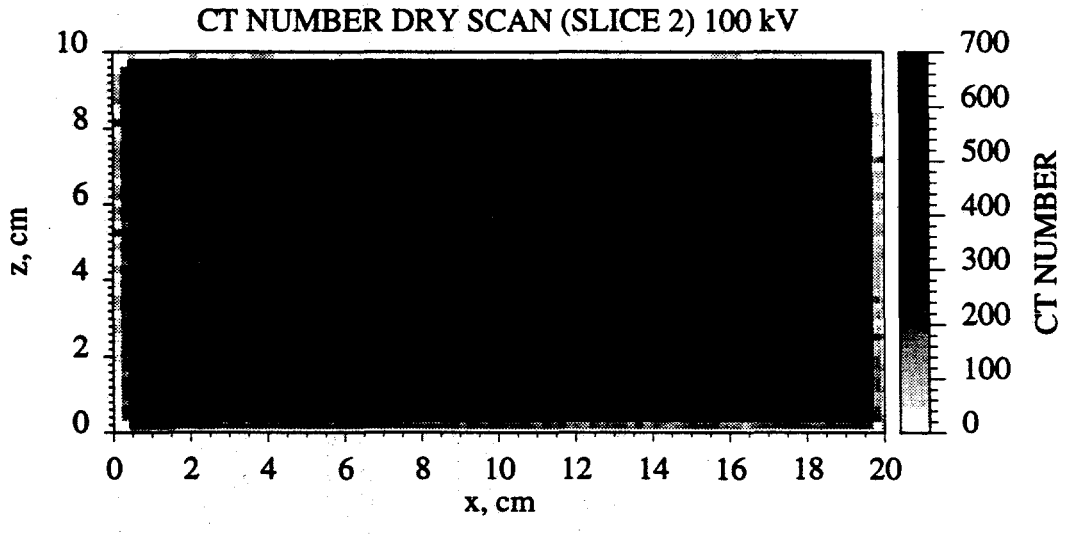

Figure 3.1.3 CT number maps for dry scans at 100 kV.

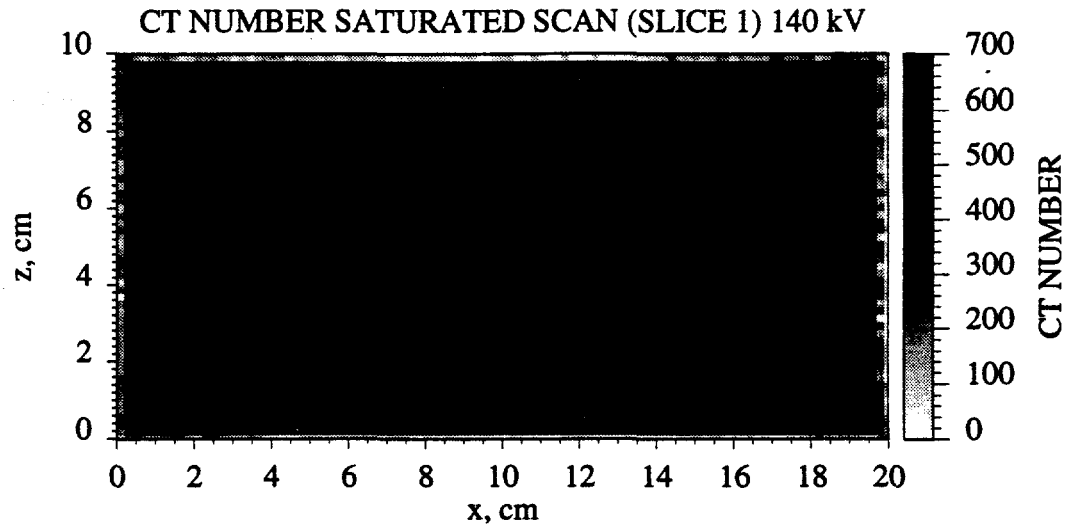

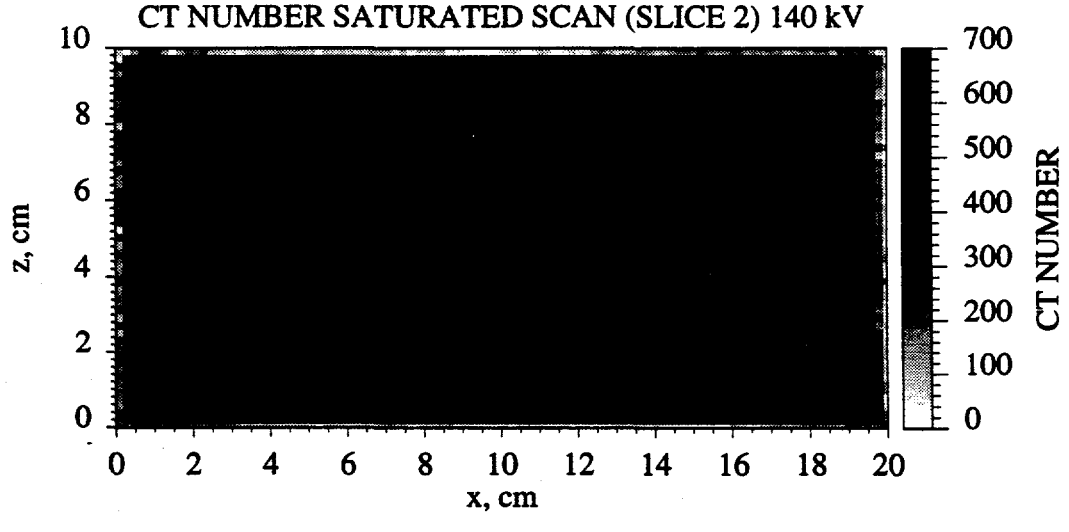

Figure 3.1.4 CT number maps for the model 100% saturated with water at 140 kV.

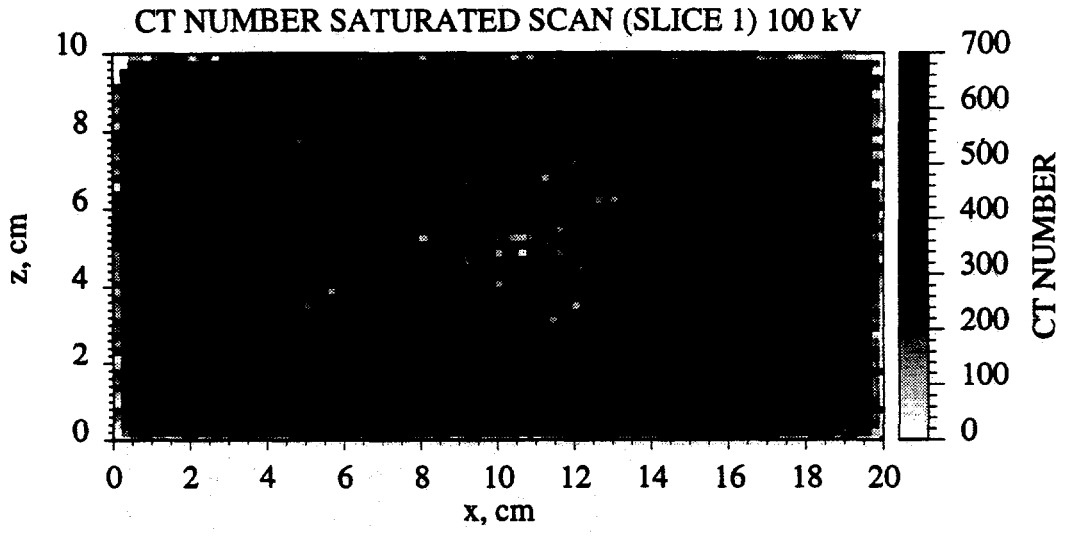

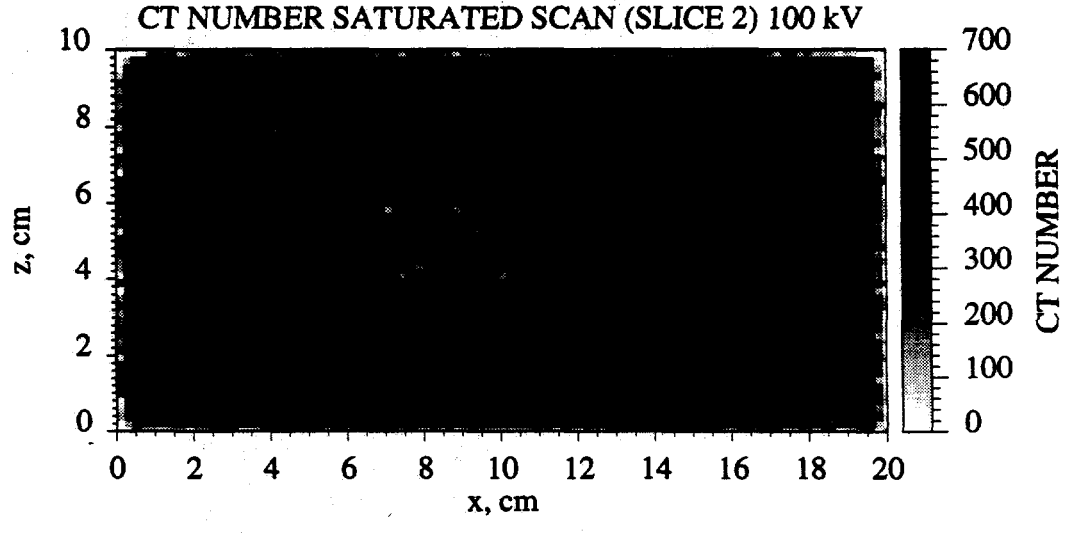

Figure 3.1.5 CT number maps for the model 100% saturated with water at 100 kV.

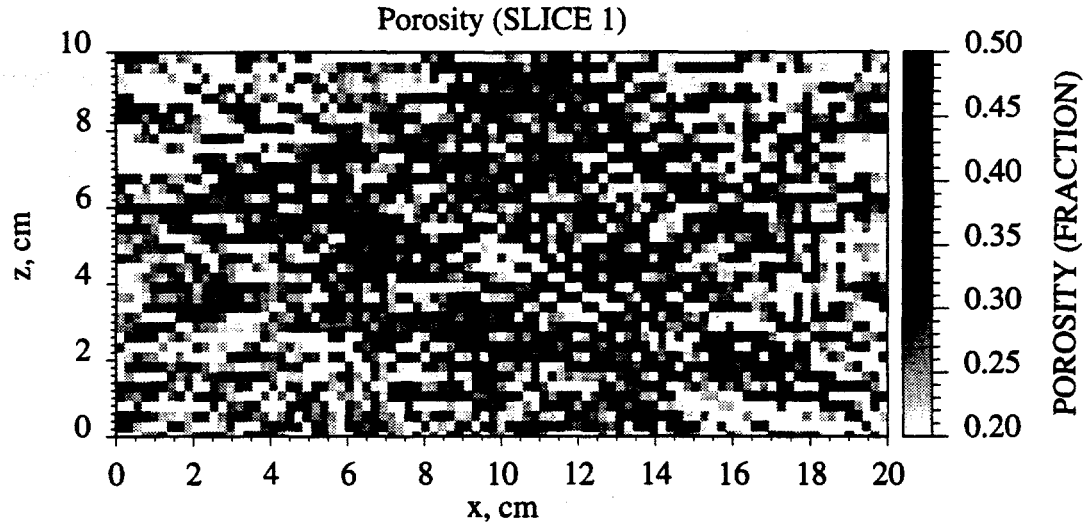

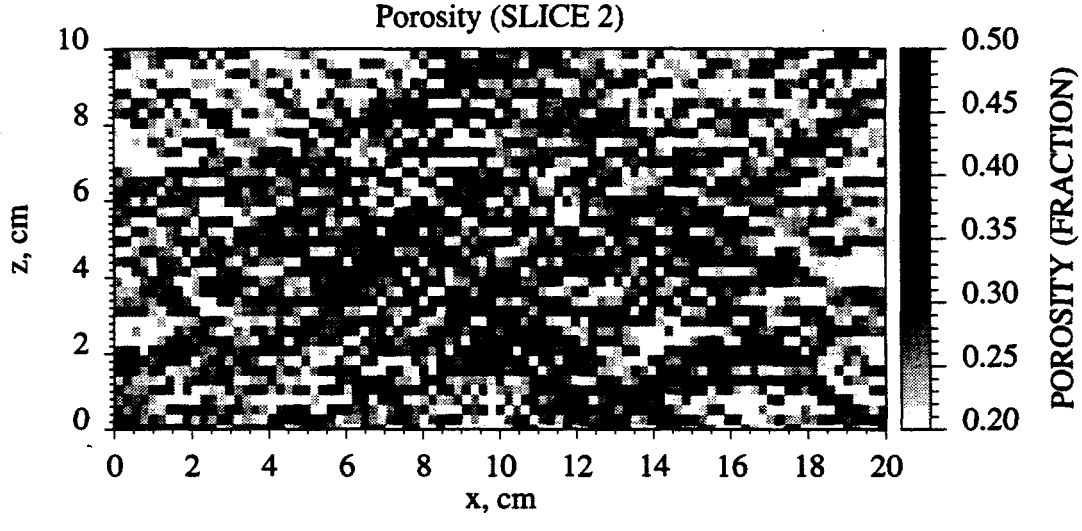

Figure 3.1.6 Porosity maps for two different core slices.

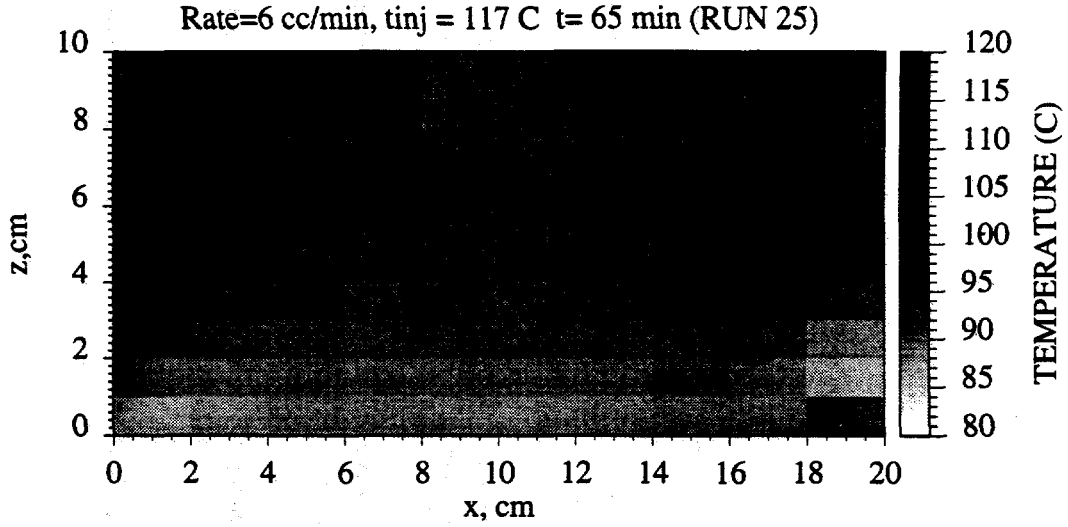

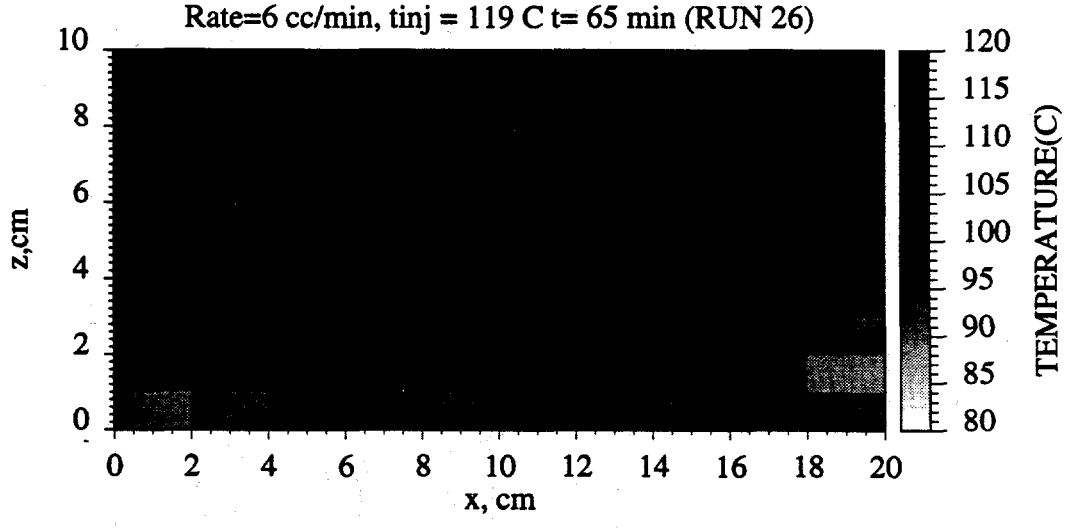

Figure 3.1.7 Temperature maps at t = 65 min.

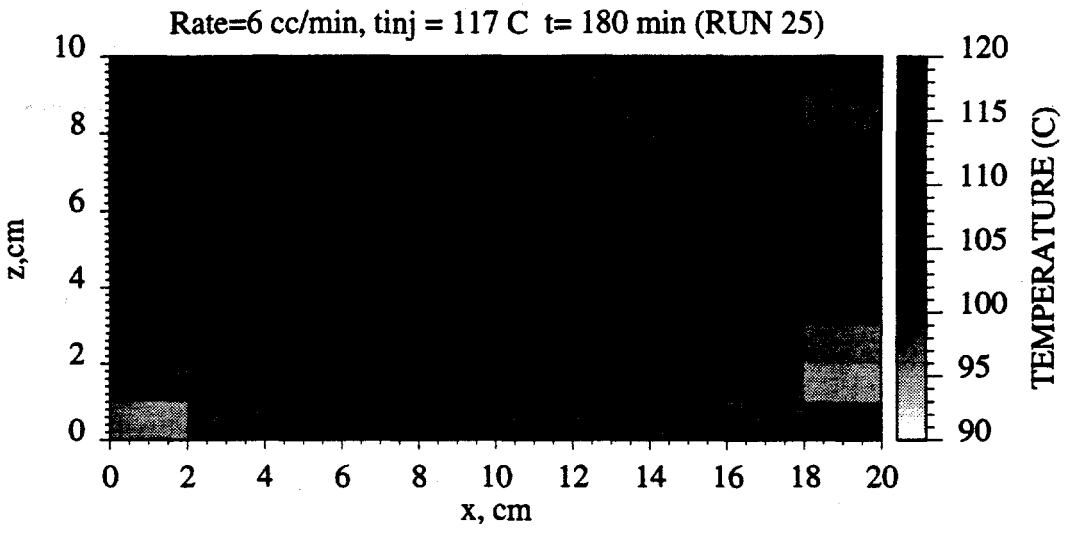

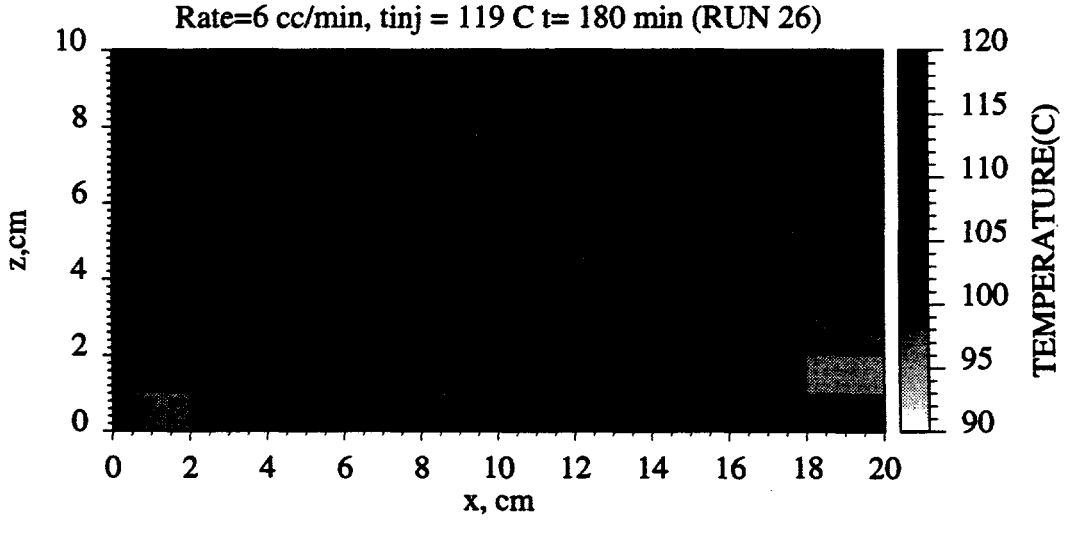

Figure 3.1.8 Temperature maps at t = 180min.

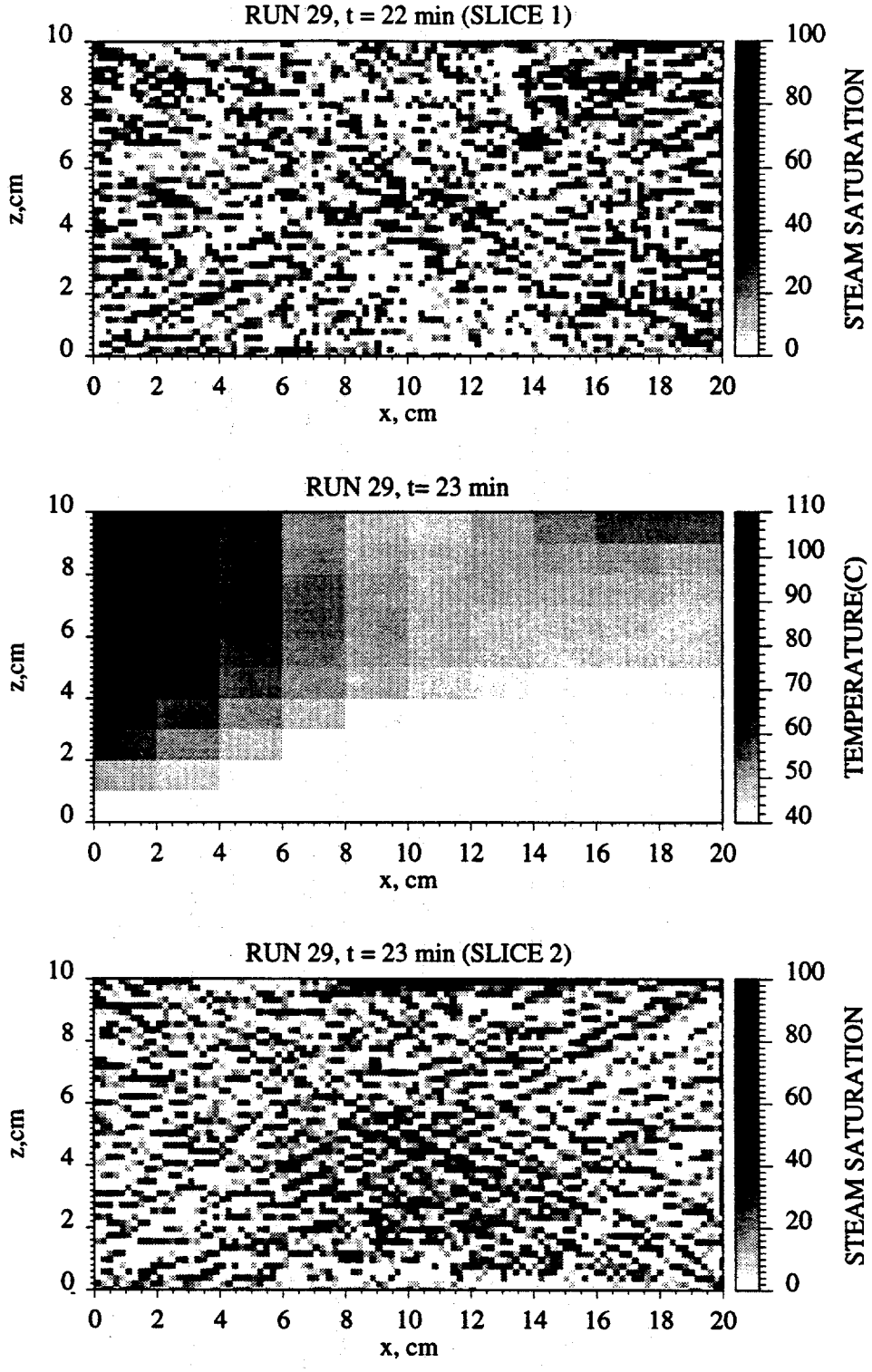

Figure 3.1.9 Steam saturation and temperature maps at t = 23 min.

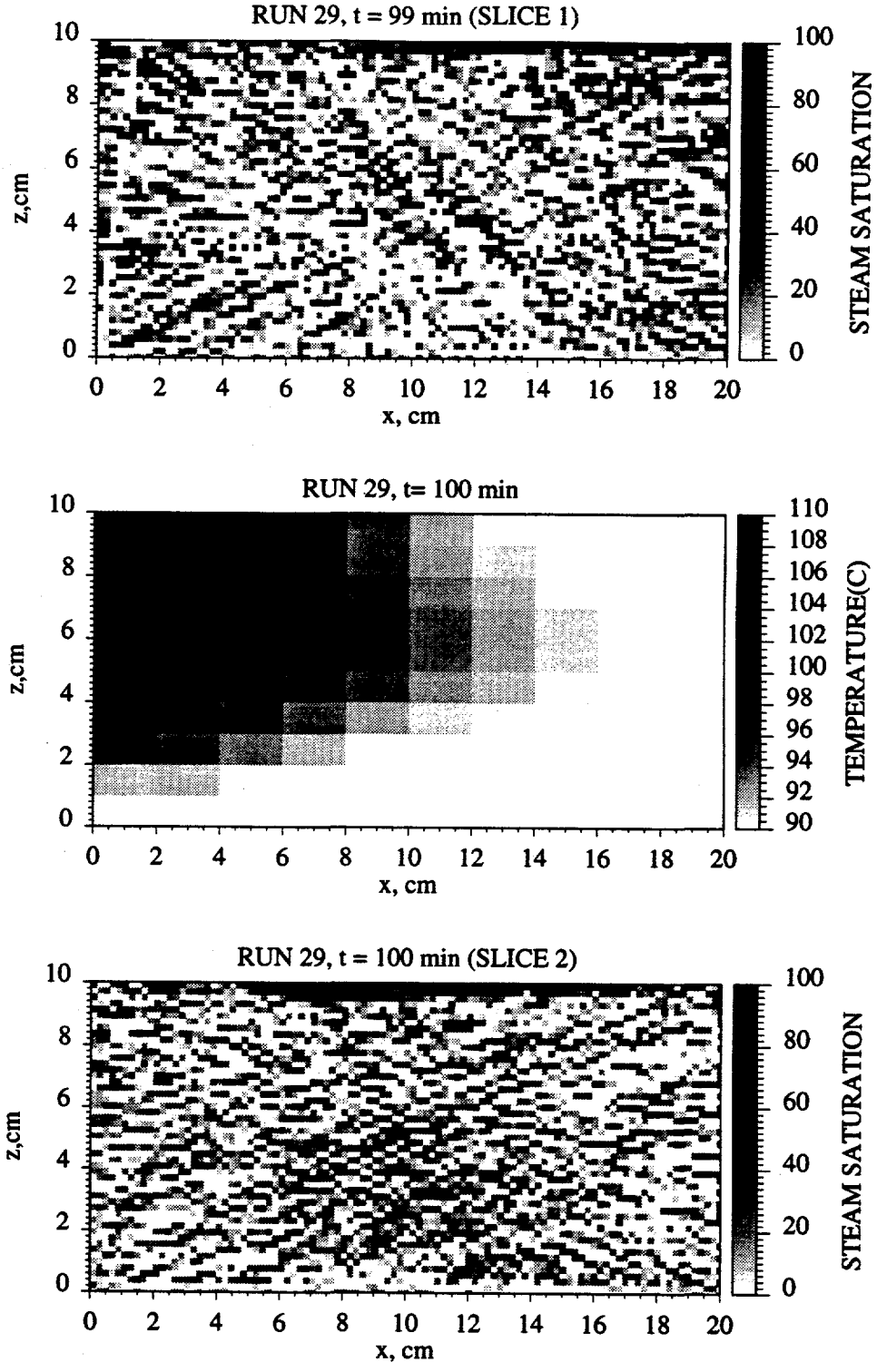

Figure 3.1.10 Steam saturation and temperature maps at t = 99 min.

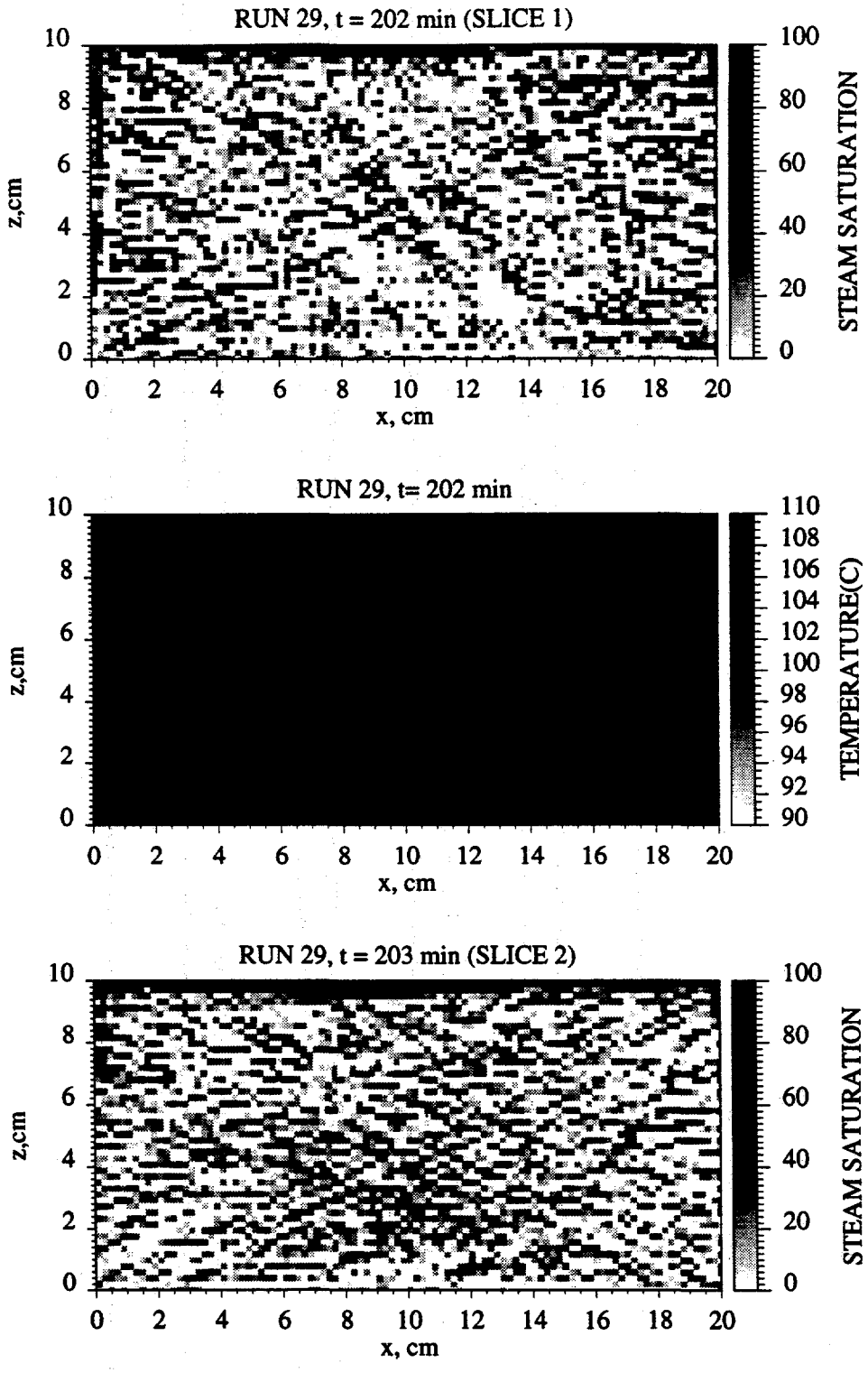

Figure 3.1.11 Steam saturation and temperature maps at t = 202 min.

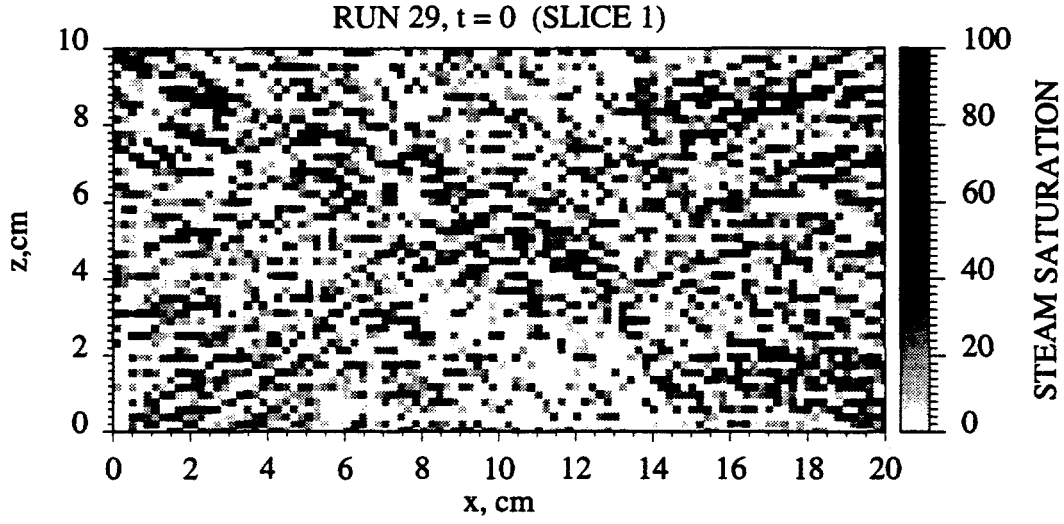

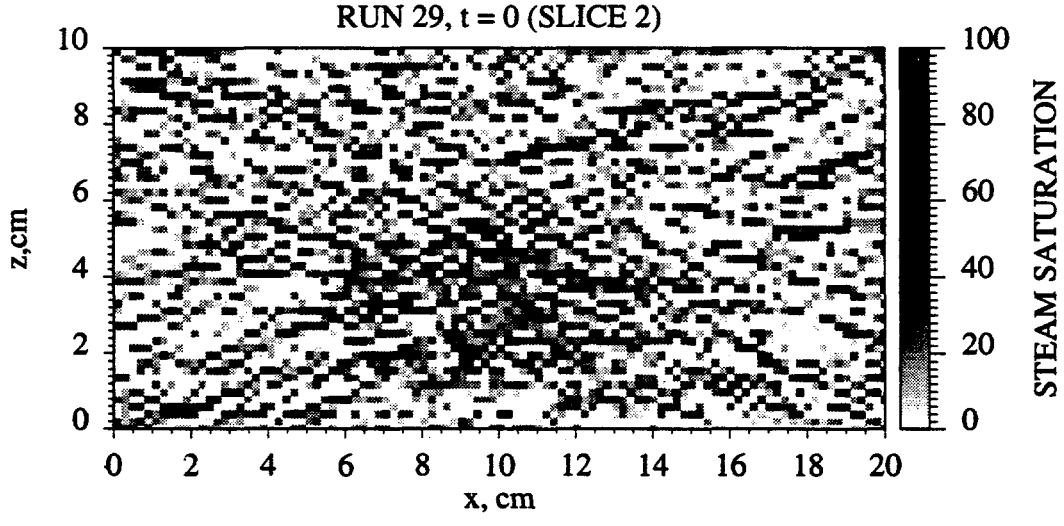

Figure 3.1.12 Steam saturation maps at t = 0.

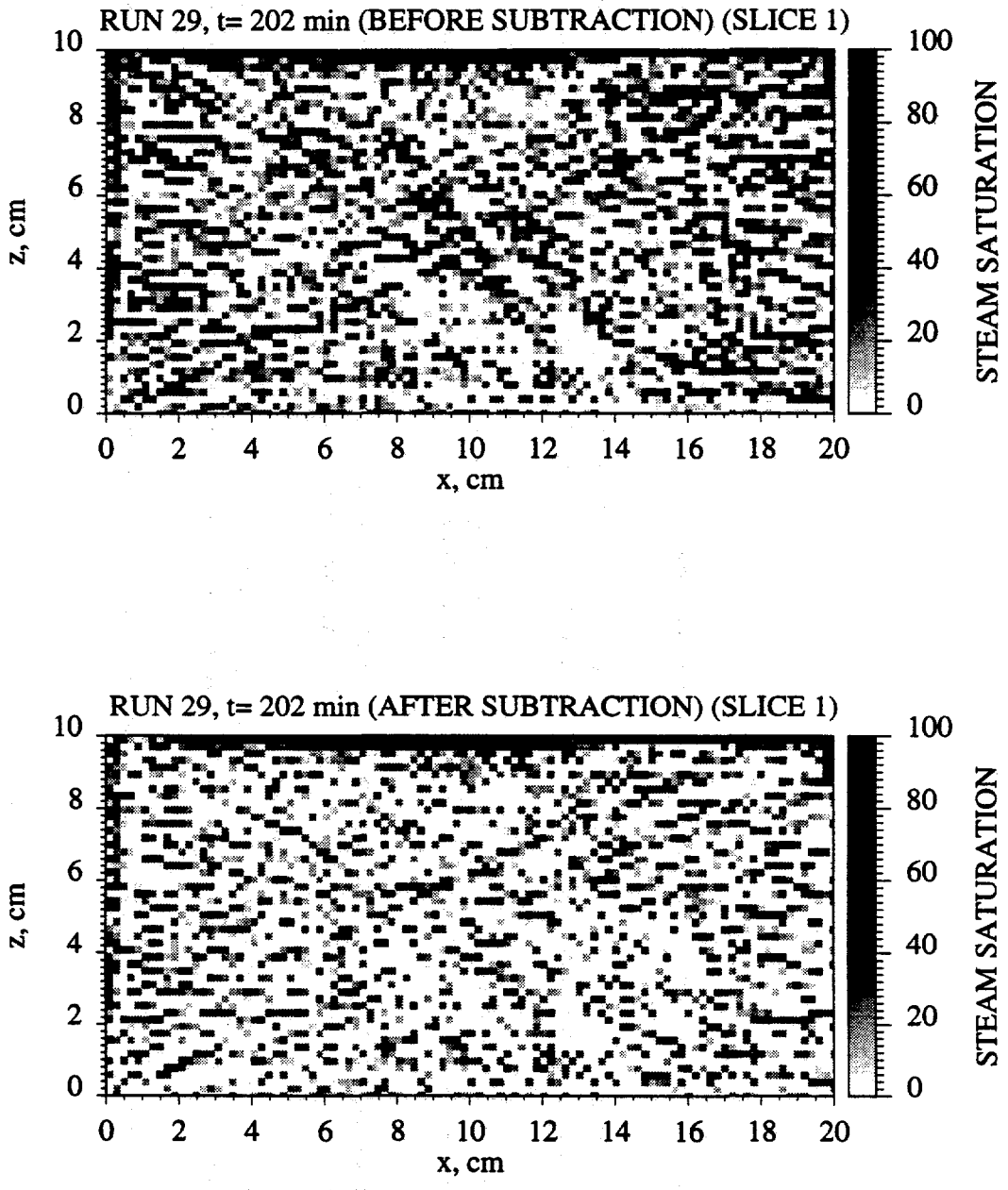

Figure 3.1.13 Steam saturations before and after subtraction (Slice 1).

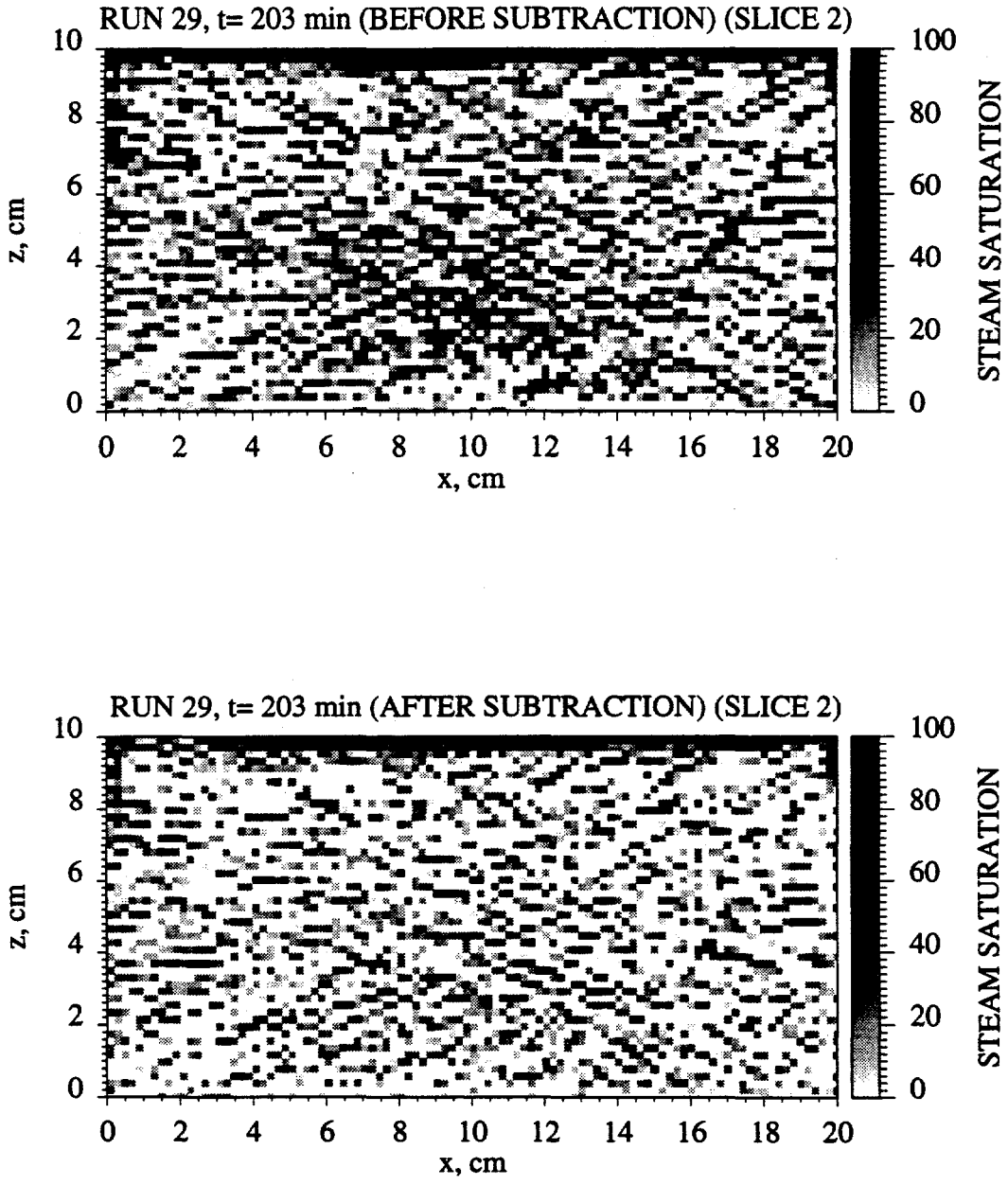

Figure 3.1.14 Steam saturations before and after subtraction (Slice 2).

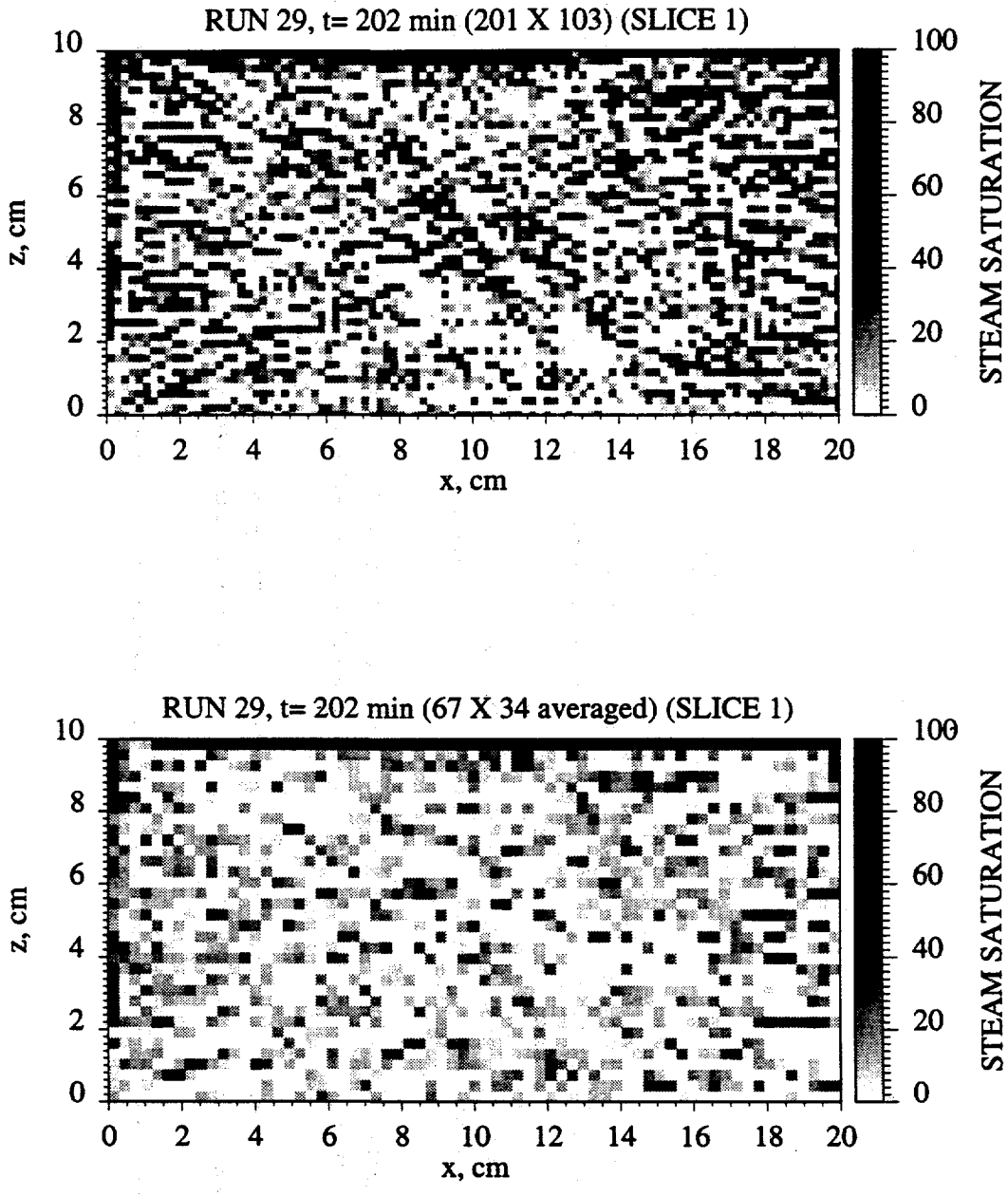

Figure 3.1.15 Averaged steam saturation maps (Slice 1).

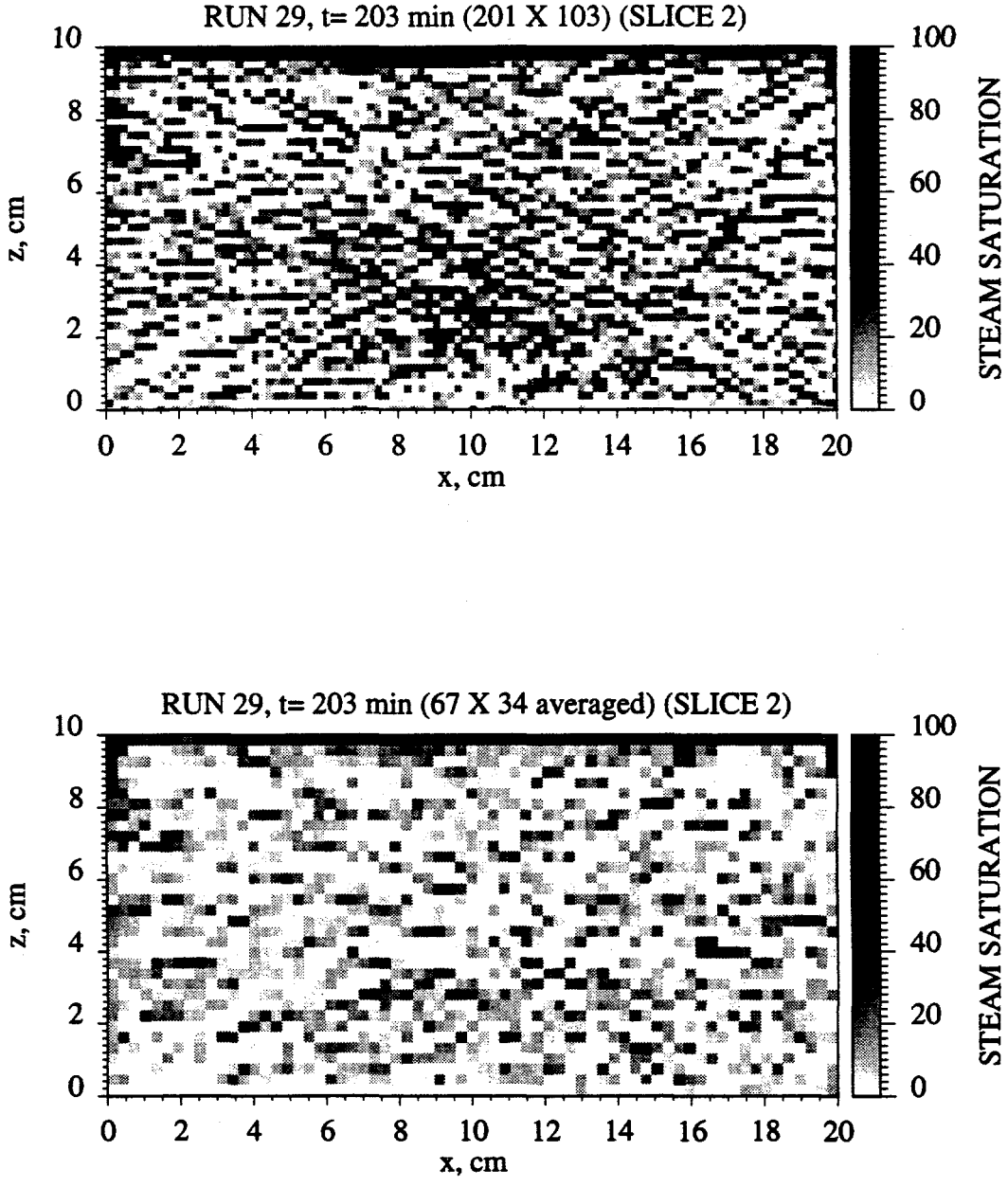

Figure 3.1.16 Averaged steam saturation maps (Slice 2).

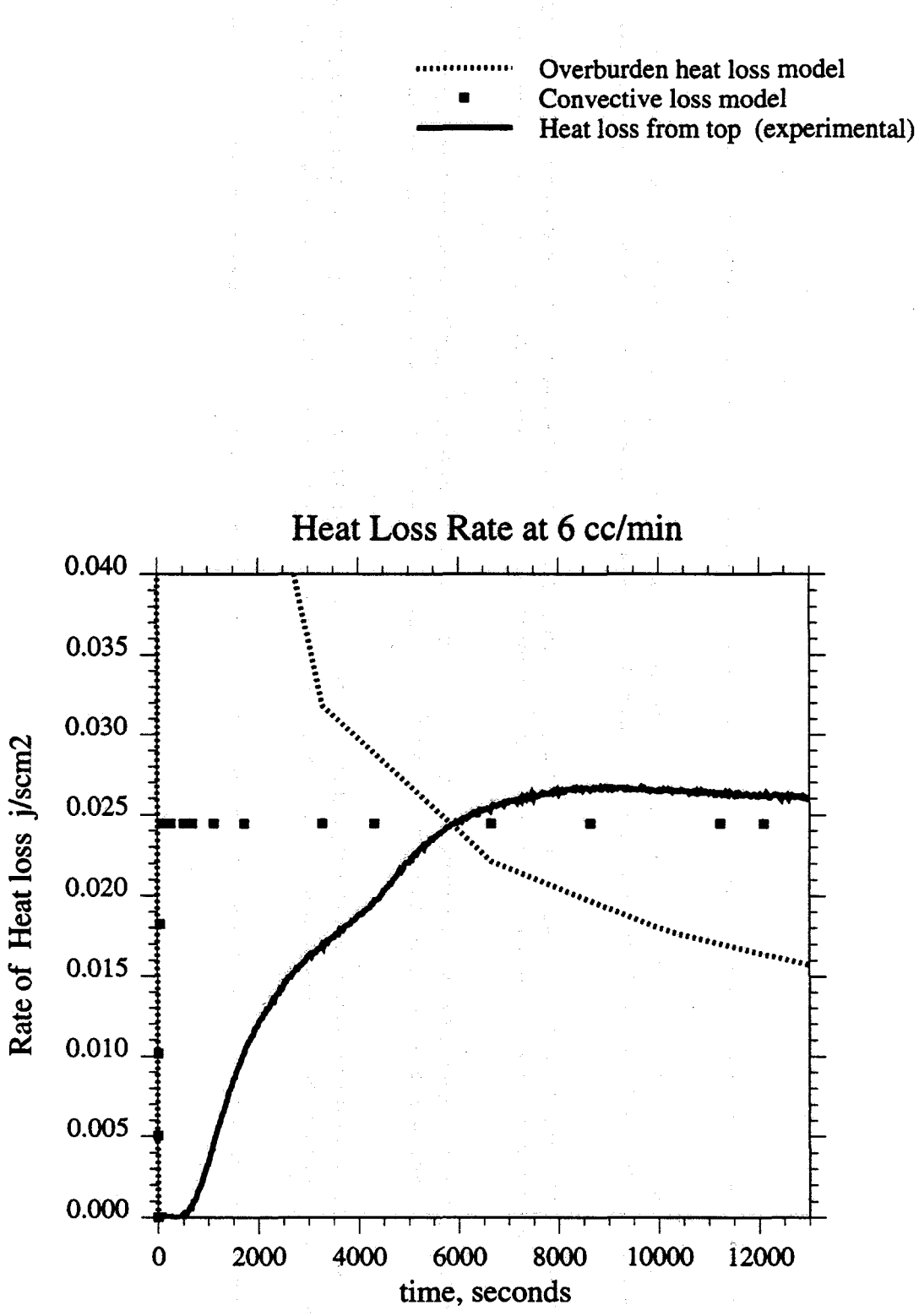

Figure 3.1.17 Comparison of heat losses from different models.

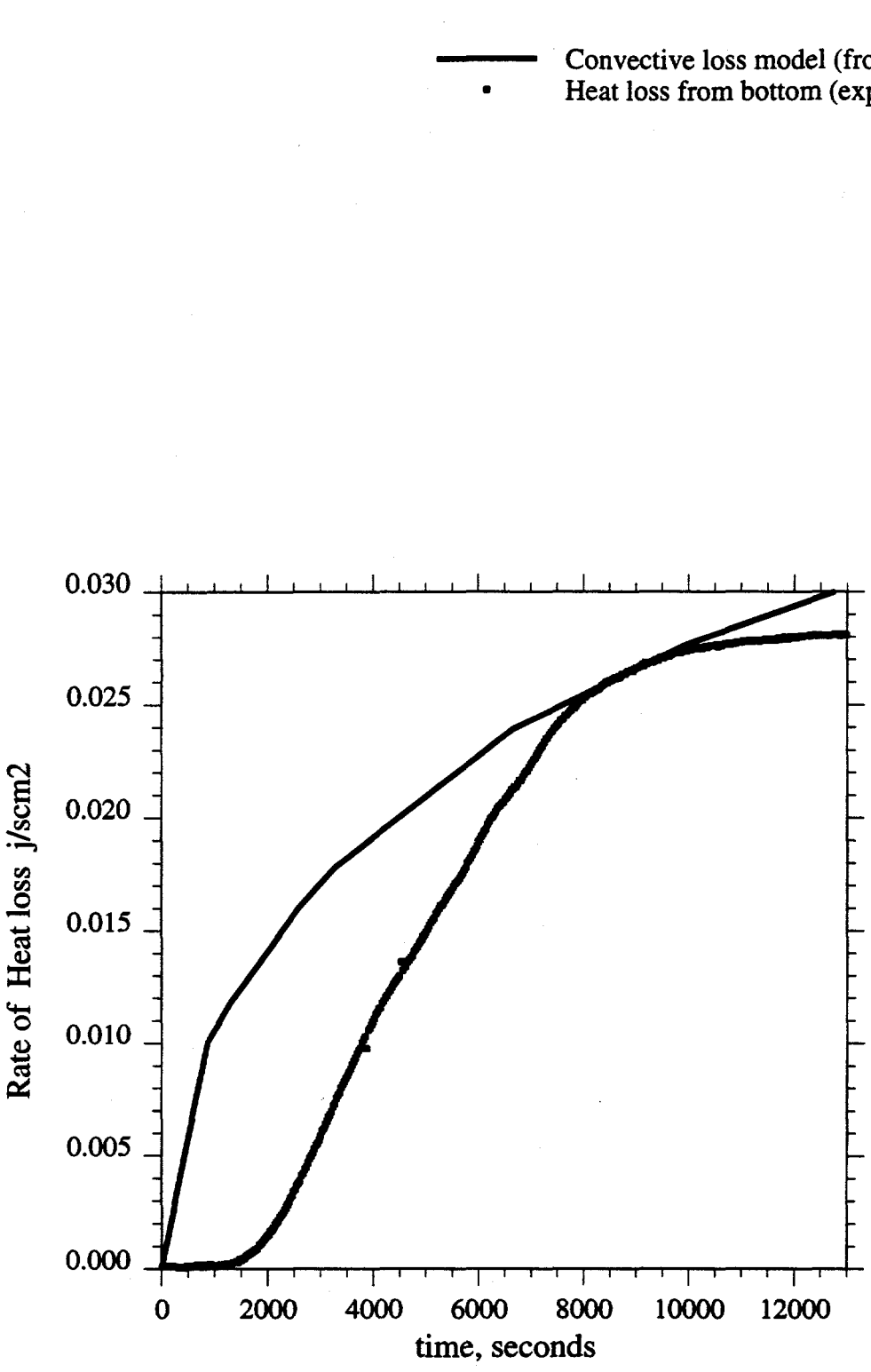

Figure 3.1.18 Heat loss from the bottom of the model.

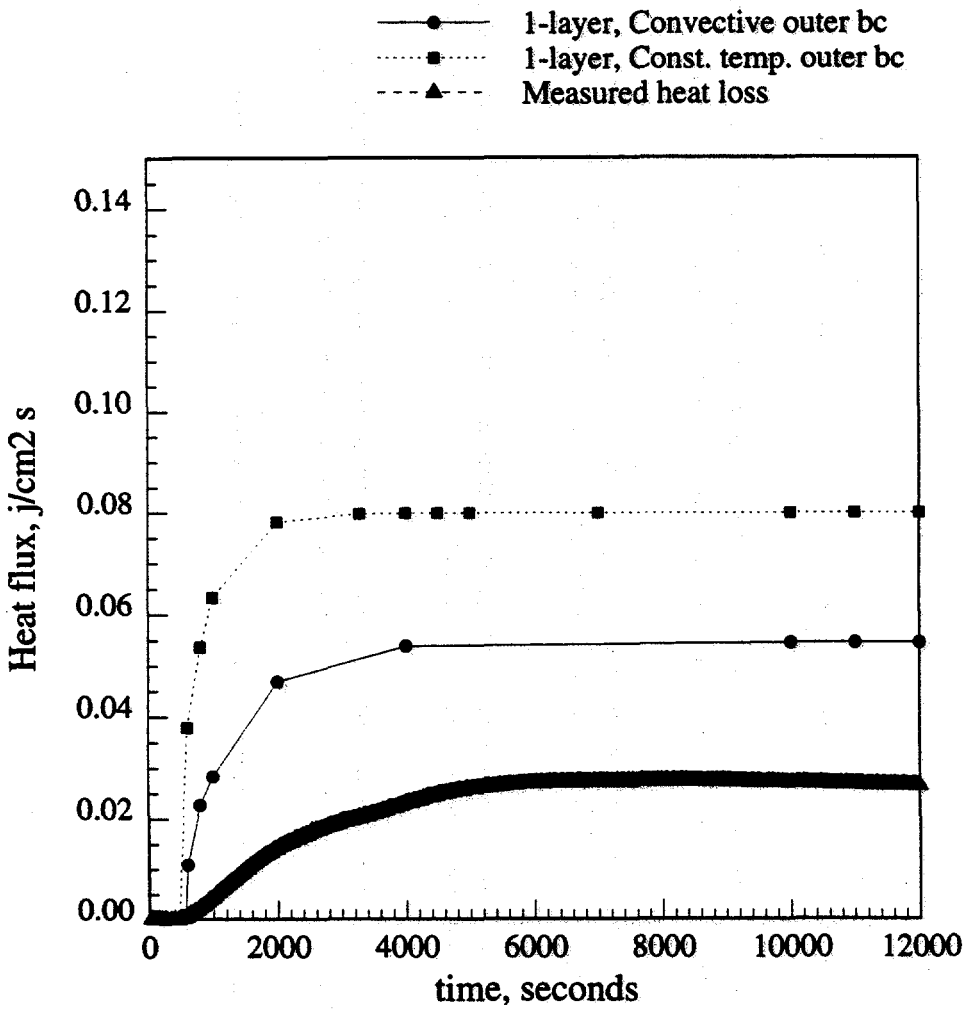

Figure 3.1.19 Heat losses from Case 1 and Case 2.

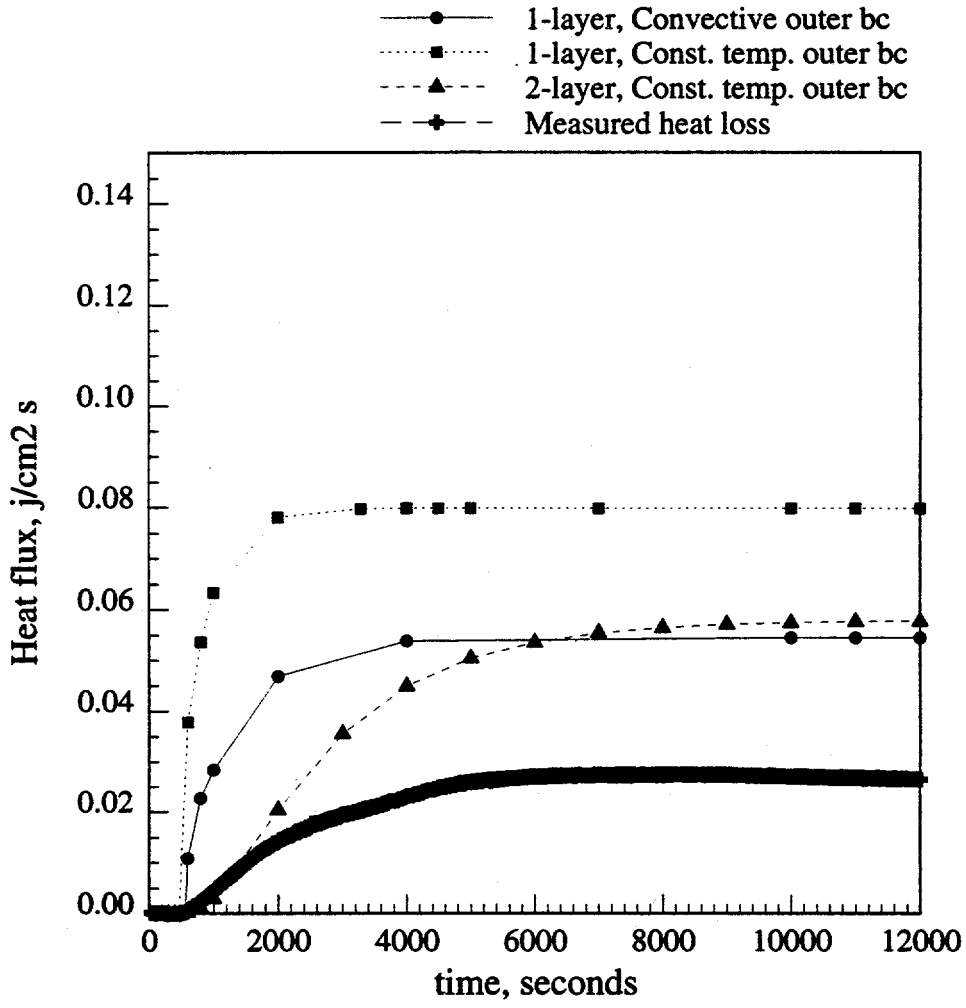

Figure 3.1.20 Heat losses from Case 1, Case 2 and Case 3.

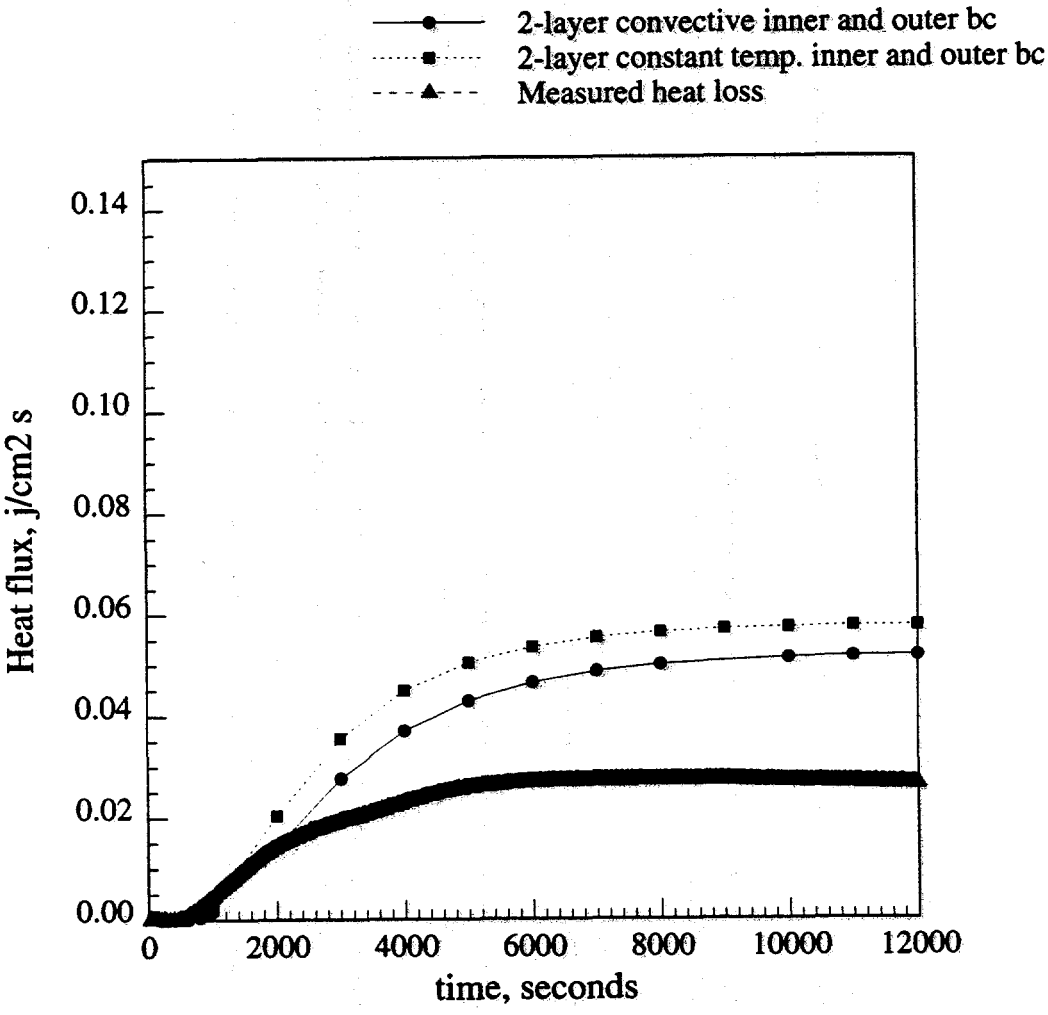

Figure 3.1.21 Heat losses from Case 3 and Case 4.

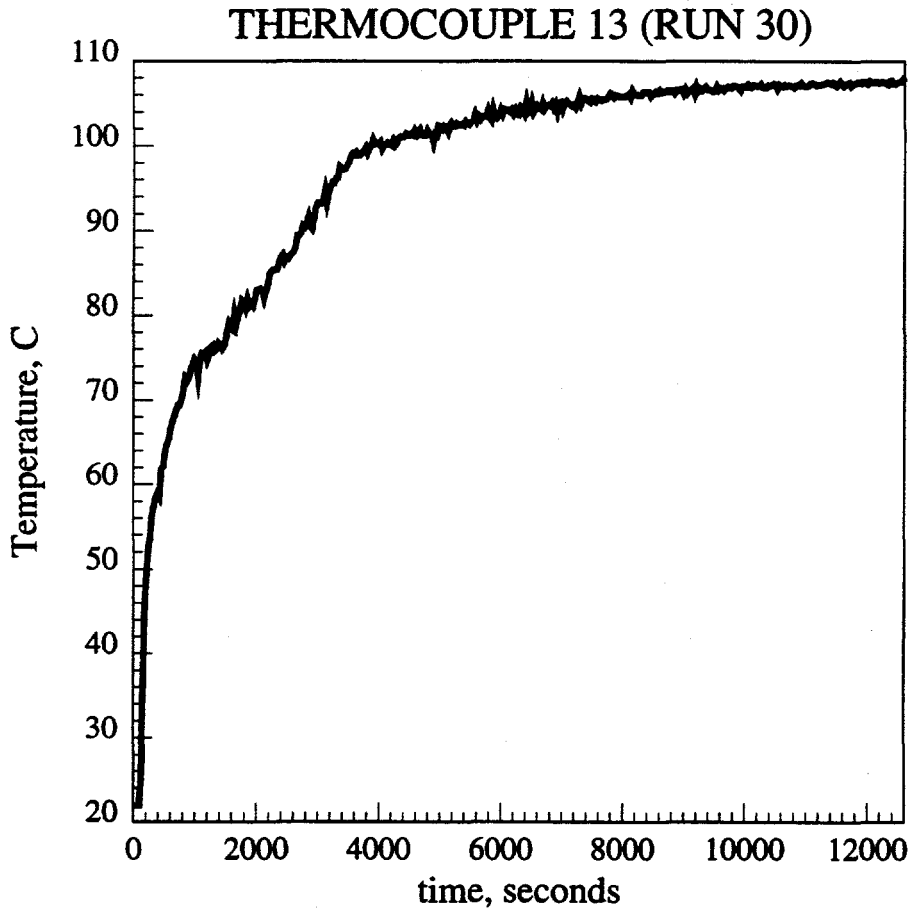

Figure 3.1.22 Temperature measurements from T/C 13.

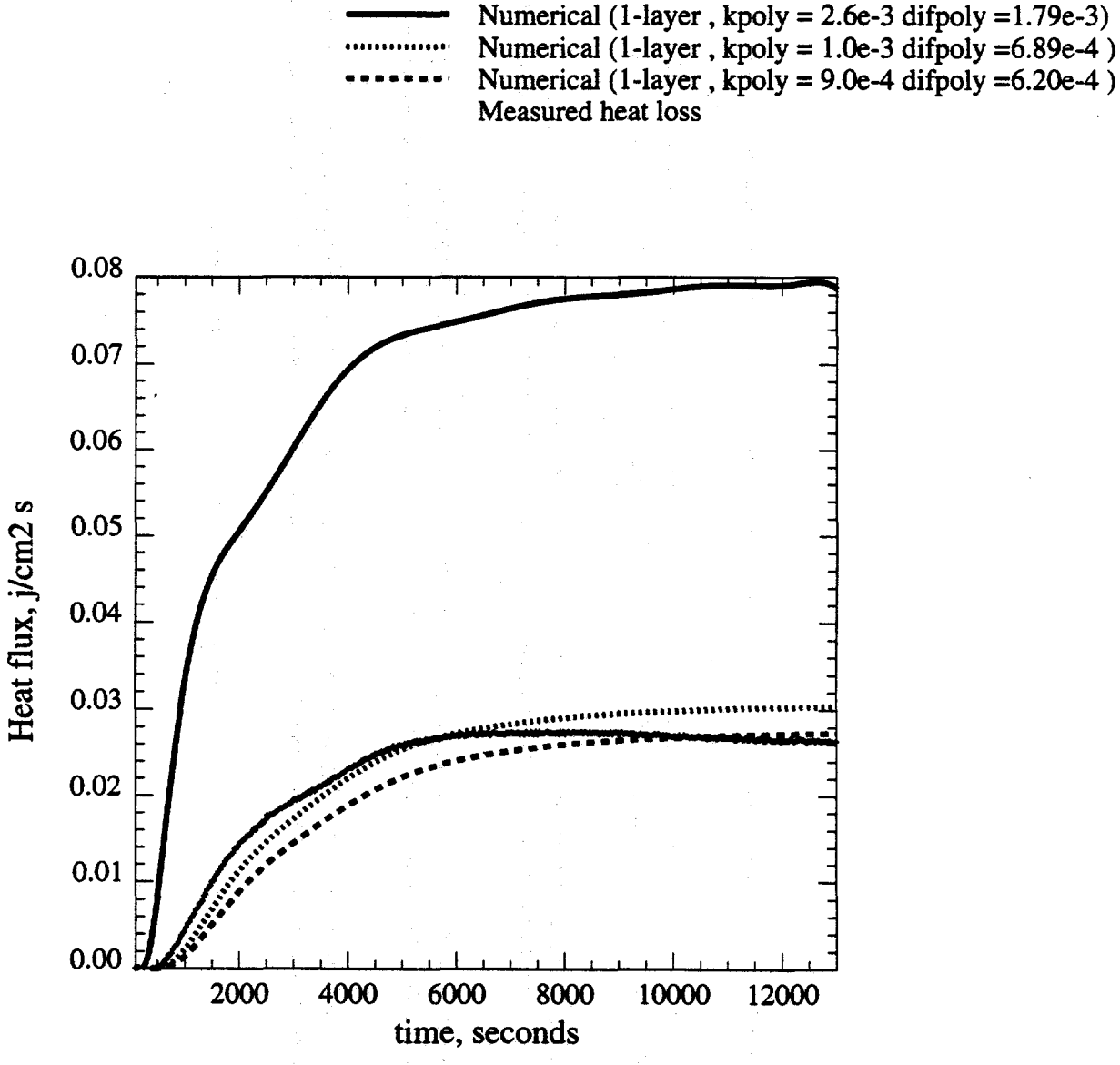

Figure 3.1.23 Heat losses calculated from finite difference solution.

3.2 DISPLACEMENT STUDIES USING A THREE-DIMENSIONAL LABORATORY STEAM INJECTION MODEL
(Bakul Sharma)

3.2.1 INTRODUCTION

The aim of this research project is to use the SUPRI 3-D steam injection laboratory model to further investigate the mechanisms of some of the thermal recovery processes.

Invented for medical purposes in 1972 (Haunsfield, 1972), CT scanners have been used extensively in petroleum engineering applications. They are useful tools for measuring in situ saturation, porosity determinations and core flood experiments. Most of the experiments in which CT scanners have been used to investigate the mechanisms of some EOR processes were carried out in linear models, leading to poor representation of gravity override and channeling. CT scanners were not used for applications with higher temperature and pressure, as seen in thermal recovery processes. Metallic core holders required for laboratory simulation of thermal EOR processes made it difficult to use X-ray absorption techniques. Demiral *et al.* (1992) designed and constructed a three dimensional laboratory model to measure temperature, pressure and heat loss data. The model was designed so that the construction materials were not limiting factors during scanning.

Demiral *et al.* carried out runs where water was displaced by steam, by steam foam without nitrogen, steam foam with nitrogen, and by nitrogen foam alone. They made two-phase saturation measurements in the CT scanner during these runs. Similar experiments will now be carried out for displacement of oil, with three-phase saturation measurements in the CT scanner.

3.2.2 OBJECTIVES

(a) Determine the accuracy of three-phase saturation measurements using the CT scanner.

(b) Better understanding of the mechanisms of steamflooding.

(c) Better understanding of the effect of surfactant on steamflood mechanism.

3.2.3 EXPERIMENTAL SETUP

The experimental setup is shown in the figure. The injection end has two liquid chromatography pumps to inject water or surfactant solution and to feed the steam generator with distilled water. One extra pump has been added for oil. The 3-D steam model with dimensions of $20 \times 20 \times 7.5$ cm simulates one quarter of a five spot pattern. Aluminum, Teflon and Fiberfrax have been used as supporting and insulating materials. A top cover helps to compress the sand to assure that there is no gas space above the pack. The injection well system allows injection of steam with a quality ranging from 0 to 100% through the total depth of the well. Heat loss from five sides of the model are measured by means of heat flux sensors. Temperature and pressure variation with time can be recorded at three different levels in the model at regular intervals along the flow direction. Sixteen center thermocouples are placed at a level of 3.810 cm from the bottom

of the model. Nine top and nine bottom thermocouples are placed at 6.985 cm and 0.635 cm from the bottom. Sixteen pressure taps are located at the same locations as the center thermocouples. The model was packed with unconsolidated 100 mesh sand. A back pressure regulator maintains constant pressure at the producing corner of the model. A cooler condenses the produced steam. Water and oil production at the outlet will also be measured in order to compare the CT determined water and oil saturations with the volumetric values.

The CT scanner presently available is a Picker International SYNERVIEW 1200SX X-ray scanner. This is a second generation machine allowing automatic switching of energy levels from 80 keV to 140 keV and a 512×512 pixel imaging capability.

The model can be scanned at six different locations (through the 1.5 cm clearance between the thermocouples) during the experiments. The total scan time for six slices is around 4 minutes (for 12 number of scans). A reference mark has been made on the model so that the same locations will be scanned each time.

3.2.4 WORK COMPLETED

(a) All pressure transducers were connected back after checking and cleaning.

(b) A setup for the study of sand size effects on pressure drop was made. A few runs were conducted, and it was observed that pressure drop did not go above 3 psi even at higher flow rates with the model packed with fine sand (100 mesh).

(c) The model was, therefore, packed with -100 mesh unconsolidated sand.

(d) Rewiring was done on the heaters used to control the temperature of the steam/hot water generated and injection well temperature, because they were found to be shorting.

(e) Test runs were conducted to check for leaks and functioning of the instruments. All leaks were fixed.

(f) The existing codes for data logging had to be slightly modified because they were not compatible with our system.

(g) The model was set up adjacent to the new CT scanner for carrying out the experiments. This involved setting up the data logger and computer system, and some rewiring.

(h) A couple of runs were conducted to check for proper functioning of the data logging system.

(i) A few calibration runs were made with the new CT scanner using dual voltage. The results are being analyzed.

3.2.5 FUTURE PLAN AND EXPERIMENTAL PROCEDURE

(a) CO_2 will be used to displace air.

(b) The model will then be flushed with water to remove the CO_2 in the pores.

(c) Oil will then be pumped into the system until no traces of water are found at the outlet.

(d) For the steamflood runs, steam will be injected until oil production is negligible. Temperature, pressure, saturation, heat flux, and production measurements will be made at breakthrough and other predetermined times.

(e) Similar measurements will be made for a surfactant steamflood, with surfactant slug introduced at the breakthrough of steam.

(f) The main experiments will be started shortly. Quite a few experiments are expected to be completed by the end of the spring quarter, with the possibility of preliminary analysis of most of the results.

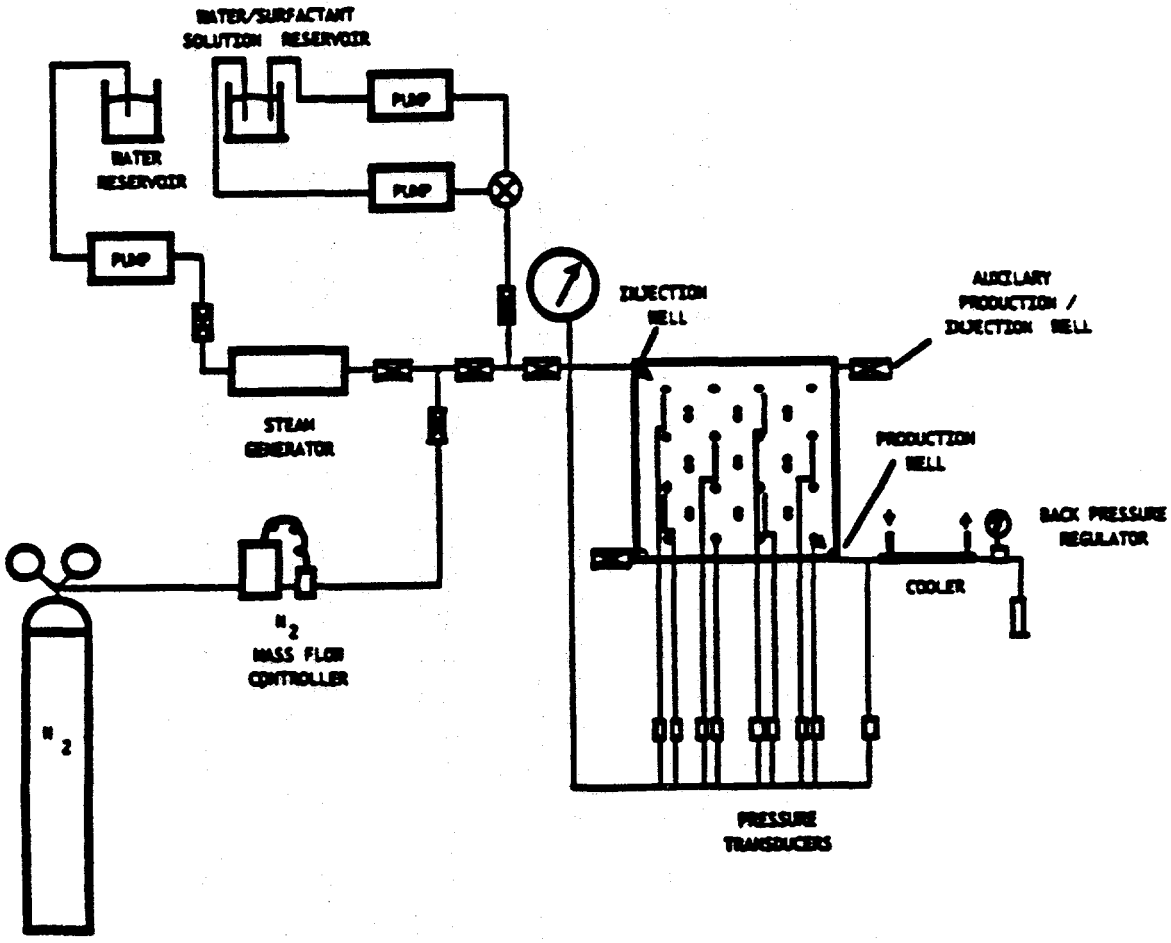

Figure 3.2.1 Schematic of the experimental setup

3.3 PORE LEVEL VISUALIZATION OF FOAM/OIL FLOW IN A SANDSTONE REPLICA MICROMODEL
(F.C. Woody)

3.3.1 OVERVIEW AND OBJECTIVES

Steam injection is the most widely used enhanced oil recovery technique and is particularly suited for heavy oil reservoirs, where other methods, such as waterflooding, often fail. The injected steam has a much lower density and viscosity than the oil and water it is attempting to displace. This results in severe gravity over-ride and channeling through high permeability zones, leaving the bottom of the formation and low permeability zones unswept. Foams have been used as a method of mobility control in steam floods, mitigating the problems of channeling and over-ride and resulting in an efficient displacement.

At present, the basic phenomena by which foam flooding works is not known. In particular, it is unclear under what circumstances injected surfactant forms a stable foam and how it reacts with the oil phase. A quantitative description of foam flooding based on a knowledge of the pore level processes by which the oil is displaced is lacking. It is our hope that this understanding can be used to develop a mathematical model of foam flooding that can be used to predict performance at the field scale.

In this project, we will study the pore level processes in foam flooding in a sandstone micromodel. The micromodel is an exact representation of a slice through a Berea sandstone etched onto a silicon wafer. It honors the microscopic heterogeneity of the rock, but, being two dimensional, loses some of the continuity of a three dimensional sample.

A novel micromodel fabrication technique has been pioneered at Stanford (Hornbrook *et al.*, 1991, 1992). A high quality photograph of the rock section is digitized. The image, which is approximately 500 mm across, is replicated many times to fill an area 5 cm squared. This image is reproduced as a chrome on glass mask. The grains are opaque and the pores are transparent. A coating of photoresist is placed on a silicon wafer. Ultraviolet light shines through the mask onto the wafer. The light kills the photoresist, so after exposure the flow path image exists as clean silicon for the pores, and silicon still coated with photoresist for the grains. A dry etch technique is then used to create the network of pores and grains onto the wafer. The maximum etch depth is between 5 and 30 um and is controlled by the thickness of photoresist on the wafer. After etching, a glass plate is placed over the wafer by anodic bonding. Two inlet ports are needed to perform three phase flow experiments where the capillary pressure differences between gas and water and between oil and gas can be controlled independently. Several similar micromodels have been constructed with exactly the same pore structure, which enables exact comparisons of the results from different experiments to be made. The manufacturing process is shown schematically in Fig. 3.3.1 and the experimental set-up is shown in Fig. 3.3.2.

Preliminary experiments of foam flow in such micromodels have already been performed on one type of oil and with one surfactant concentration (Hornbrook *et al.*, 1991,1992). We plan to perform many more experiments on a wide range of oils and surfactants to assess the circumstances in which foam flooding is effective and to find the pore level processes by which high oil recoveries can be achieved. We will also vary the

foam injection procedure, since this can have a dramatic effect on recovery, particularly for the displacement of residual oil.

The observed displacement processes can be coded into a numerical network model. This simulator represents the pore space as an array of pore spaces connected by narrower throats. The position of the fluids is controlled by capillary forces and so it is possible, theoretically, to compute the capillary pressures at which different displacement events will occur. These predictions can be compared with the observed processes. From simulations of systems containing hundreds of thousands of pores, averaged properties of flow can be computed. It is these properties that are used in conventional transport models to predict oil recovery at the field scale. The simulator can be used to predict capillary pressure and relative permeability under different flow conditions, for different foam systems and for different types of pore structure. In particular, the simulator will be used to estimate the residual oil saturation in the presence of foam, and the effect of oil and surfactant properties on recovery. The model can be tuned on the experimental data until it can reliably predict the pore scale events seen in the micromodel. The model will test whether or not the conventional characterization of multiphase flow based on saturation dependent relative permeabilities and capillary pressures adequately describes the full range of phenomena seen in foam flow. The final result will be a pore level tool that can reliably predict the averaged displacement properties under a wide range of circumstances and which is not dependent on a particular functional form of the averaged parameters.

3.3.2 EXPERIMENTAL APPARATUS

In order to fully evaluate pore level interactions, several pieces of equipment have been acquired and utilized to provide both direct and indirect data. The experimental set-up is shown schematically in Fig. 3.3.2.

* The syringe pump used is critical to all observations. As the experiments conducted have been characterized by constant rate injection, the stability of the pump is critical.The rate applied to the system is consistent with typical field production rates of afoot per day.

3.3.2.1 Direct Observation

The principal pieces of equipment required are a high quality reflected light microscope, a video camera, a cassette recorder, a television monitor and a computer.

1. A Nikon microscope has been purchased for the visualization. It is a reflected light microscope, which when connected to a video monitor, allows for the observation, recording and analysis of pore level processes.

2. The video camera employed is a Sanyo closed-circuit TV camera with a universal microscope adapter attached to it. The image viewed is sent via coaxial cable to the VCR.

3. The VCR used in experimentation is a Mitsubishi high resolution model. Along with a detailed recording of the experiment, it provides frame by frame advance capabilities enabling one to pinpoint more accurately displacement events. The image is then routed to the TV monitor.

4. The television monitor is a Sony, high definition color model. It permits the viewing and analysis of the experiment and the analysis of pore level displacement processes.

5. Finally, the image is sent to the computer, a Macintosh IIcx. Image analysis software on the computer allows for the capture of displacement events, and provides editing tools to eliminate noise.

3.3.2.2 Indirect Observation

Pressure data is collected through the use of pressure transducers, demodulators, and a data logger.

1. Celesco differential pressure transducers are used to measure inlet and outlet pressures during experimentation. Since preliminary work requires only two active ports, two transducers are employed - one at each end. The positive leads are open to atmosphere, while the negative ones are connected to pressure ports. 25 psi pressure plates are attached to the transducers. Experience has shown that pressures in excess of 40 psig can rupture the micromodels as presently constructed.

2. Electrical signals generated from the pressure transducers are sent to demodulators. The demodulator converts the fluctuating voltages to psig values.

3. The psig values are plotted on a Soltec data logger. The particular data logger being used is of a graphical nature, plotting inlet and outlet pressure next to each other versus chart recording speed.

3.3.3 PRELIMINARY EXPERIMENTS

In order to create a basis from which to compare oil/water/air and oil/surfactant/air results, water/air and surfactant/air experiments were performed. The surfactant, AOS 1618, was chosen so that a comparison to previous research could be made. This Shell Development Company product is an alkansulfonate, and should be suitable for both heavy and light oil experiments. Surfactant concentrations were determined from the known active substance weight percent. The following is a brief explanation of the procedure and the results.

3.3.3.1 Procedure

Prior to each run the micromodel is vacuumed, and the equipment recalibrated. The vacuum on the micromodel and plumbing is broken upon exposure to a column of deionized water, or a solution of deionized water and surfactant. As a result of exposure, the micromodel, almost instantly, is completely saturated with fluid. Several pore volumes of air is drawn into a 10cc B/D syringe and the syringe attached to the pump. The outlet is then opened to atmosphere, and the experiment is ready to begin. The constant rate injection pump is activated and pressure buildup commences. During experimentation, displacement events are viewed and recorded. Once breakthrough occurs, pressure drops significantly, and when no more fluid is produced, the experiment is terminated.

3.3.3.2 Results

Water/Air Interaction: During the runs, pressure drop builds gradually it reaches about 12 psi and then declines rapidly after breakthrough. Visually, a continuous, although tortuous path of air is observed from inlet to outlet. This is consistent with previous research. The air is observed traveling in directions different from the overall direction of pressure drop - indicative of local dominance of capillary forces above viscous forces. Following the air from inlet to outlet one begins to anticipate the next pathway taken. This likely reflects air's inclination to take path of least resistance, which is through the largest pores. Figure 3.3.3 represents a five step progression of air displacing water. The continuity of the air stream can be observed as well as the fact that the air always passes through the largest available pore throat at each stage in the displacement.

0.001% wgt. Surfactant/Air Interaction: Based upon direct observations alone, there wasn't any significant difference between this concentration and the previous water/air experiments. Continuous air flow paths were observed across the micromodel. However, indirectly, pressure drops almost doubled, reaching up to 18 psi. Upon re-examination, more of the micromodel itself is required for air to breakthrough, and more fluid is produced in the process. It is apparent that the low surfactant concentration still had some effect on air path tortuosity, by forming blocking lamellae.

0.01% wgt. Surfactant/Air Interaction: During experimentation, the effect of this concentration is quite obvious. Numerous air lamellae are observed throughout the micromodel. The lamellae typically extend, in size, for a couple of pores and terminate. The pathway from inlet to outlet is difficult to observe as routes in every direction can be argued. No snap-off or break and reforming of lamellae was observed. The lamellae seem to have formed initially, and reside in larger pores until enough pressure is applied to force them through adjacent pores. Once again, pressure drops double from the preceding concentration. Drops up to 43 psi were recorded. After breakthrough, however, pressure drops much more gradually, as the discontinuous air trains arrive at the outlet from different and circuitous routes. Finally, a greater amount of fluid was produced. Figure 3.3.4 reveals air interacting with 0.01% wgt. surfactant solution.

3.3.4 CONCLUSIONS

1. The experimental apparatus works well. Pore level events were viewed and measured as desired.

2. It is apparent that increased surfactant concentrations have an affect on air mobility. Increased production occurred as a result of increased concentration.

3. Experiments including oil are necessary to gain a basic understanding of lamellae formation and propagation. The conventional description of foam flow in porous media is the population balance approach. Here lamellae are continually formed by snap-off at narrow throats. In wider pores the lamellae break, and the foam reaches a point of equilibrium between formation and breaking of lamellae. Air flow occurs by breaking lamellae. This has been observed directly in micromodels with relatively large pore spaces, approximately ten times larger than the realistic pores in this model. However, the preliminary results of this study indicate that the lamellae are very stable and no snap-off or breaking events were seen. Thick, stable

lamellae were seen in narrow throats. Air flow was accompanied by slippage of lamellae along the pore walls. This is a quite different mechanism and reveals the importance of a micromodel with a realistically sized pore space.

3.3.5 FUTURE WORK

Based upon the preliminary findings, the following is planned and under way:

1. Preparations for oil/water/air and oil/surfactant/air experiments have begun. Here we wish to observe the basic pore level mechanisms by which oil interacts with the foam, and the circumstances inwhich the oil will destroy the foam.

2. Physical aspects of multiphase interactions can be quantified based upon an understanding of micromodel pore geometries.

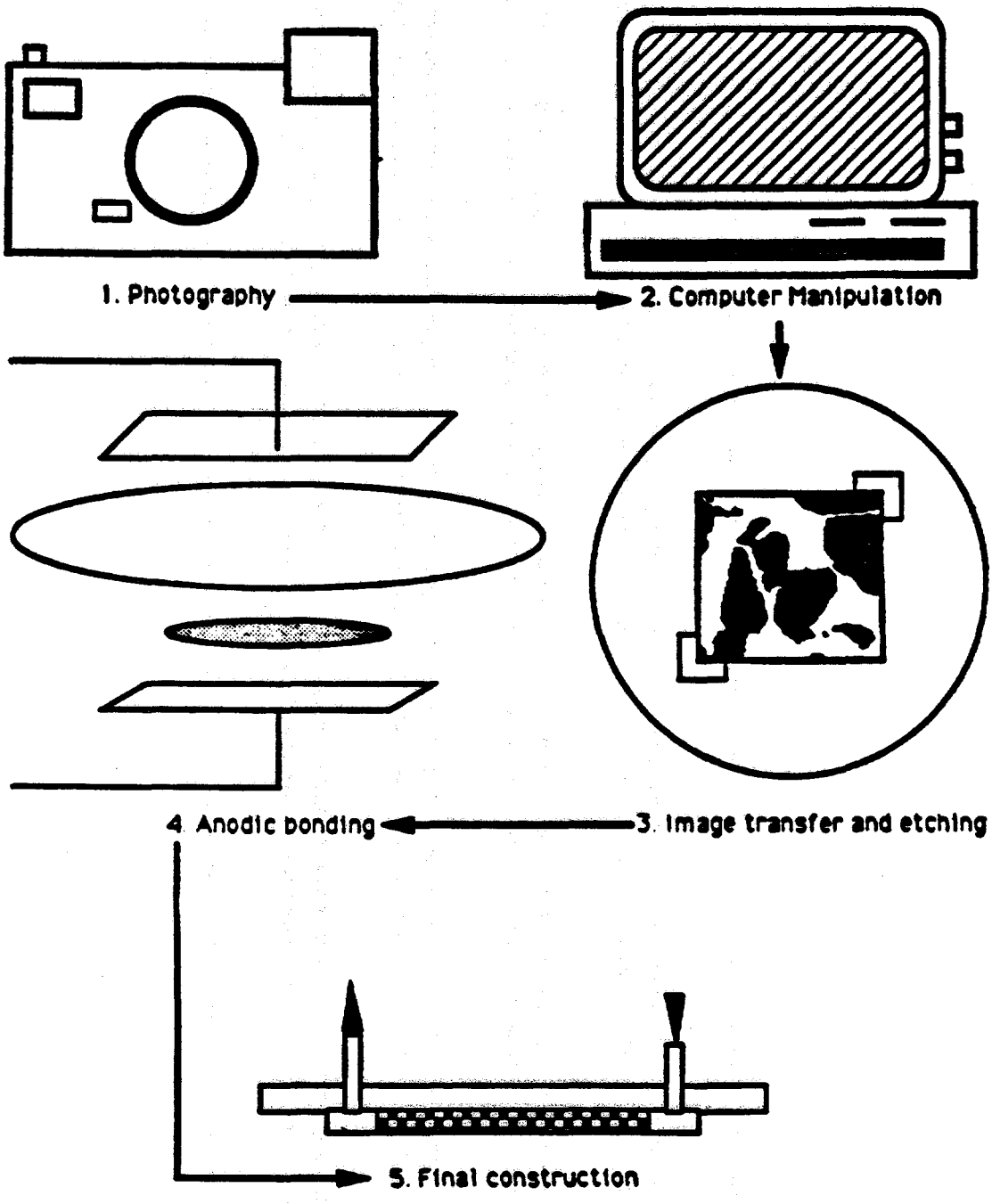

Figure 3.3.1 Schematic of the manufacture of a silicon etched micromodel (Hornbrook, 1992)

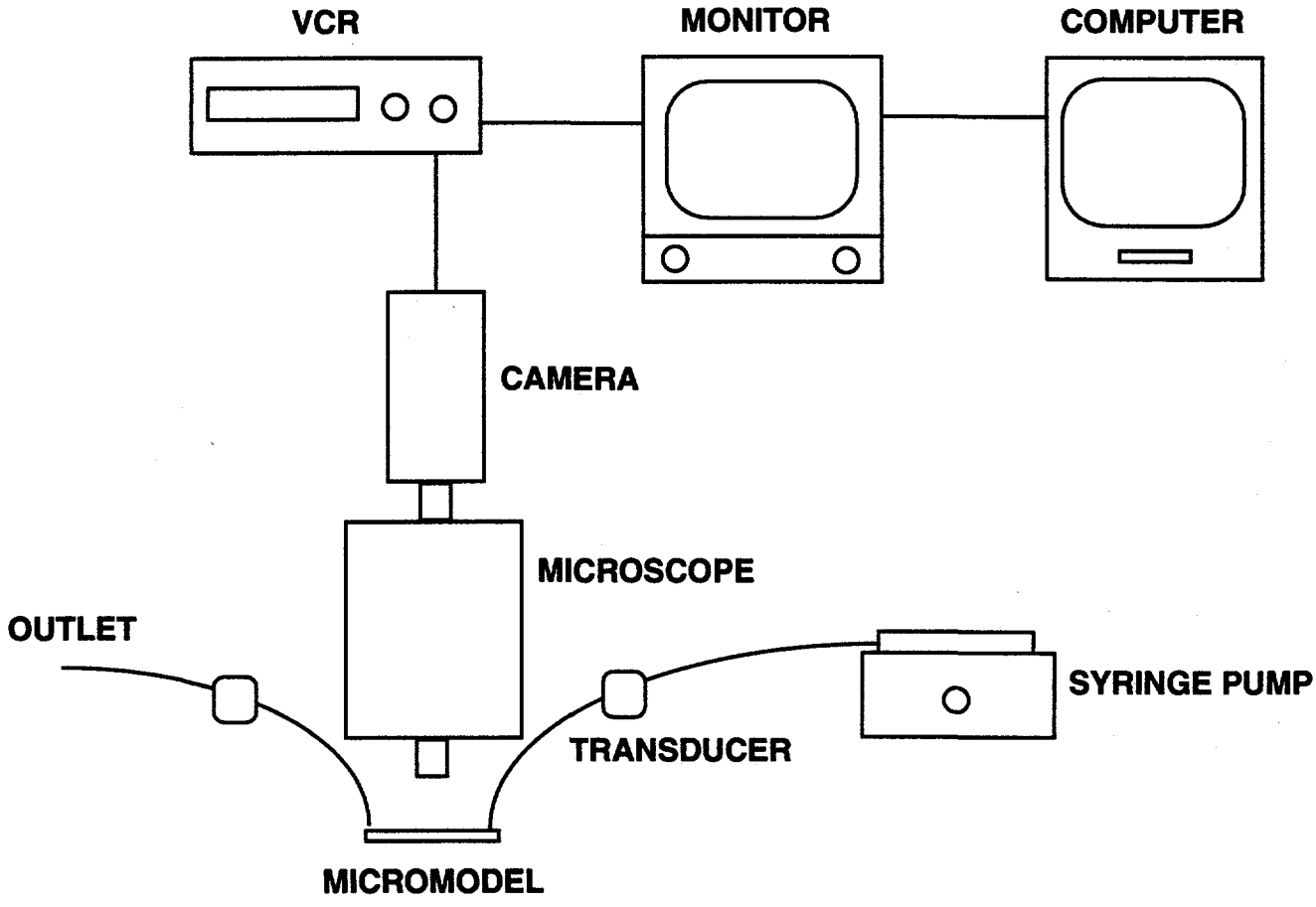

Figure 3.3.2 Experimental apparatus schematic.

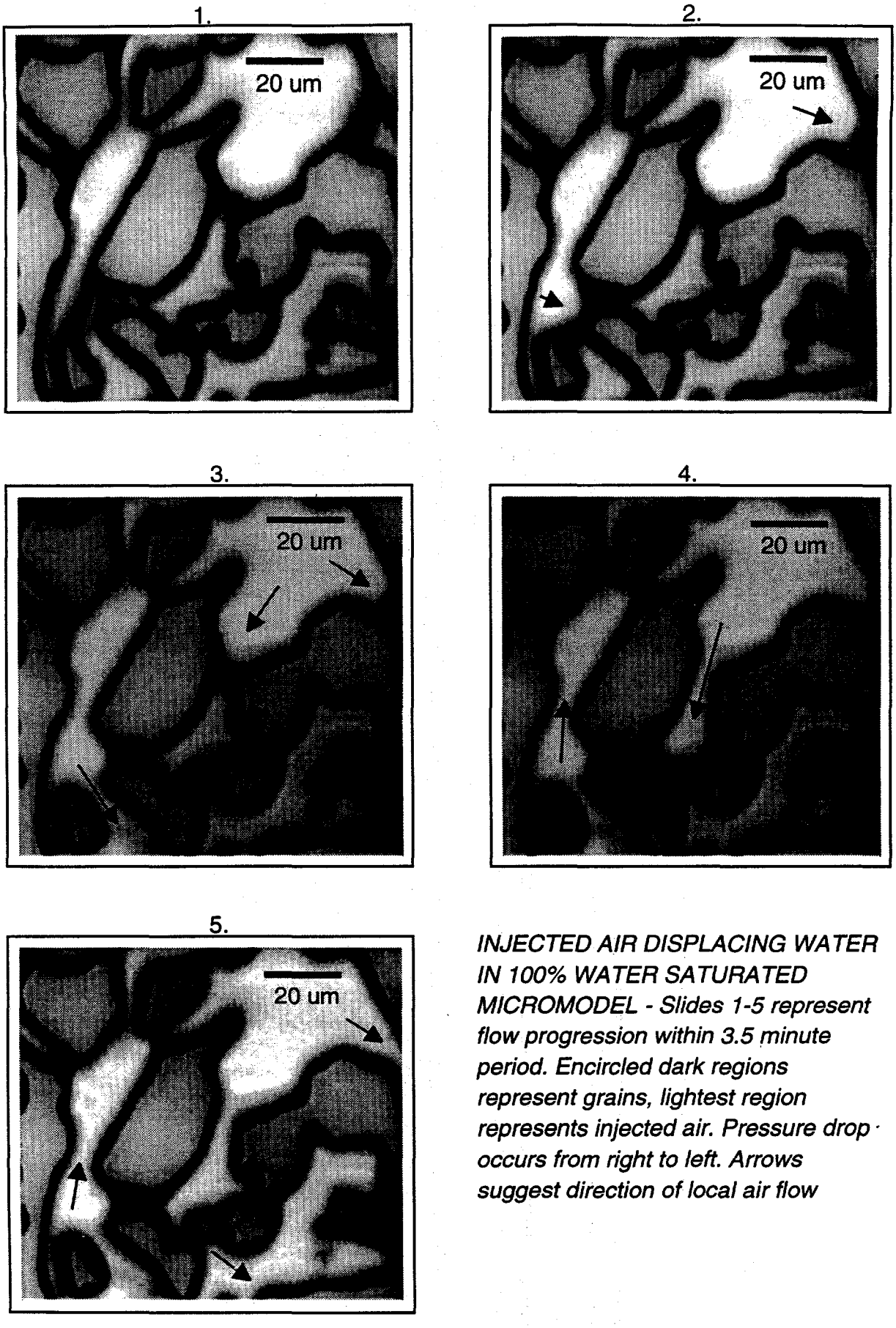

INJECTED AIR DISPLACING WATER IN 100% WATER SATURATED MICROMODEL - Slides 1-5 represent flow progression within 3.5 minute period. Encircled dark regions represent grains, lightest region represents injected air. Pressure drop occurs from right to left. Arrows suggest direction of local air flow

Figure 3.3.3 Air displaces water in water-filled micromodel.

1.

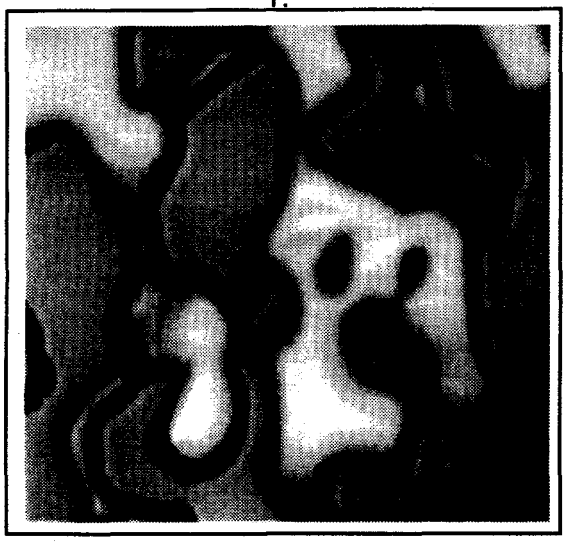

2.

3.

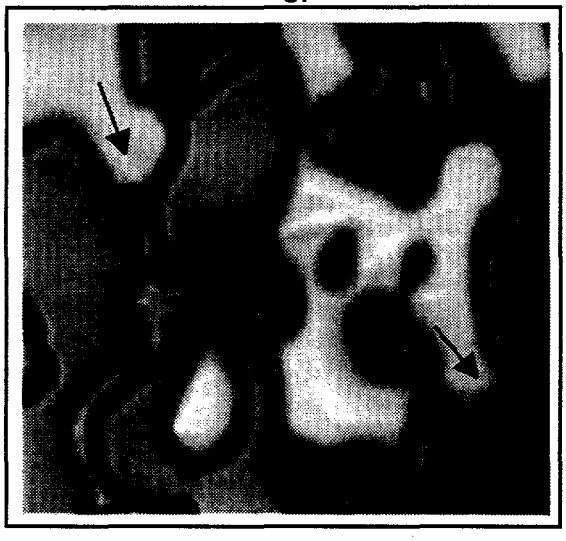

4.

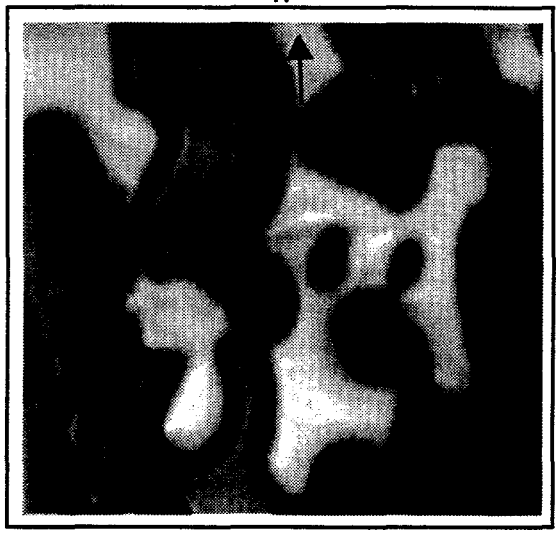

5.

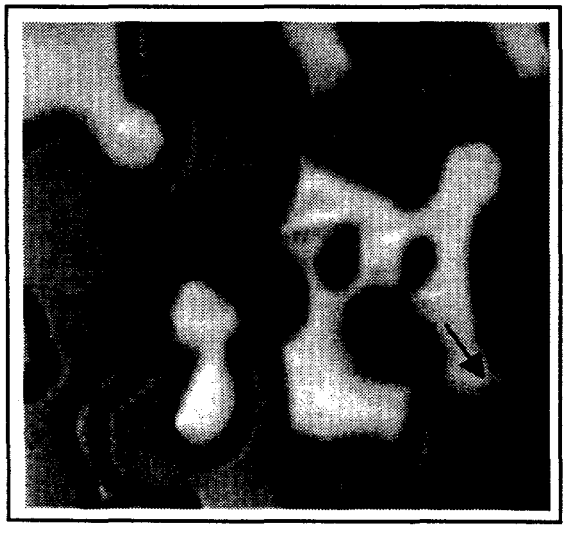

INJECTED AIR DISPLACING SURFACTANT/WATER SATURATED MICROMODEL (0.01% wgt. AOS1618) - Slides 1-5 represent flow progression within 8 minute period. Encircled dark regions represent grains, lightest region in each slide represents injected air. Pressure drop occurs from right to left. Arrows suggest direction of local air flow.

Figure 3.3.4 Air displaces surfactant/water solution in micromodel.

3.4 MICROMODEL FOAM FLOW: A LITERATURE REVIEW

(Tony Lolomari)

3.4.1 ABSTRACT

The use of micromodels in foam flow visualization is relatively recent. Previous research on foam flow in micromodels was reviewed, to evaluate the published techniques and their relative merits and demerits, and the information derived from the micromodels (flow mechanisms of foam).

The literature review will provide insight into further avenues of research in this area with the novel micromodel construction procedure we have now.

3.4.2 LITERATURE REVIEW

Foams can be used to improve the sweep efficiency (vertical or horizontal) in miscible and steam enhanced oil recovery (EOR) processes Although the study of foam in porous media started in the late 1950s with the work of Bond and Holbrook (1958) research in the use of micromodels is relatively recent. These models can help provide a better insight into the mechanisms. The types of micromodels commonly employed to date are bead/sandpack, etched glass and etched silicon.

3.4.2.1 Early Work (Up to 1977)

Fried (1961), using capillaries observed that foam bubbles subdivided into smaller bubbles as they entered the sand and passed through pore constrictions. He concluded that the foam moved as "plug-type, non Newtonian flow where all the shear takes place at the flow-channel boundaries".

Marsden and Khan (1966), using circular capillary tubes treated foam as a combined liquid and gas, which behaved like a single non-Newtonian fluid when flowing through a medium.

Raza and Marsden (1967), did an experimental study of the flow of fine-textured, aqueous foams through Pyrex tubes packed with sand and Pyrex beads. They concluded that the foams had the flow behavior characteristics of pseudoplastic fluids.

David and Marsden (1969), using circular capillary tubes proposed that foam flowed as a single body. This is known as the homogenous flow mechanism, in which foam is considered to be a continuum; the gas and liquid flowing at the same rate and the foam behaving as a single fluid with a high apparent viscosity.

Up until the mid-eighties, there had been a number of conflicting results on the nature of foam. Bernard *et al.* (1965), Holm (1968), and Mast (1972) indicated that the gas component of foam flowed through porous media by breaking and reforming films, while the liquid was transported as a free phase through the film network. Bernard and Holm (1964), Marsden and Khan, and Nahid (1971) suggested further that the liquid flow could be treated according to Darcy's law. Kolb (1964], Nahid, and Mast also suggested that a portion of either gas or liquid or both are trapped in the porous medium, while the flowing phases flow according to Darcy's law.

However, none of these proposed early mechanisms adequately accounted for all the observed properties of the foam in porous media. The only general agreement was that foam generally hindered the flow of gas in porous media.

Kanda and Schechter (1976) performed experiments with anionic and nonionic surfactants in sandpacks and found that the permeability to gas was a sensitive function of the surfactant solution wettability, and the presence of salts in the surfactant solutions did not affect the results.

3.4.2.2 Recent Work (Up to 1992)

Haraski and Lawson studied the behavior of foam lamellae in smooth capillary tubes in 1983. They investigated:

1. Foam quality, which is the ratio of gas volume to total volume

2. Foam texture which is the average bubble size in relation to capillary size

3. Interfacial tension gradients created when surfactant is swept from the front of a bubble to the rear.

A comprehensive literature review was carried out in 1986, by Marsden. He outlined the various contradictions in the literature and also outlined some major advances in the study of foam. Marsden pointed out that foam viscosity was a function of its flow rate, flow history and surfactant concentration; and foam was fluid of high apparent viscosity which acted like a non-Newtonian fluid in most cases. Some of the problems that he cited that remained to be solved had to do with the chemical aspects of surfactants such as their chemical and microbiological degradation, thermal stability and adsorption on mineral surfaces or oil/water surfaces.

In 1986, Sarathi did a review on previous research in flow visualization studies with micromodels and their merits and demerits. He summarized the limitations in the use of micromodels as:

1. The difficulty in obtaining an etch of specific depth repeatedly.

2. The introduction of microscopic heterogeneities into the model via the etching process.

3. The fact that 2-D models do not permit as much continuity with multiple fluid phases as do 3-D models.

4. Pores in the micromodel being usually larger than those in reservoirs, resulting in different Peclet numbers. The Peclet number is defined as the ratio of convective to dispersive transport. Lake (1989) defines the Peclet number, N_{pe} as:

$$N_{pe} = uL / \phi K_t \qquad (3.4.1)$$

where u is the superficial velocity, L is the length, ϕ is the porosity and K_t is the longitudinal dispersion coefficient.

5. Greatly differing pore structures between micromodels and reservoirs due to the inability to capture extreme variations in rock characteristics such as heterogeneity, pore geometry and wettabilty.

Sarathi concluded by stating that although micromodels could be useful in studying displacement processes and fluid distribution on the pore level, their limitations should be borne in mind when interpreting their results.

Sanchez and Schechter (1986) investigated the conditions under which foam bubbles were formed or destroyed using simplified capillary tube models. They obtained an expression for the rate of generation of foam bubbles based on geometric and fluid properties. They performed steady state experiments which demonstrated that: only trace quantities (in the order of 2.6 parts per million by weight) of surfactant are needed to affect the relative permeability of gas. They concluded that the relative permeability to gas was a sensitive function of the wetting phase film thickness. This film thickness was believed to be most sensitive to wettability.

Owete and Brigham (1986) studied the flow behavior of foam using micromodels (etched silicon wafers) with a homogenous and heterogeneous pore structure. In their experiments, they discovered that air was propagated by displacement of lamellae in long bubbles flowing and extending across several pore lengths, while the liquid flowed through the network of films. The surfactant concentration as well as the pore structure were varied and these affected the mechanisms observed. In the heterogeneous model (much more realistic), they observed snap-off occurring at pore constrictions and the resultant bubble break-and-re-form process.

Radke and Ransohoff (1986) categorized the various mechanisms of foam generation within glass bead packs as snap-off, lamella leave-behind, and lamella division, with snap off being the primary mechanism for strong foam formation. They also developed a simple model (based on the concept of a germination site) to predict the onset of snap-off and found a critical velocity above which a stable foam was generated by both snap-off and lamellae division mechanisms, and below which only the unstable foam was obtained by the leave-behind mechanism.

Khatib *et al.* (1986) studied the stability of foam lamellae as determined by capillary pressure using sand and beads packed in glass and acrylic tubing. Their results indicated that as the fractional flow of gas was increased, the capillary pressure measured during a foam displacement approached a characteristic value, which they termed the limiting capillary pressure. The limiting capillary pressure was a function of the type of surfactant and its formulation, the gas velocity, and the permeability of the medium. They stated some of the consequences of such a limiting capillary pressure as:

1. A limit on how high above the free water level discontinuous-gas foams (containing moving lamellae) and continuous-gas foams (containing only stationary lamellae) can exist in an oil reservoir.

2. An easy calculation of the relative gas mobility from the capillary pressure curve, relative liquid mobility function, and the ratio of gas to liquid fractional flows when the limiting capillary pressure was maintained in a porous medium.

The destabilizing effect of crude oil on foam was observed by Nikolov *et al.* by studying bulk-foam/oil interactions in 1986. They showed that the surfactant type and concentration directly influenced the stability of the emulsion structure. They concluded that the interactions between the oil phase and foam lamellae were complex. These

interactions often involved the migration of emulsified oil droplets from the foam film lamellae into the Plateau borders where various factors, such as the pseudoemulsion film tension, droplet size and number of droplets may all contribute to destabilize the foam. They also found the stability of the emulsion and foam films to be dependent upon the micellar microstructure within the film.

A summary of the various flow mechanism patterns in the literature was given by Mahmood and Brigham in 1987 as:

1. Bubble flow, in which foam flows as a homogeneous fluid with gas uniformly dispersed in the surfactant solution.

2. Intermittent flow, in which foam flows such that liquid is transported through a continuous network of liquid membranes acting as a free phase, while the gas flows as a discontinuous phase through breaking and reforming of bubbles.

3. Plug flow, in which foam flows as plugs that are characterized by high shear rates near the boundary between the foam and the conduit.

4. Trapped-Gas flow, in which foam flows such that it traps some gas in the porous medium while the remainder flows as a free gas phase according to Darcy's law.

5. Segregated flow, in which foam flows only through gas channels carrying a small amount of surfactant solution with it.

6. Membrane flow, in which foam is generated as lamellae at specific locations in a porous medium possessing specific pore constrictions that aid its generation.

7. Tubular-Channel flow, in which foam flows through channels consisting of tubular bubbles moving along and extending over several pore spaces.

Lau and O'Brien (1988) used sandpacks to show the effects of spreading and nonspreading oils on foam propagation through porous media. Their results showed that the presence of a spreading oil increased the time to generate a foam, decreased the propagation speed of the foam, and broke the foam faster than a nonspreading oil.

Spreading is determined from free surface energies, expressed in spreading coefficients. For a flat surface, the oil spreading coefficient is given by:

$$S_{po} = \sigma_{wg} - \sigma_{go} - \sigma_{ow} > 0 \qquad (3.4.2)$$

where S_{po} is the oil spreading coefficient, σ is the interfacial tension, and subscripts o, w, g represent the oil, water and gas phases respectively. A positive spreading coefficient indicates spreading. Spreading only possible if the oil penetrates the foam/gas interface. A droplet of oil can be drawn up between the two adjacent foam bubbles so that it can bridge the two bubbles. This process occurs if the oil entering coefficient, E_o is positive E_o is given as (Ross, 1950):

$$E_o = S_{po} + \sigma_{go} \qquad (3.4.3)$$

Equation (3) indicates that E_0 is always greater than S_{po}. There are three possibilities:

1. $E_0 < 0$. If E_0 is negetive, then S_{po} must be negetive. Here the oil will neither spread nor be drawn up into the foam. It will not destabilize the foam by any of the above mechanisms.

2. $E_0 > 0$, $S < 0$. In this case the oil will be drawn into the lamellae, but would not spread at the interfaces.

3. $E_0 > 0$, $S > 0$. In this case oil will be drawn up into the lamellae and then spread along the interfaces. An isolated oil droplet is eventually formed and this consequently leads to rupture of the foam bubble.

Huh *et al.* (1988) studied the mechanisms associated with gas permeability reduction in terms of microscopic heterogeneity, the presence of an oil phase, surfactant concentration and flow rate at elevated temperature and pressure (90^0 F and 1320 psia). They performed 33 displacements, and their main conclusions were:

1. Upstream and downstream snap-off and bubble division were equally important as foam generation mechanisms.

2. The mixing of fluids and the aspect ratio of the porous medium were the most important factors in foam generation.

3. The wettability of the micromodel was changed to intermediate or oil wet by saturating it with crude oil. Consequently, foam generation was greatly reduced due to lack of surfactant solution at foam generation sites.

4. Improved sweep efficiency with higher surfactant concentrations and higher flow rates.

5. Simultaneous injection of CO_2 and surfactant solution resulted in better foam generation and increased sweep efficiency compared to the injection of single phase CO_2.

Manlowe and Radke (1988) performed direct visual studies of foam flow in etched-glass micromodels containing residual oil and demonstrated that foam decayed as a result of breakage of pseudoemulsion films. They did not find any correlation between oil spreading and foam stability. They proposed that pseudoemulsion film rupture was the general destabilization mechanism.

Jimenez and Radke (1989) presented a hydrodynamic theory based on a single lamellae flowing through a periodically constricted cylindrical pore to predict the relationship between critical capillary pressure and velocity in an oil free porous medium. From the results of their analysis, they concluded that this critical capillary pressure could be associated with a critical permeability or a critical wetting liquid saturation for a given medium through the Leverett J-function.

Hanssen and Jakobsen (1989) observed through etched glass micromodels foam to exist as a network of liquid films which did not move through the pore channels. This observation indicated that gas flow occurred by a film breaking and reforming process.

Sanchez and Hazlett (1989) performed a study of the generation and flow of gas and surfactant solution through an oil-wet porous medium using glass bead packs. Their experimental results are outlined below:

1. Gas permeability reduction was essentially identical for both water-wet and oil-wet media for the same surfactant concentration.

2. Foam formation in the initially oil-wet medium was a result of the initial hydrophobic surface being altered to hydrophilic by the addition of surfactant.

3. A substantial shift in the liquid phase relative permeability of the oil-wet porous medium indicated a wettability alteration.

Schramm and Novosad (1990) evaluated the possible correlation between basic surface properties and observed foam/oil interactions in a glass micromodel whose etch depth was approximately 70 microns. They concluded that there were three distinct types of possible foam behavior: (1) stable foams, (2) intermediate stability foams, and (3) unstable foams. Emulsification of the oil into the foam structure with subsequent penetration and rupture was the proposed mechanism for the foam destruction.

Kuhlman (1990) performed a series of high-pressure CO_2 foam/light oil microvisual experiments. He deduced that the main reason for the deleterious effect of oil on foam was the high concentration of light hydrocarbons in the oil and oil wetness of the porous medium. Compositional changes caused by vaporization and condensation during a CO_2 flood reduced emulsification near the oil bank. Then, increased mobility control observed when soluble $C0_2$ hydrocarbons had been stripped from the oil. He asserted that water could become the spreading phase when enough $C0_2$ soluble hydrocarbons had been stripped from the oil. This result suggested that water spreads in foams near CO_2 injectors and that oil spreads in foams deeper in the reservoir. He also observed a decrease in the foaming ability of a surfactant by hydrocarbons which had the same size as the hydrophobe of the surfactant. This phenomenon occurred even without the presence of a separate oil phase.

Chambers and Radke (1990, 1991) furnished an in-depth treatment of capillary phenomena in foam flow. These capillary phenomena dominate events at the pore scale (all foam generation and breaking mechanisms apart from lamella leave-behind and division are due to capillarity). In the former, they gave an apparent justification for extrapolating the 2-D micromodel observations to 3-D capillary phenomena. In the latter, they describe the various foam generation and termination mechanisms with micrographs as recorded from the micromodel.

Persoff *et al.* (1991) investigated the flow of foam in a sandstone core at elevated pressures. Their results showed that for a fixed liquid velocity and a wide range of gas velocities, the pressure drop was essentially independent of the gas flow rate over a change of about two orders of magnitude. They also observed a trend of constant liquid saturation for changing foam mobility, emphasizing the fact that foam mobility was not a unique function of saturation. They concluded that the most crucial factor controlling foam flow resistance was the bubble texture (bubble size and size distribution).

Hornbrook *et al.* (1992) developed a new micromodel procedure that allowed for an almost exact 2-D replication of a porous medium and used it to observe foam/oil interactions qualitatively. The highlight of this novel procedure is that all the disadvantages

outlined by Sarathi (1968) except for the loss of three-dimensional continuity are eliminated. They performed two sets of experiments:

1. Slug surfactant displacement of oil, in which the oil appeared to be the wetting phase. The oil occupied the small pores, while the surfactant occupied the larger pores. These conditions yielded an efficient displacement of the oil.

2. Foam displacement of oil, in which the surfactant appeared to be the wetting phase. The foam was observed to break upon contact with the oil resulting in an inefficient displacement of the oil. There was also an early breakthrough of the surfactant with a corresponding low fractional recovery of oil.

The authors concluded that injection procedure strongly influenced the oil displacement efficiency.

Schramm *et al.* (1992) in an extension of their earlier work (1990) formulated a model that described the observed foam stabilities for a light crude. In their previous work, they used a heavy crude, but those results were essentially similar to those obtained with the light crude. They did qualitative observations of foam behavior and quantitative measurements of foam lamella breakage frequency with a micromodel. They observed three types of foam/oil interactions: (1) quite stable foams, (2) intermediate-stability foams and (3) unstable foams. All instances of foam lamella rupture appeared to be from the imbibition of emulsified oil droplets into the foam. They also performed flow experiments in Berea sandstone cores (at residual oil saturation) in which they evaluated a mobility reduction factor for different foams.

Their results showed that the observed foam behavior in the micromodels matched phenomenological model predictions and were consistent with the mobility reduction factors and incremental oil recoveries obtained from the corefloods. This work suggested that trends observed in micromodels could indeed be scaled up to the core level.

There was one other reference that I could not review (because it was unavailable) that I think might be relevant: "A Generalized Entering Coefficient to Characterize Foam Stability Against Oil in Porous Media," by Radke *et al.* (1993).

3.4.3 RECOMMENDATIONS

From the foregoing, it can be seen that many of the experiments performed have only provided qualitative results. Quantitative relationships regarding the effects of gas velocity, permeability, surfactant formulation, capillary pressure, etc. are yet to be established or verified.

I think it is important that we:

1. Establish the operative mechanisms of foam/oil interactions, our final goal being the recovery of residual oil in enhanced oil recovery (EOR) process,

2. Investigate the effects of wettability in the micromodels and contact-angle values on foam stability;

3. Use a wide range of surfactants, concentrations and crudes in our displacement experiments. This will help refine our knowledge of the stability of foam in the presence of oil.

4. Combine the micromodel work with core flood experiments. The core displacements should also be combined with computer tomography (CT) methods, to enable some degree of visualization at the core scale.

3.5 FOAM MECHANISMS STUDIES
(Louis M. Castanier and Jan Erik Hanssen)

3.5.1 NOTE AND ACKNOWLEDGEMENTS

This paper was presented at the Reservoir Utilization through Technical Help (RUTH) seminar in Stavanger, Norway (September 1994). It covers work performed at the Rogaland Research Institute under the RUTH program. My sabbatical leave during the Spring and Summer of 1994 was funded by the Fulbright foundation.

Although funding for this study was not provided by the US. Department of Energy or the SUPRI-A Industrial Associates, we feel that the topic is very similar to our own foam flow mechanism project and that this paper will be of interest to tour SUPRI supporters. We are grateful to the RUTH program and the Fulbright Foundation for their support.

Foam Mechanisms Studies

Louis M Castanier, Jan Erik Hanssen

Abstract
Observations of flow mechanisms for foam systems have been conducted in realistic size micromodels (models with pore sizes equal to the size of sandstone pores). As a first step, blocking tests were simulated using an AlphaOlefinSulfonate (AOS) of 16 carbon atoms chain length foamer in concentrations ranging from 0 to 1% by weight active. The results were compared to previous work in larger size micromodels.
The foam behaviour was strinkingly different in the two systems. While in the large pores of previous investigations film generation and breackage appeared to be the dominating mechanisms by which the gas mobility is reduced, in the realistic size system most of the pressure drop across the model appears to be caused by an elastic liquid network made of liquid on solid and liquid in gas films. The events of breackage and formation of lamelae and lenses are rare as compared to the large size systems. Sliding of lamellae over the liquid films covering the grains was often observed as was liquid backflow against the main pressure gradient in the gas phase. Coalescence of two neighbouring lamellae frequently occurred and caused formation of thick liquid lenses. The blocking was almost complete, resulting in no flow under gas pressure gradients of up to 20 bars per meter.
In order to further investigate the causes of the sliding of the lamellae over the grain covering liquid films, Atomic Force Microscopy was used to investigate the solid liquid interface. Unespected results were obtained when a surfactant solution was put in contact with a surface of mica. Instead of the mono or bilayers of surfactant molecules expected to be found adsorbed at the surface, a thick layer of surfactant was found. Agregates of a large size (60 nanometers and more in diameter) are present at the top surface of this layer when the surfactant solution is above the critical micelle concentration (CMC). More experiments are in progress to better define the amount of surfactant used in this layer. The presence of this previously unknown layer could be an explanation to the elastic behavious of the liquid phase observed in the micromodel. It could also parly explain the sliding of some lamellae without breackage frequently seen in the experiments.
Further work will include coinjection tests as well as an investigation of the effect of crude oil on the flow mechanisms. The results obtained in the micromodels should be compared to similar tests made in sandpacks under similar conditions. Oil resistant surfactants will also be tested at that stage.

Introduction

Foam as an enhanced oil recovery method has been sucessfully tested in a variety of fields and conditions (Castanier, Hanssen, Castanier and Hanssen). Predictive modelling of foam flow is however not possible to date except through the use of empirical simulators. The first step towards modelling and optimization of foam flow in porous media is to identify and describe the flow mechanisms at the pore level. Numerous studies have been done in a variety of systems ranging from glass beads to cores , encompassing glass etched micromodels and slabs of rocks. The present work aims at understanding foam flow mechanisms at the pore level through visualisation in realistic micromodels.
Most of the techniques used in the past present problems. Bead packs have a regular pore geometry which causes the foam texture to be incorrect. Etched glass micromodels have pores and necks an order of magnitude bigger than the reservoir rocks, slabs and cores do not allow easy visualisation of the flow at the pore level. The goal of the design and construction of the `realistic´micromodels is to eliminate those problems.
This study uses new silicon micromodels designed and built at Stanford University. The design and construction of such models can be found in Hornbrook et al (1991) and Hornbrook, Pettit and Castanier (1992). For the experiments conducted at RF, a thin

section of Berea sandstone was used as a pattern to manufacture the models. Pore sizes range from 0.5 to 200 microns and the depth of the channels is about 15 microns. The etching of the channels is vertical as verified by Scannin Electron Microscopy. The surface of the model is silicon oxyde which provides for a water wet surface.
This report presents a brief summary of the state of the art knowledge of foam flow at the pore level made through selected literature review, describes the experimental setup and operating procedures and discusses the results. No conclusions will be drawn at this early stage but speculations on possible future work in terms of modelling and experimental effort are presented at the end.

Commonly Accepted Concepts of Foam Flow Mechanisms in Porous Media.
It would be outside the scope of this work to completely review the extensive literature on foam flow through porous media, instead we will briefly describe some of the main concepts generally believed to be correct to date.
Foam was at first assumed to flow through porous media as a homogenous mixture of liquid and gas with a higher viscosity than both components. This concept has now been proven wrong through measurements of liquid and gas velocities as well as direct observations in micromodels.
There is a consensus today in the literature on the fact that liquid and gas flow at different velocities. Liquid films (termed lamellae or lenses) separating the gas phase in discrete bubbles are generated by various mechanisms (snap off, leave behind, division) and destroyed by gravity drainage and excessive pressure gradients. An equilibrium is reached between those processes and a population balance can be established between creation and destruction of those films. The number and strength of the films at a given moment determines the resistance to gas flow. Disjoining pressure seems to be an important parameter to determine film strength (Bergeron and Radke). This concept was found through large size micromodel observations and capillary tubes experiments. For more details on those concepts, the reader can refer for example to Falls et al. 1988, Hanssen 1992, Hirasaki, 1989, Radke and Ettinger, 1992, Radke and Gillis, 1990, Radke and Ransohoff, 1988. Attempts to model foam flow using the population balance method have been made by several researchers. The simulators created using this method are however cumbersome and require as input parameters that have not been well defined experimentally such as number of bubbles or lammella as a function of surfactant presence and concentration. Most authors have matched core floods to obtain those parameters. Application of such simulators to field performance prediction is dificult to implement to date because of the scaling problem.
The presence of oil complicates the problem. Generally oil reduces film strength and numbers. Although the interaction of oil and foam has been studied (Wasan et al. 1988, Radke and Manlowe 1990, Hombrook et al. 1992, Dalland et al. 1994) much remains to be done to fully explain how oil affects foam. As a result modelling of foam flow in presence of oil is still more an art than a science.

Experimental Apparatus and Procedure
A schematic of the experimental set up is presented in figure 1. The micromodel is placed under an Olympus microscope connected to a videocamera. A differential pressure transducer allows measurement of the pressure gradient across the model. Gas flow rate is measured by collecting the produced gas in a test tube at the outlet of the model. Because of the small volume of the pores it is impossible to measure the liquid saturation in the model directly. Saturation estimates can however be made from the pictures recorded via the videocamera. A pressure cylinder connected to a compressed gas bottle provides the driving force for saturating the model and flowing gas under constant pressure conditions (blocking mode). A syringe pump on loan from IKU can be used for constant rate experiments.

In the blocking mode experiments, the model is first saturated with a surfactant solution and gas is then introduced at constant pressure. Gas flow rate is recorded which allows an estimate of the mobility reduction caused by the foam. Coinjection experiments (constant rate) only involve flowing a given ratio of gas and surfactant solution through the micromodel. Presssure is recorded during such runs. Visual observations are made through the microscope and recordings can be made on demand via the videocamera.

Results to date and Discussion

Most of the experiments performed to date are in the blocking mode. Six runs were carried on at concentrations of AOS 16 of 0, 1, 10,100,1000 and 10,000 ppm respectively. Distilled water was used in all experiments without any inorganic salt added.

The base case run without surfactant yielded expected results. The entrance pressure for the gas to penetrate into the model is about 12psi (0.80 bars). This is in line with Berea capillary pressure data and comparable with values calculated from the neck sizes at about 10 psi (.67bars). The gas follows channels consisting mainly of large pores and invades preferentially the large pores as expected because gas is the nonwetting phase. The smaller channels remain filled with water. This is again consistent with multiphase flow theories. As the model is strongly water wet, a thin water film remains around the grains but does not show significant movements as the gas flows.

Increasing the surfactant concentration first to 1ppm then to 10ppm showed only a small change in behaviour except for the fact that the entrance pressure was reduced to 7.5 psi (0.5bars). At 100 ppm concentration, the entrance pressure is 5 psi (.34bars) and the gas invades the smaller pores network. This is consistent with measured surface tension data for the AOS 16 surfactant. A pattern of alternating small liquid slugs followed by larger gas bubbles was observed. No lamellae could be seen at those concentration. The liquid network around the grains is now thicker than at very low concentrations

At 1,000 ppm concentration, lamellae start to appear. Most of the time they are rather insolated and stagnant at a pressure gradient of up to 15 psi (1bar) across the micromodel. Most of the lamellae are in fact lenses of liquid bridging the narrow parts of the model. Figure 2 shows examples of those. Some thiner lamellae are also present in the larger pores (fig.3). The liquid films around the grains are thick and the dead end pores act as liquid reservoirs, emptying when the films strech and filing up again as the part of the model under observation becomes quieter . This type of behaviour is illustrated on fig.4. In (a), a lamella is positionned at a pore neck. Under the effect of pressure gradient in the gas phase, it moves towards the pore. The liquid film around a nearby pore thickens at the same time (b) . The lamella jumps to the next pore without rupture (c). A new lameela appears at the initial position by sliding from the nieighbouring pores (d). The lamellae exibit elastic type behaviour, almost no breakage was observed. generation events are also quite rare in the system. The prevalent mechanism of flow seems to be for the gas to force the lamellae to slide without breacking on the films covering the grains then jump from one grain to the next (fig.4). One can also observe frequent coalescence of two neighbouring lamellae separated by a slowly diseapearing gas bubble. Such events are shown on fig.5. In this illustration , coalescence of two lamellae is first observed and is shown in parts (b,c,d,e) then the resulting lamella jumps across a pore and divides (f). this results in the formation of several lenses and a large film bridging the pore as seen in frame a. If the pressure gradient is higher at the same site, 'bulk'type foam can be observed sliding along the grains. This is shown on frame g. As the local gradient deceased, the system slowly goes back to equilibrium positions as shown in frame h. This mechanism is obviously controlled by an interplay between the gas diffusion across the liquid films and the capillary forces pulling the two lamellae together. The liquid network often seems to wiggle as gas slugs flow by it. Figure 6 shows a typical case where a thin film briges a large pore (a) . Under events occuring outside the field of view, the liquid film around the grains thickens (frames b and c), then returns to position (a). One must note the role of the dead end pores acting as liquid reservoirs. This 'elastic' behaviour of the liquid network

both around the grains and as lenses and lamellae surrounded by gas has not been to our knowledge reported before this work but seems to be an important part of the gas mobility reduction observed in presence of foam.
As pressure across the model was increased to about 40 psi (2.6bars), the number and activity level of the lamellae increased but the expected breacking and reforming of the lamellae did not occur (see figure 5 frames g and h for example). Sliding is the main transport method, sometimes coupled with jumps that become more frequent as the pressure gradient increases. Some formation of additional lamellae was observed by division during the jumps. A slower lamella apears after a fast jumping one when enough liquid is present at the site (figure 5 frame f). A few snap off events were detected at one site. This is obviously controlled by the liquid supply at this site with the liquid being transported by the film network surrounding the grains. The forces exerced by the liquid on the lamellae against the gas flow are so strong that backwards movement of lamellae was frequently observed against the pressure gradient in the gas phase as indicated by the lamellae curvature . This generally occurs during the transition when a lamella bridging a large pore goes back to a lense bridging a narrow channel.
The observations discussed above are very different from observations that can be made in larger geometry micromodels. The ratio between lamellae thickness and length is much larger in realistic micromdels than in common etched glass models. The role of the liquid films covering the grains is also more important because the liquid transport through this films is easier and faster in reservoir sized networks. Dead end pores also greatly affect the flow behaviour, specially by acting as reservoirs for the liquid network. Generation and breakage of lamellae are much less frequent in realistic size systems than in the large scale micromodels used by a majority of researchers on foam.

Atomic Force Microscopy Results
As the blocking foam behaviour in the models appear to strongly depend on sliding of lamellae along the surfactant coverred grain surface, investigation of the solid liquid interface is of interest. A nanometer (Atomic Force Microscope) located in the physics department of the Technical University at Munich (Germany), was used to image a mica surface in contact with solutions of the same AOS 16 surfactant used in our experiments. Mica is strongly water wet and presents surface properties close to those of silica. A detailled analysis of the results would be outside the scope of this report but will be expanded in a future publication. We will only here present the conclusions to date in broad terms. Details of the equipment and its use can be found in Professor Gaub´s group publications. For the purpose of this study the goal was only to obtain a qualitative idea of the rock/surfactant solution interface.
It is generally accepted that surfactant molecule adsorbe at the rock surface. In theory, mono or bilayers of surfactant molecules will cover the surface if enough adsorbtion occurs. The behaviour observed in our system was different. A thick (several hundred nanometers)multilayer of surfactant was at the mica surface. This layer behaved elastically under the nanometer needle. It deformed when disturbed and then came back to its original position after some time. Above the CMC, macrosystems were observed on top of the layer. Their sizes range from 60 to 150 nanometers, way bigger than the expected miscelles from AOS 16. These systems are soft and are easilly disturbed by the nanometer needle. When spread over the multilayer of surfactant, they stay where they are, just adding more layers to the surfactant mass.
The presence of this thick surfactant multilayer at the rock/liquid interface has not been previously reported. Similar concepts have been mentionned in the biology literature for surfactant like materials such as albumin. For enhanced oil recovery, the implications of this find are important. In particular, models of surfactant adsorbtion will need to take that problem into account.

In terms of foam flow, that layer could be the substrate on which the gas liquid films can slide. The ample supply of surfactant that it provides stabilizes the films thus explaining the very few rupture events observed. The observations of varying thickness of the liquid films around the grains can also be explained by that surfactant layer at the rock surface attracting water and reacting under gas pressure changes. It could also be a contributing factor to the large residual liquid saturation observed in blocking foam in the realistic micromodels.

Some Preliminary Conclusions

The mechanisms of foam flow under constant pressure in a realistic sized micromodel differ greatly from the accepted theory. In particular, sliding and jumps seems to be the main transport mechanism instead of breaking and reforming of films. The contribution of the liquid network around the grains and in the smaller pores is important and needs to be further studied. The population balance models are probably valid but need to be refined to take into account the liquid network elastic behaviour.

Examination of the rock surface showed a thick surfactant layer which also needs to be studied further. This could have implications not only for foam studies but for surfactant flooding as well.

Obviously more work needs to be done. Suggested studies are repeat experiments in coinjection mode at constant rates instead of constant gas pressure, further examination of the surfactant layer discovered by atomic force microscopy and use of different types of surfactants. Effect of oil on the pore level mechanisms of flow is also an important aspect of the problem that needs further attention.

Acknowledgements

Numerous persons and organizations contribute to this work. Hildegard Tengberg-Hansen has run the realistic micromodels experiments. Mariann Dalland contributed comments and suggestions. The models were made in the Petroleum Engineering Department at Stanford University. Last but not least, special thanks are due to the E 22 group at the Technical University in Munich where professor Gaub and his students gave access to a nanometer and provided help and advice in interpreting the results. Financial support from the Fulbright Foundation and the RUTH program is gratefully ackowledged.

Selected Bibliography

1. Castanier, L.: "Steam with additives: Field projects of the '80s," *Journal of Petroleum Science & Engineering* (1989) **2**, 193-206.
2. Dalland, M., Hanssen, J.E., and Kristiansen, T.S.: "Oil interaction with foam under static and flowing conditions in porous media," *Colloids and Surfaces A: Physicochem. Eng. Aspects* (1994) **82**, 129-140.
3. Dullien, F.A.L.: *Porous Media – Fluid Transport & Pore Structure,* Academic Press, (1979).
4. Ettinger, R.A.: "Foam Flow Resistance in Berea Sandstone," MS Thesis, Univ. of California, Berkeley (1989).
5. Falls, A.H., *et al.*: "Development of a mechanistic foam simulator: The population balance and generation by snap-off," *SPE Reservoir Engineering* (August 1988) 884-892.
6. Gauglitz, P.A.: "Coalescence during division: A mechanism of lamella rupture in porous media," *Proc.*, AiChE National Meeting, Chicago (1990)
7. Gillis, J.V.: "Tracer Detection and Structure of Stationary Lamellae during Foam Flow through Berea Sandstone," PhD Thesis, Univ. of California, Berkeley (1990).
8. Hanssen, J.E., Jakobsen, K.R., and Meling, T.: "Interaction of gas-blocking foam with oil in model porous media," *Progress in Colloid & Polymer Science* (1990) **81**, 264-265.

9. Hanssen, '.E.: "Foams for gas flooding," *SPOR Monograph: Recent advances in Improved Oil Recovery Methods for North Sea Sandstone Reservoirs*, S.M. Skjæveland and J. Kleppe (ed.), Norwegian Petroleum Directorate, Stavanger (1992) 277-283.
10. Hanssen, J.E.: "Foam as a gas-blocking agent in petroleum reservoirs. II: Mechanisms of gas blockage," *Journal of Petroleum Science & Engineering* (1993) **10**, No. 2, 135-156.
11. Hanssen, J.E.: "Foam as a gas-blocking agent in petroleum reservoirs. I: Empirical observations and parametric study.," *Journal of Petroleum Science & Engineering* (1993) **10**, No. 2, 117-134.
12. Hanssen, J.E. and Holt, T.: "Foam processes: An evaluation of field experience towards foam application in Norwegian reservoirs," Report RF, Stavanger (1993).
13. Hirasaki, G.J.: "The Steam-Foam Process," *Journal of Petroleum Technology* (May 1989) 449-456; complete text available from Society of Petroleum Engineers as a Supplement to SPE 19505.
14. Holt, T. and Kristiansen, T.S.: "Foam flooding using alpha olefin sulfonates," *Proc.*, 5th European Symposium on Enhanced Oil Recovery, Budapest (1989)
15. Hornbrook, J.W., Castanier, L.M., and Pettit, P.A.: "Observation of foam/oil interactions in a new, high-resolution micromodel," Paper SPE 22631 presented at the 1991 66th SPE Annual Technical Conference and Exhibition, Dallas.
16. Jímenez, A.I.: "Stability of Thin Liquid Films: Theory and Application to Foam Flow in Porous Media," PhD Thesis, Univ. of California, Berkeley (1991).
17. Isaacs, E., Best, D.A., and Tam, E.S.: "A discussion on the mechanism of foam flow through porous media," *Proc.*, 3rd Int. Conf. on Heavy Crude and Tar Sands, (1985) United Nations, New York, 518-533.
18. Kovscek, A.R. and Radke, C.J.: "Fundamentals of foam transport in porous media," *Foams: Fundamentals and Applications in the Petroleum Industry*, L.L. Schramm (ed.), Advances in Chemistry Series, American Chemical Society, Washington, DC (1993) **242**, .
19. Kovscek, A.R. and Radke, C.J.: "Simulation of foam transport in porous media," Paper SPE 26402 presented at the 1993 68th SPE Annual Technical Conference and Exhibition, Houston.
20. Manlowe, D.J.: "Pore-Level Mechanisms of Foam Destabilization by Oil in Porous Media," MS Thesis, Univ. of California, Berkeley (1988).
21. Minssieux, L.: "Oil Displacement by Foams in Relation to their Physical properties in Porous Media," *Journal of Petroleum Technology* (January 1974) 100-108.
22. Novosad, J.J. and Mannhardt, K.: "Modelling adsorption of foam-forming surfactants," *Revue de l'Institut Français du Petrole* (1988) **43**, No. 5, 659-671.
23. Owete, O.S. Castanier L.M. and Brigham, W.E.: "Flow Behavior of Foam: A Porous Micromodel Study," *SPE Reservoir Engineering* (August 1987) 315-323.
24. Owete, O.S. and Brigham, W.E.: "Flow of foam through porous media," Report SUPRI TR-37, Stanford University Petroleum Research Institute, Stanford (1984). 113 pp.
25. Patzek, T.W.: "Description of Foam Flow in Porous Media by the Population Balance Method," *Surfactant-Based Mobility Control*, D.H. Smith (ed.), ACS Symposium Series, American Chemical Society, Washington DC (1988) **373**, 326-343.
26. Prieditis, J.: "A Pore Level Investigation of Foam Flow Behavior in Porous Media," PhD Thesis, Univ. of Houston, Houston (1988).
27. Radke, C.J. and Ransohoff, T.C.: "Mechanisms of Foam Generation in Glass-Bead Packs," *SPE Reservoir Engineering* (May 1988) 573-585.
28. Radke, C.J. and Jímenez, A.I.: "Dynamic stability of foam lamellae flowing through a periodically constricted pore," *Oil-Field Chemistry: Enhanced Recovery and Production Stimulation*, J.K. Borchardt and T.F. Yen (ed.), ACS Symposium Series, American Chemical Society, Washington (1989) **396**, 461–479.
29. Radke, C.J. and Gillis, J.V.: "A Dual Gas Tracer Technique for Determining Trapped Gas Saturation during Steady Foam Flow in Porous Media," Paper SPE 20519 presented at the 1990 65th SPE Annual Technical Conference and Exhibition, New Orleans.

30. Radke, C.J. and Manlowe, D.J.: "A Pore-Level Investigation of Foam-Oil Interactions in Porous Media," *SPE Reservoir Engineering* (November 1990) 495-502.
31. Radke, C.J. and Chambers, K.T.: "Capillary phenomena in foam flow through porous media," *Interfacial Phenomena in Petroleum Recovery*, N.R. Morrow (ed.), Surfactant Science Series, Marcel Dekker, Inc., New York and Basel (1991) 191-255.
32. Radke, C.J. and Ettinger, R.A.: "The influence of texture on steady foam flow in Berea sandstone," *SPE Reservoir Engineering* (April 1992) 83-90.
33. Schramm, L.L., Turta, A.T., and Novosad, J.J.: "Microvisual and coreflood studies of foam interactions with a light crude oil," Paper SPE/DOE 20197 presented at the 1990 SPE/DOE 7th Symposium on Enhanced Oil Recovery, Tulsa.
34. Schramm, L.L. and Novosad, J.J.: "Micro-visualization of foam interactions with a crude oil," *Colloids and Surfaces* (1990) **46**, 21-43.
35. *Foams in the Petroleum Industry*, Schramm, L.L. (ed.), Advances in Chemistry Series, American Chemical Society, Washington (1993)
36. Wasan, D.T., Nikolov, A., and Huang, D.: "Foams: Basic Properties with Application to Porous Media," *Langmuir* (1986) No. 2, 672-677.
37. Wasan, D.T., *et al.*: "Effect of Oil on Foam Stability: Mechanisms and Implications for Oil Displacement by Foam in Porous Media," Paper SPE 15443 presented at the 1986 61st SPE Annual Technical Conference and Exhibition, New Orleans.

PROJECT 4: RESERVOIR DEFINITION

To develop and improve techniques of formation evaluation such as tracer tests and pressure transient tests.

There are no students presently working on this project.

PROJECT 5: FIELD SUPPORT SERVICES

To provide technical support for design and monitoring of DOE sponsored or industry initiated field projects.

5.1 STEAM DRIVE OPTIMIZATION
(Amita Garg)

5.1.1 ABSTRACT

Steam drive is employed in heavy oil reservoirs to improve oil mobility by reducing the viscosity of reservoir fluids, and provides the additional benefit of producing a hydrocarbon rich vapor phase. The light components are condensed at the condensation front and mix with the oil in place to produce a lower viscosity crude oil. Thus steam drive can be an efficient and successful method of heavy oil recovery. Though there have been many steam drive pilots and large-scale operations, an optimization of the steam injection process has not been fully researched.

The objective of this research was to determine an optimal injection schedule to minimize steam use and maximize oil recovery. This objective was achieved by applying economic constraints on steam drive production performance calculations. The primary steps include:

1. Developing a representative steam-drive model to convert heat injection into an oil recovery prediction,

2. Incorporating an economic model to relate injection and handling costs with production revenue,

3. Optimizing the economic function using a multivariable, nonlinear optimization technique.

A general optimization method has been developed to maximize net present value by adjusting injection rate. Prior to steam breakthrough the maximum injection rate feasible is recommended, then after breakthrough, reductions in injection rate provide the most economically efficient recovery history.

5.2 STEAMFLOODING A WATERFLOODED RESERVOIR -- PERFORMANCE EVALUATION AND PREDICTION

(Sameer Joshi)

5.2.1 SUMMARY

This paper was prepared for presentation at the 1995 Western Regional Meeting held in Bakersfield, March 8-10, 1995.

SPE 29669

Steamflooding a Waterflooded Reservoir -- Performance Evaluation and Prediction

Sameer Joshi, Stanford University, Mike C. Wood, Union Pacific Resources Co.,
L.M. Castanier and W.E. Brigham, Stanford University

SPE Members

This paper was prepared for presentation at the 1995 Western Regional Meeting held in Bakersfield, CA, U.S.A., 8-10 March, 1995.

ABSTRACT

The Wilmington Steamflood of Union Pacific Resources Co. (UPRC) at Long Beach, CA was initiated in 1989, in a previously waterflooded reservoir. Average initial reservoir oil saturation, at the start of the steamflood, was 35%.

Field production data were studied, to derive an overall energy balance for the steamflood, to calculate the steamflood capture efficiency and predict further steamflood performance. Heat-losses due to produced fluids were calculated. Predicted production schedules from the model were history-matched with field production data.

All steamflood calculations were carried out using a PC-based spreadsheet program. The major results were as follows:

- The capture efficiency of the Wilmington steamflood was calculated at 60%. This is an acceptable value, taking into account the fact that the reservoir had previously been waterflooded to a low oil saturation of 35%.
- The calculated heat balance showed a high heat-loss, not only to adjacent formations, but also through produced fluids. Of the cumulative heat injected up to the time of the study, 21% had been lost to vertical conduction and 21% through produced fluids.
- Predicted production schedules indicated that up to 43% of the oil in place (at steamflood initiation) would be recovered by the steamflood.

WILMINGTON STEAMFLOOD

The Wilmington Oil field, Los Angeles County, California is the third largest in the U.S., after Prudhoe Bay and the East Texas fields, on the basis of cumulative oil production, with a total of 2.4 billion barrels produced. A good description of the initial pilot steam flood carried out by UPRC in this field from 1982-1989 is given by Lim et al., 1993 [1]. The pilot 20 acre steamflood is now part of the main 130 acre Wilmington Steamflood. The portion of the field studied had initially been waterflooded to a low oil saturation of 35% before the main steam flood was initiated in 1989.

The steam flooded reservoir is unconsolidated sandstone in the Tar Zone (T, D1 and D3 members) with average gross and net thicknesses of 170 feet and 128 feet respectively. Average reservoir pressure was estimated at 350 psig in 1993. The steam flood project has a surface pattern area of 129.73 acres divided into approximately 17 individual seven-spot patterns, each of 7.5 acres. Average well depth is 2500 feet. The oil in place at steam flood initiation was calculated at 18 million barrels with a movable oil volume of 12.9 million barrels, assuming an initial oil saturation, S_{oi}, of 35% (at steam flood initiation), a final oil saturation S_{or} of 10% and an average porosity of 40%. Volumetric

References and illustrations at end of paper.

calculations were carried out using a three-dimensional surface modeling and visualization program on a Unix workstation. All other calculations were carried out using PC based spreadsheet programs. Reservoir and production data was obtained from UPRC records and computer databases. Production data was available from the time of steam flood initiation in May 1989 up to July 1993.

The method of analysis followed in this study was essentially as follows:

1. Determine a heat balance for the steam flood project by calculating the following heat-loss mechanisms:
   - Surface steam distribution network
   - Determine Injection well-bores
   - Produced fluids
   - Vertical conduction to adjacent formations
2. After accounting for the above heat-losses, calculate a saturated steamed area and, thus, a steam zone volume.
3. From the steam zone volume, calculate a displaced oil rate versus time and attempt a history match with the recorded production rates. This step also determines the capture efficiency of the steamflood.
4. Use the history matched model to predict future oil production under different assumed operating scenarios.

It was determined that the largest amount of heat loss out of the steam flood area was to the adjacent formations and by way of produced fluids, each being 21% of the cumulative injected heat up to July 1993. As of July 1993, 4.79 million barrels of oil had been produced by the steam flood. It is predicted in the present study that 7.8 million barrels of oil will be recovered by the time the pattern area is fully saturated with steam. The capture efficiency of the Wilmington steamflood was calculated at 60%.
The following sections will describe the models used and results obtained.

CALCULATION OF HEAT-LOSSES

The first step of the analysis consisted of calculating the magnitude of heat losses in different subsystems of the steam flood system. Heat losses were calculated, as mentioned earlier, for the following subsystems:

1. Surface steam distribution network
2. Injection well-bores
3. Produced fluids
4. Vertical conduction to adjacent formations

Surface Steam Distribution Network

The distribution network consisted of a total length of about 18,900 feet of different sizes of surface pipelines which conveyed steam from the generator to the well heads. Pipes varied in size from 1.5 inches to 14 inches, with insulation thicknesses ranging from 1 inch to 4 inches. The basic equation used to calculate heat-losses per unit length, $\dot{Q}_{ls}$ is Reference [2], Equation 10.1 (page 125).

$$\dot{Q}_{ls} = \frac{(T_b - T_a)}{R_h} \quad \text{.....(1)}$$

where T_b is the bulk temperature of the fluid in the pipe, T_a is the ambient temperature and R_h is the specific thermal resistance (thermal resistance per unit length) of pipe or wellbore, given in units of (BTU/ft-Day-°F)$^{-1}$ {1 BTU = 1055.056 Joule; 1°F= 1.8(temperature in °C)+32}. A steam temperature of 580 °F, ambient temperature at 60°F and an average wind speed of 20 mph normal to the surface pipelines was assumed, with steady state conditions.

For a pipe covered with insulation, R_h is given by Reference [2] Equation 10.2. (page 126). If scale deposits, contact thermal resistances, thermal resistance due to pipe and the film coefficient of heat transfer between steam and pipe are neglected, the equation reduces to

$$R_h = \frac{1}{2\pi}\left[\frac{1}{\lambda_{ins}} \ln \frac{r_{ins}}{r_o} + \frac{1}{h_{fc} r_{ins}}\right] \quad \text{.....(2)}$$

where:

λ_{ins} = thermal conductivity of the insulation,
r_o = outer radius of the pipe,
r_{ins} = outer radius of the insulation,
h_{fc} = heat transfer coefficient due to forced convection on the outer surface of the insulation.

h_{fc} can be calculated using Reference [2], Equation 10.4 (page 129).

$$h_{fc} r_{ins} = 18 v_w^{0.6} r_{ins}^{0.6} \quad \text{.....(3)}$$

where v_w is the wind speed in miles per hour normal to the pipeline.

The calculated heat-loss rates for different insulated pipe sizes used in the field are shown in figure 1. The heat loss distribution between different insulated pipe sizes used in the field is shown in figure 2. The highest heat-loss contribution is from the 3 inch and 14 inch pipelines which account for a loss of 28.8 MMBTU/D (57.5% of the total pipeline heat-loss). The total loss due to all pipe was calculated as 50 MMBTU/D which is 0.5% of the cogenerator output. The total length of pipe in the field is 18,900 feet.

Heat-Losses in Injection Wells

The specific thermal resistance is given by Reference [2] Equation 10.6 (page 129). After neglecting insignificant terms it reduces to

$$R_h = \frac{1}{2\pi}\left[\frac{1}{\lambda_{ins}} \ln\frac{r_{ins}}{r_o} + \frac{1}{h_{rc,an} r_{ins}} + \frac{1}{\lambda_{cem}} \ln\frac{r_w}{r_{co}} + \frac{f(t_d)}{\lambda_E}\right] \quad \text{.....(4)}$$

Here:

r_w = well radius,
λ_{cem} = thermal conductivity of the cement
λ_E = thermal conductivity of the earth,
$h_{rc,an}$ = the radiation and convection coefficient of heat transfer for the annulus,
$f(t_d)$ = the time function that reflects the thermal resistance of the earth.

$f(t_d)$ is a function of the dimensionless time t_d given by

$$t_d = \frac{\alpha_E t}{r_w^2} \quad \text{.....(5)}$$

where α_E is the thermal diffusivity of the earth in square feet per day and t is the time in days.

An iterative procedure is used to find both R_h and $h_{rc,an}$. An example calculation is shown in Reference [2] (page 130). Calculations for an average injection well in Wilmington indicates that the heat-loss rate varies with time as shown in figure 3. An average Wilmington well is 2500 feet deep, with a well radius of 10 inches, casing diameter of 7inches and tubing diameter of 3.5inches.

Using an average value of the heat-loss rate over 10 years, the total heat loss due to all injection wells is calculated at 130 MMBTU/D which is about 1.5% of the cogenerator capacity. Thus the total heat-loss due to surface pipelines and injection wells is calculated at 2% of the total cogenerator output. This is a low value and indicates that the insulation methods adopted for the steam injection distribution system are adequate.

Heat-Loss through Produced Fluids

Heat-loss through produced fluids is the heat transported out of the reservoir by the produced oil and water. The factors determining this are the oil and water flow rates, the bottomhole flowing temperatures and the fluid specific heats and enthalpies.
The oil and water production rates are known. The bottomhole flowing temperature was determined from the average surface flow line temperature using an adaptation of Ramey's equations, given by Reference [2], Equation 10.13 (page 133). Assumptions made while deriving the equation were

- The system is at steady state, except for conduction heat-losses into the earth
- Friction pressure drop is negligible
- Vertical heat-transfer is by convection only
- Heat-losses to the formation are radial

In this calculation an average value of the specific heat over the given temperature range was used. The specific heats of the fluids were calculated using Gambill's correlations, given for liquid hydrocarbons and oil by,

$$c_o = \frac{(0.388 + 0.00045T)}{\sqrt{\gamma_o}} \quad \text{.....(6)}$$

where c_o is the specific heat (BTU/lb-°F), γ_o the specific gravity and T the temperature (°F).

For saturated water, the corresponding relation is,

$$c_W = 1.0504 - 6.05\times10^{-4} T + 1.79\times10^{-6} T^2 \quad \text{.....(7)}$$

where c_W is the specific heat (BTU/lb-°F), and T is the temperature (°F)

Average values of specific heats for the operating temperature range were used in the calculations.

Figure 4 plots the measured flow line temperatures and corresponding BHT's. The total heat-loss rate due to produced fluids and that due to water alone are plotted in figure 5. The difference between the two rates is very small, as expected, since at an oil cut of 10% the majority of fluid production is water, which also has a higher specific heat than oil. The heat-loss due to produced fluids as a percentage of the cumulative heat injection since the start of the steamflood (May 1989) is shown in figure 6. It can be seen that a large fraction of the injected heat (21% up to 7/93) is lost through produced fluids. At present, this heat is not being effectively utilized. The magnitude of the heat-loss suggests that it may be feasible to try to recover some of this heat by means of a heat exchange process.

Adjacent Formation Heat-Losses

The Marx and Langenheim method was used to calculate adjacent formation heat-losses. Since the varying average monthly heat-injection rates were known, it was decided to use Ramey's generalization of this method to variable rates of heat injection. See References [3] and [4]. The main assumptions of this model are:

- The pressure drop due to the flow is sufficiently small such that the steam zone temperature throughout the reservoir is constant and equal to the temperature of the injected steam
- Heat-losses from the reservoir are only by vertical conduction to adjacent formations
- There is a piston-like vertical displacement of the steam front

Myhill and Stegemeier (1978) [5] have pointed out that for this heat-loss model (and its extensions) to be applicable, it is not necessary that the heat front be vertical. It is only necessary that the total volume of the steam zone can be represented by the expression (Ah/2) where A represents the sum of the upper and lower surface areas where the steam zone contacts the adjacent layers and h the vertical distance between them. For example, a sloped but straight front that is advancing linearly. A comparison by Satter and Parish in 1971 [6] of the heat-losses obtained with the Marx and Langenheim model and those calculated from a numerical simulator has shown that the difference between the results varies from 0.5% to 3.5%, depending upon the injection rates and pressures.

The major variables involved in this model are:

- The heat injection rate history
- Gross formation thickness
- Formation and adjacent formation thermal parameters (thermal conductivity and heat capacity)
- Elapsed time

The rate of advance of the steam front is determined by the heat loss to the adjacent strata. If the heat injection rate can be expressed by constant monthly average values then the heat remaining in the reservoir at any time is given by Reference [2], Equation 5.20 (page 47). This equation was used to calculate the percentage of the net injected heat that remained in the reservoir at any time. Figure 7 shows the percentage of the cumulative net injected heat since 5/89 that is lost to adjacent formations. It can be seen that the rate of heat loss was very high initially but then decreased. By the end of May 1993, 27% of the net injected heat had been lost to the adjacent formations. The cumulative heat-loss data is summarized in Table 1. A distribution of the cumulative injected heat as of 7/93 is shown in Figure 8.

CALCULATION OF PRODUCTION RATES

A simple analytical steamflood model based on Ramey's generalization of Marx and Langenheim's method [3, 4] was used to predict oil production rates. A history match was obtained using the model and was further used to predict future oil production rates for 3 different cases.

After accounting for adjacent formation heat losses, the model calculates a saturated steamed area and thus a steam zone volume. The model assumes that all the movable oil in the steam zone is displaced. From this a displaced oil rate can be calculated. However, this calculated rate will differ from the actual oil production rate due to the following reasons:

- The amount of oil displaced out of the steam zone will depend upon the sweep efficiency
- All of the displaced oil will not be produced

To account for these effects a capture efficiency E_c is defined which is the fraction of the displaced oil that is actually produced. The capture efficiency for the Wilmington steamflood was determined by trying to match the measured production rates with the calculated production rates. It was found that the calculated rates had to be multiplied by a factor of 0.60 to obtain a good

history match. This value also provided a good match with the measured cumulative production. Thus it was concluded that the capture efficiency for the Wilmington steamflood is 60%. The unadjusted rates matched well during later times, but were too high initially. A comparison by Myhill and Stegemeier [5] of results from different steam drive field projects indicated that the capture efficiencies varied from 0.66 to 1.1 (a value of 1.1 indicates that oil is being produced from outside the pattern area by factors such as gravity drainage). This comparison is shown in Table 2. The calculated vs. actual production rates are shown in figure 9 after reducing the calculated rates by the capture efficiency. Future production rates were predicted for three different cases:

Case 1: Constant steam injection rate of 25,000 bbls/D
Case 2: Constant steam injection rate of 21,000 bbls/D. which corresponds to the scenario of full injection into Phase 1C and Phase 2 while maintaining the current steamflood. This is the present case in the oilfield.
Case 3: Steam rate decreasing by 3,000 bbl/D every year, which corresponds to the scenario of drilling a new pattern every year outside the current pattern area, with each pattern requiring an injection rate of 3,000 bbl/D. The predicted rates are shown in figure 10. The predicted data is summarized in Table 3.

Cases 1 and 2 indicate that the recovery from the present steamflood at the time saturated steam fills up the area will be 7.8 million bbls of oil which is 43% of the calculated OOIP (18 million bbls) at steamflood initiation. Since the model assumes a vertical displacement front with no gravity override, steam breakthrough may occur earlier than the predicted steam fillup date, with correspondingly lower production rates and recovery, thereafter.

CONCLUSIONS

1. The pipeline and tubing insulation are adequate in controlling heat-losses.
2. A high proportion of heat-loss is due to produced fluids and the adjacent formations as 21% of the injected heat had been lost through produced fluids and 21% to adjacent formations by July 1993.
3. Based on a simple model, the capture efficiency for the Wilmington steamflood was calculated at 60%, as compared to values of between 66% and 110% for other steamfloods.
4. Over 7.3 million bbls of the OOIP (43%) will be recovered when saturated steam has filled the steamflood area.
5. The current steamflood (Case 2) is predicted to decline at a nearly constant rate of 193 BOPD/yr.

NOMENCLATURE

α_E	Thermal diffusivity of earth
γ_o	Specific gravity of oil
λ_{cem}	Thermal conductivity of cement
λ_E	Thermal conductivity of Earth
λ_{ins}	Thermal conductivity of insulation
BOPD	Barrels of oil per day
BTU	British Thermal Unit
c_o	Specific heat of oil
c_w	Specific heat of water
E_c	Capture efficiency
F	degree Fahrenheit
$f(t_d)$	Time function reflecting thermal resistance of earth
h_{fc}	heat transfer coefficient due to forced convection on outer surface of insulation
$h_{rc,an}$	Radiation and convection coefficient of heat transfer for annulus
$\dot{Q}_{ls}$	Heat loss per unit length
R_h	Specific thermal resistance
r_i	inner radius of pipe
r_{ins}	Outer radius of insulation
r_o	Outer radius of pipe

S_{oi}	Initial oil saturation
S_{or}	Residual Oil saturation
T_a	Ambient temperature
T_b	Bulk temperature of fluid in pipe
v_w	Wind velocity

ACKNOWLEDGEMENTS

The authors wish to thank the management of Union Pacific Resources Co. for permitting the use of data acquired by them.

REFERENCES

1. Lim et al.: SPE 26615, 1993.
2. Prats, Michael: "Thermal Recovery", SPE Monograph Volume 7,1982.
3. Ramey, H., J.: Discussion of Marx and Langenheim paper, Petroleum Transactions (Volume 216), p. 364, 1959.
4. Ramey, H., J.: Correction of equation given in reference 3, JPT, p. 658, July 1961.
5. Myhill N., A.,and Stegemeier, G., L.: "Steam Drive Correlation and Prediction", JPT, 1227-1232, (Nov. 1972).
6. Satter, A., and Parrish, D. R.: "A Two Dimensional Analysis of Reservoir Heating by Steam Injection", SPEJ, Vol. 11, p. 185-197, 1971.

CONVERSION FACTORS

1 Barrel = 1.589 873 E-01 cubic metres.

1 acre = 4.046 856 E+03 square metres.

1 foot = 3.048 000E-01 meter.

1 psig = 6.894 757 E+03 pascal.

1 inch = 2.540 000E-02 meter.

1 mph (mile per hour) = 1.609 344 kmph (kilometer per hour)

Table 1.Wilmington Cumulative Heat Loss data

Date	Cumulative Heat (MMMBTU)	Percentage Heat Losses Due To			Cumulative Net (MMMBTU)	Cumulative Loss to Over/Underburden	Percent Retained
		Pipe	Oil	Water			
Dec-89	2,711.27	2.00%	0.25%	5.65%	2,497.00	12.39%	79.71%
Dec-90	6,372.65	2.00%	0.62%	12.30%	5,421.52	16.43%	68.65%
Dec-91	9,198.24	2.00%	0.87%	15.79%	7,482.17	18.90%	62.45%
Dec-92	13,007.84	2.00%	1.05%	19.63%	10,056.81	20.02%	57.29%
Jul-93	15,215.28	2.00%	1.06%	19.95%	11,714.19	21.26%	55.73%

Table 2.Wilmington Capture Efficiency Compared with other Steamfloods

Field	Ec
Brea ("B" sand)	1.08
Coalinga (section 27, zone 1)	1.13
El Dorado (N-W pattern)	0.40
Inglewood	0.68
Kern River	0.81
Schoonebeek	0.81
Slocum (Phase 1)	0.62
Smackover	0.78
Tatums (Hefner steam drive)	0.77
Tia Juana	0.63
Yorba Linda ("F" sand)	1.06

Wilmington	0.6

as calculated in this study.

Table 3. Summary Predicted Data

	Case 1	Case 2	Case 3
Fillup Date	Dec. 1996	Mar. 1998	
Decline Rate	246 BPD/yr	193 BPD/yr	
OilRate (BOPD)			
12/93	2849	2137	2309
12/94	2579	1944	1559
12/95	2329	1752	885
12/96	2117	1560	269
12/97		1392	218

Figure 1. Pipeline Heat Loss rates

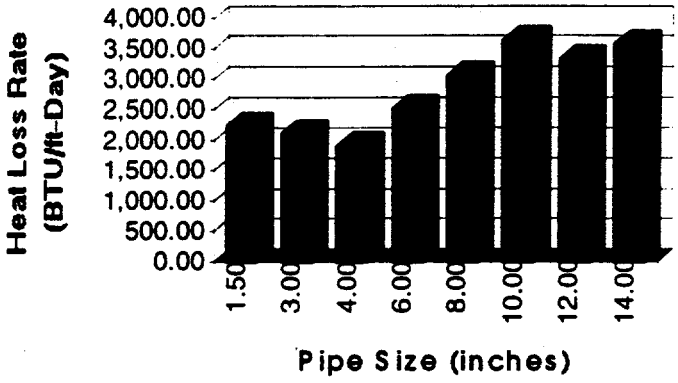

Figure 2. Pipe Heat Loss Distribution

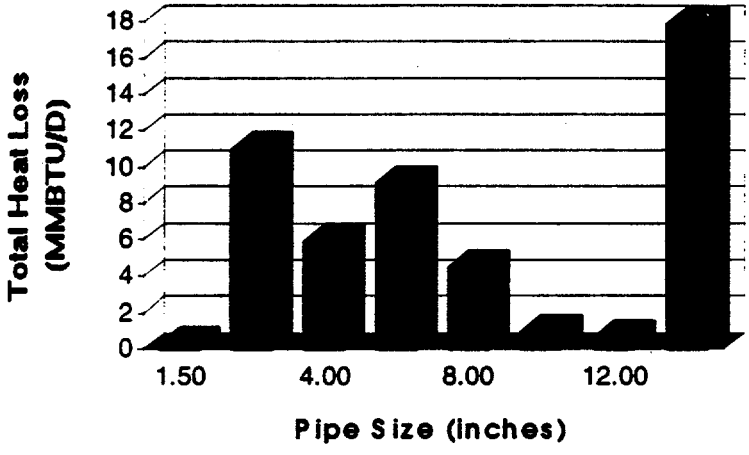

Figure 3. Injection Well Heat Loss rate

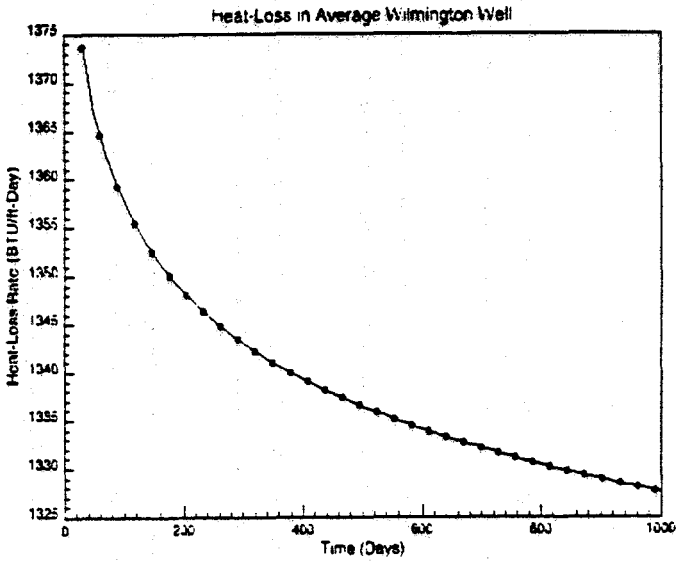

Figure 4. Calculated Bottomhole Temperatures vs. Surface Temperatures

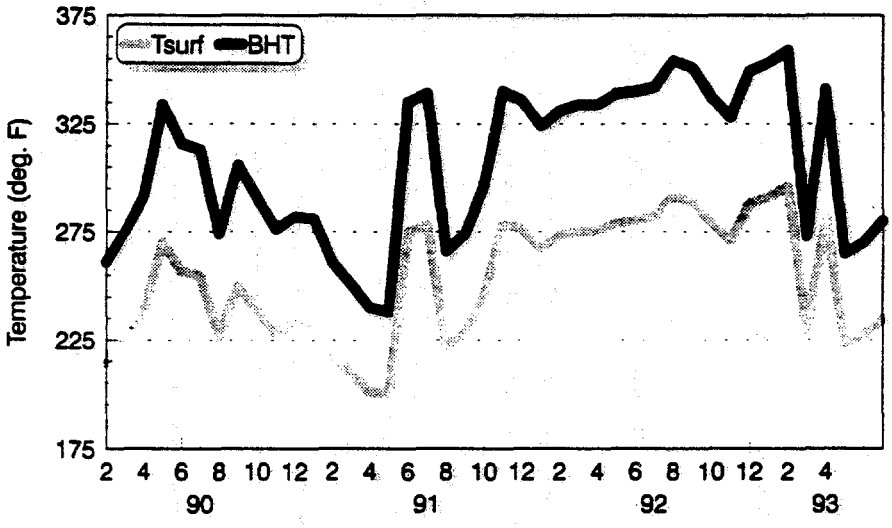

Figure 5. Water and Total Heat Losses

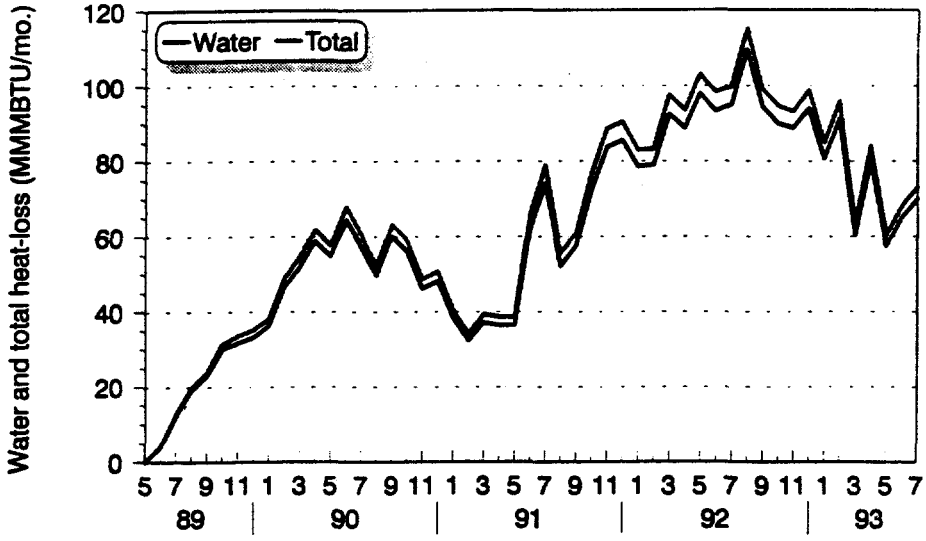

Figure 6. Cumulative Heat Loss to Produced Fluids

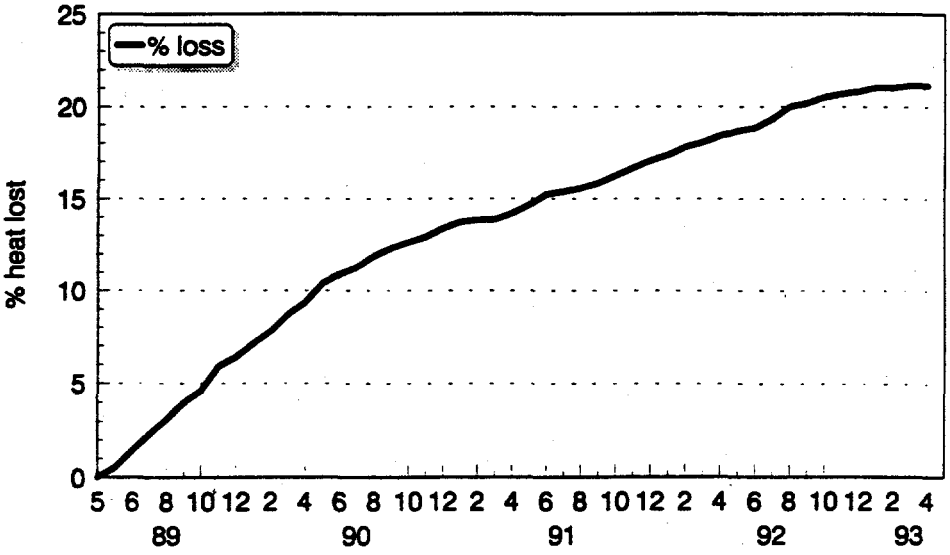

Figure 7. Cumulative Heat Loss to Adjacent Formations

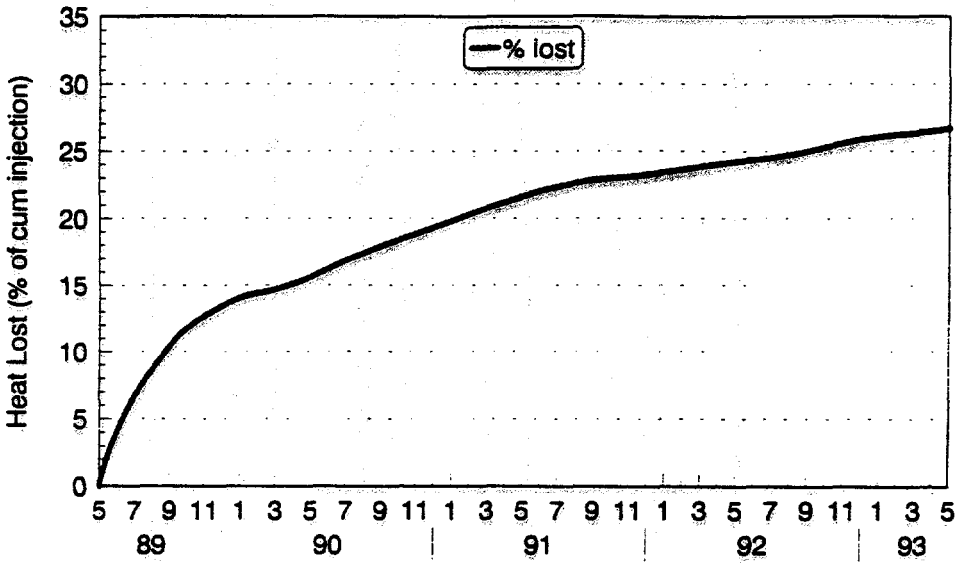

Figure 8. Distribution of Cumulative Injected Heat (7/93)

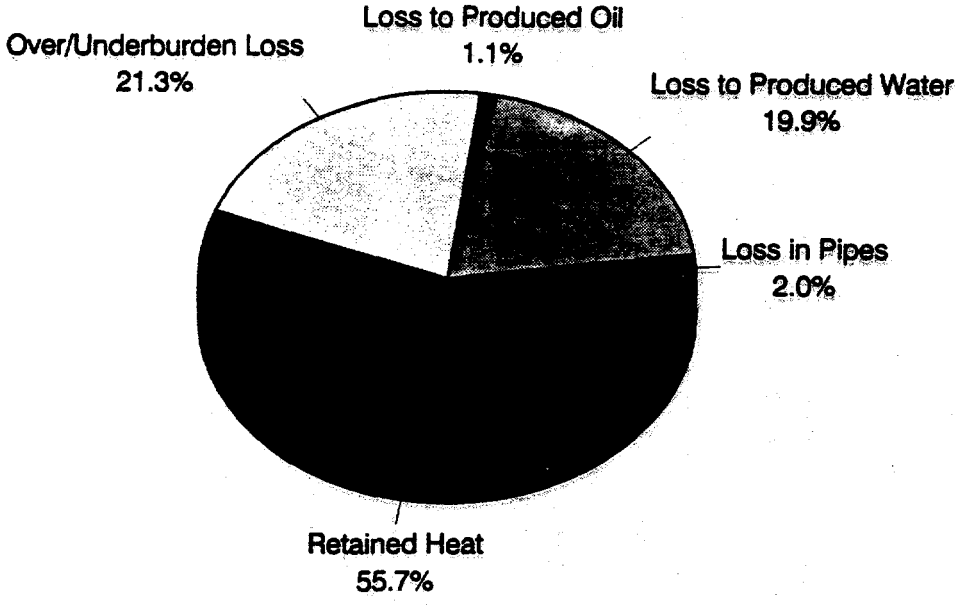

Figure 9. History Match (Calculated vs. Actual Rates)

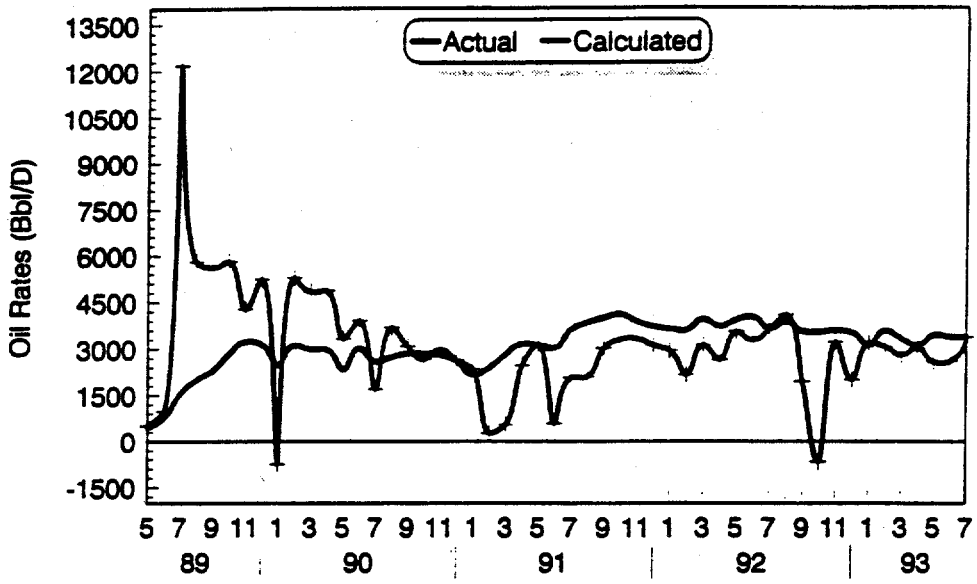

Figure 10. Predicted Production Rates

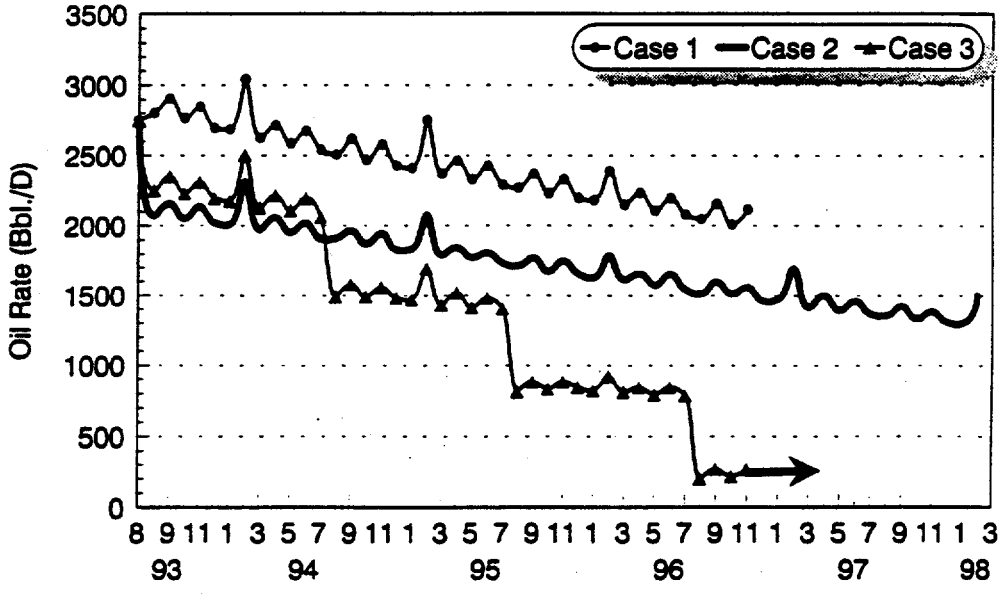

5.3 PILOTFLOODING FOR ENHANCED RECOVERY

(William E. Brigham)

5.3.1 SUMMARY

This paper was prepared for presentation at the IEA Enhanced Oil Recovery Workshop (August 28 - 31, 1994).

PILOT FLOODING FOR ENHANCED RECOVERY

by

William E. Brigham

ABSTRACT

Pilot flooding, and the prediction and interpretation of pilot flooding results, is far more complex than is full-scale flooding of a reservoir. Certain problems are common to both systems. But, pilot systems are more complex because the flow outside the pattern is different than it is within the pattern. This variability in outer boundary conditions does not arise in balanced field wide flood patterns. As a result such items as: gas saturation, inverted versus normal pattern, reservoir pressure, and flow rate outside the pattern, all have a far greater impact on pilot flood recoveries than they do on full-scale floods.

We now have enough waterflooding field data that in most cases we have considerable confidence in our predictions of waterflood performance. Field experience on EOR projects is far less than it is for water flooding. In addition all EOR projects are far more expensive to operate than is a waterflood. Thus it becomes even more important to interpret pilot floods as intelligently as we know how.

There is a rather bewildering array of conclusions concerning pilot flooding in the SPE literature. It is possible however, to winnow the useful results from these papers and thus present a unified picture of pilot flooding for any recovery process. I will briefly discuss the work done, and the important conclusions reached. Also, I'll comment on their conclusions to clarify and sometimes to modify them.

An inverted five-spot pattern is generally useless, but it is acceptable for in-situ combustion, steam and steam with foaming additives. The normal five-spot pattern, or an enclosed pattern of any type, will generally produce reliable recovery results if the pattern is properly balanced. However, under some conditions, a more complex pattern will be necessary. If a pattern is not balanced, the recovery results can be far lower than the optimum. Since the total volume injected in a pilot must be considerably greater than the volume produced, a well-designed pilot EOR project will not show economic payout.

PILOT FLOODING FOR ENHANCED RECOVERY

by

William E. Brigham

Pilot flooding, and the prediction and interpretation of pilot flooding results, is far more complex than is full-scale flooding of a reservoir. Certain problems are common to both systems. For example, such items as pattern geometry, relative permeability relationships, reservoir heterogeneity and continuity, mobility ratio, and gravity effects influence both systems. But, in addition, pilot systems are more complex because the flow outside the pattern is different than it is within the pattern. This variability in outer boundary conditions does not arise in balanced field wide flood patterns. As a result such items as: gas saturation, inverted versus normal pattern, reservoir pressure, and flow rate outside the pattern, all have a far greater impact on pilot flood recoveries than they do on full-scale floods.

This problem was stated so clearly by Dalton *et al.*[1] that I am going to quote them directly.

> "A water flood normally consists of an array of identical well patterns. In such an array, the perimeters of the well patterns are axes of symmetry and act as impermeable boundaries. Thus, an extensive pattern water flood can be visualized as a repetition of "confined" floods. In contrast a pilot water flood involving only one or a few well patterns is "unconfined." Here the well patterns are not balanced by other flood units: hence the perimeter of the pilot area does not act as an effective boundary. Accordingly, only a portion of the fluids injected (and also of those originally contained within the pilot area) is captured by the producers of the pilot. The rest escapes into the surrounding reservoir. This usually causes amounts of oil and water produced in the pilot to be different from those recovered by a producer in an extensive water flood. Moreover, the recovery observed in the pilot can be expected to be greatly influenced by operating conditions."

They state that only a portion of the fluids originally contained in the pilot area may be captured by the producers, but later in the paper they also make it clear that fluids might flow <u>from</u> the outside <u>toward</u> the pattern wells. Thus the recovery from a pilot may either be greater than, or less than, that expected from a full-scale flood.

If we were only concerned about waterflooding, this problem of interpreting pilot floods is no longer such a serious problem. We now have enough waterflooding field data that in most cases we have considerable confidence in our predictions of waterflood performance. This statement is not true, however, when we consider enhanced oil recovery (EOR) methods. Field experience on EOR projects is far less than it is for water flooding. In addition all EOR projects are far more expensive to operate than is a waterflood. As a result, a rather minor change in recovery efficiency can have a dramatic effect on the economics of an EOP project; thus it becomes even more important to interpret pilot floods as intelligently as we know how.

There is a rather bewildering array of conclusions concerning pilot flooding in the SPE literature. It is possible however, to winnow the useful results from these papers and thus present a unified picture of pilot flooding for any recovery process. To this end, Refs. 1-4 are most helpful. I will briefly discuss the work done by the authors of each of these references, and the important conclusions reached by them. Also, I'll comment on their conclusions in an attempt to clarify them, and sometimes to modify them when such modification is warranted. From this study, a coherent picture arises concerning pilot floods of all types.

DALTON, RAPAPORT AND CARPENTER[1]

These authors looked at various pilot flooding configurations at a mobility ratio of unity, and at a high gas saturation. Actually this point of "high gas saturation" is a bit hazy, for that condition was only approximated in their results through an interplay between potentiometric model studies and flow model studies.

The flow model was indicated in their Fig. 1 on the following page. Each corner of the model was one-quarter of a particular pattern: four inverted five-spots, six inverted four-spots, one normal five-spot, or one inverted five-spot. When one of the patterns was being tested, the other three patterns were shut in and the pressure was held constant at the two outer boundaries of the model which opposed the pattern being studied.

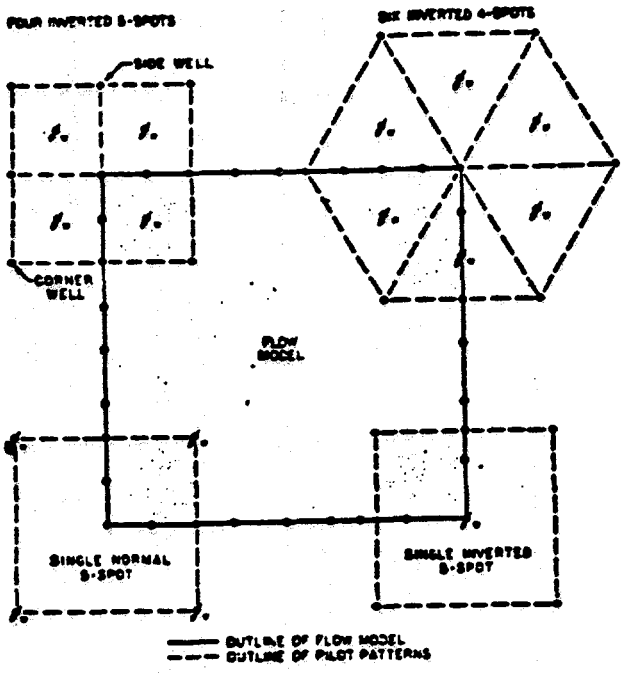

Fig. 1. Simulation of pilot patterns in flow model. (Dalton, *et al.*,[1] Fig. 1)

Their data clearly showed that both injected water and in place oil can flow away from the pilot region. This is illustrated in Fig. 2 below for the pattern with four inverted five-spots.

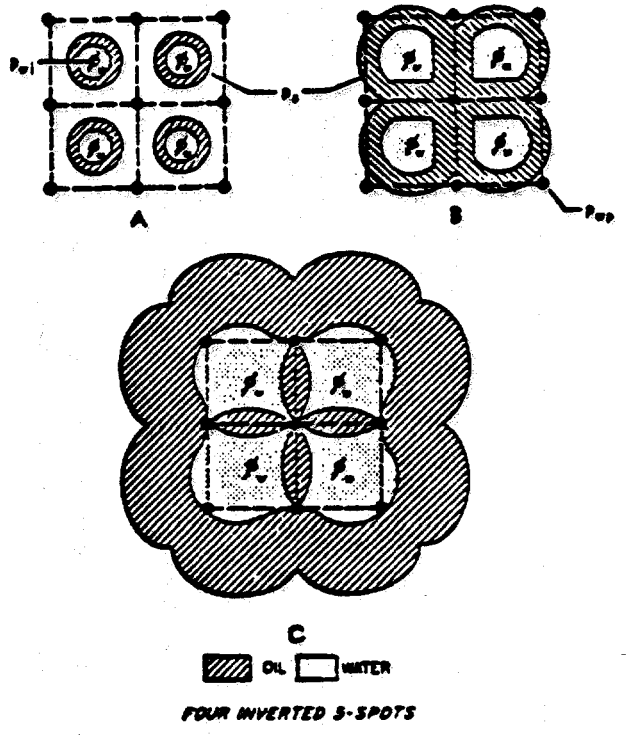

Fig. 2. Illustration of pilot oil- and water-bank development. (Dalton, *et al.*,[1] Fig. 3)

They chose to correlate their data on the basis of a "π ratio," defined as follows:

$$\pi = \frac{p_s - p_{wp}}{p_{wi} - p_s} = \frac{\Delta p_p}{\Delta p_i}$$

where

p_s = reservoir pressure, exterior boundary pressure

p_{wp} = producing well pressure

p_{wi} = injection well pressure

Since their reservoir pressure was held constant, and all their wells had the same equivalent radii, this was a valid method of correlating their data. The reason is that these pressure differences automatically set up fixed relative flow rates within and outside the patterns.

Their results can be seen from two of their figures. In Fig. 3 below is seen some of the detailed results from the pattern consisting of four inverted five-spots.

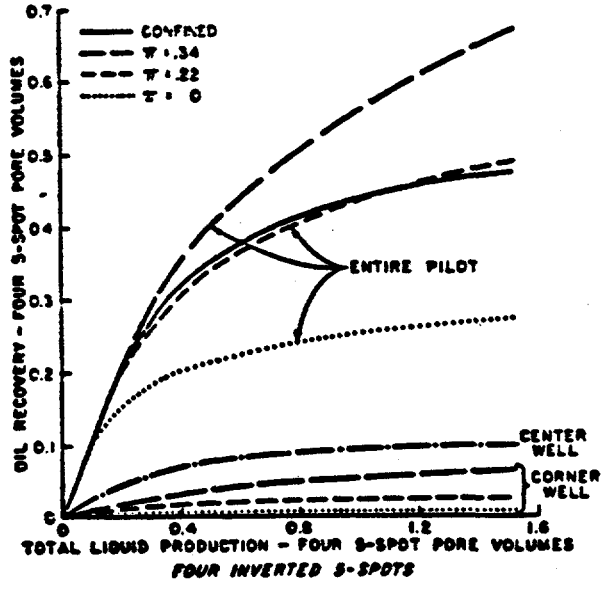

Fig. 3 Effect of operating conditions on oil recovery. (Dalton, *et al.*,[1] Fig. 5)

Notice that the recovery from the entire pattern is a strong function of the π ratio. With a π ratio of 0.22, the entire pilot recovery history fits the developed pattern closely, but clearly very close control would have to be maintained in the field to achieve this result. Even a modest change in π ratio from 0.22 to 0.34 greatly affects the recovery history.

Note the single line for the center well. There is only one line because the π ratio had almost no effect on the production from this well. Also notice that its recovery is almost exactly one-quarter of the recovery from a confined pattern, as it should be, based on the geometry. This well is totally enclosed by injectors, thus its recovery is virtually identical to that to be expected from a developed pattern. If we were producing such a pilot pattern, clearly this is the well we would study closely as a basis for our field predictions.

Figure 4 shows general recovery results for all four patterns as a function of the π ratio. From this figure it is clear that the normal five-spot is best and

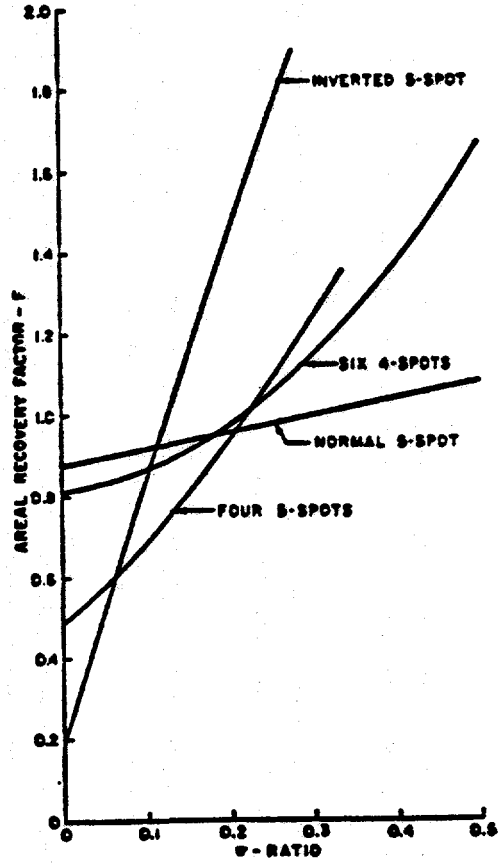

Fig. 4. Effect of operating conditions on areal recovery factor. (Dalton, *et al.*,[1] Fig. 10)

the inverted five-spot is worst. The normal five-spot gives good results for any π ratio, while the inverted five-spot is virtually useless. Thus again, from these results, we see that if a producer is surrounded by injectors it appears to behave similarly to a developed pattern. This conclusion is fairly obvious, but was not stated by the authors. It should have been, for it is an important concept for any pilot flood operating under conditions similar to those covered here. It is not confined to waterflood pilots. The authors did, however, correctly state that the normal five-spot was a good pattern to use.

We must remember that these data are limited to a system where the mobility ratio is near unity. Also, these results are for systems with a high gas saturation at the beginning of the flood. We will look to the other authors for conditions outside the data range of these results.

CAUDLE AND LONCARIC[2]

In the same year, Caudle and Loncaric[2] performed a thorough study of a normal five-spot pilot pattern. The system they studied was completely liquid filled, and they looked at various mobility ratios ranging from 0.1 to 10.0. They allowed any excess fluid to leave the pattern at a distance far removed from the pilot area. Thus the system was equivalent to a liquid filled reservoir with no producing wells near the pilot pattern. The geometry of their experimental system is seen in Fig. 5 below:

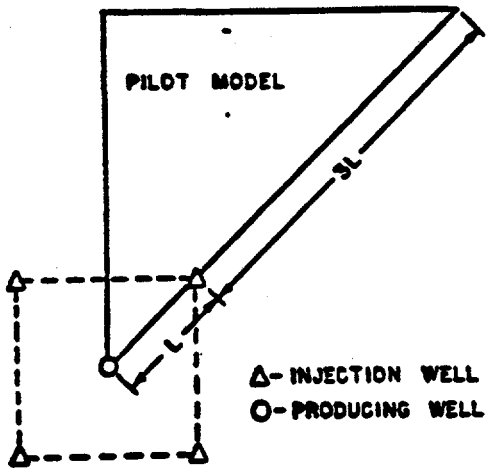

Fig. 5. A single five-spot pilot area and the fluid-flow model used in this study. (Caudle and Loncaric,[2] Fig. 1)

Any excess fluid was withdrawn from their model along the top edge of the triangle in the figure. The other two edges are no flow boundaries, for they are planes of symmetry. The distance to the top edge of the model was far enough removed from the pilot region to have little effect on the flow lines in the pilot area itself.

In this work they studied various ratios of injection to production, and determined the oil recovery as a function of these ratios and as a function of the volume injected. Remember that a fixed production ratio was also the result of the fixed π ratio discussed earlier in the work by Dalton *et al.* Caudle and Loncaric's results are seen in Figs. 6-10 following, for various mobility ratios.

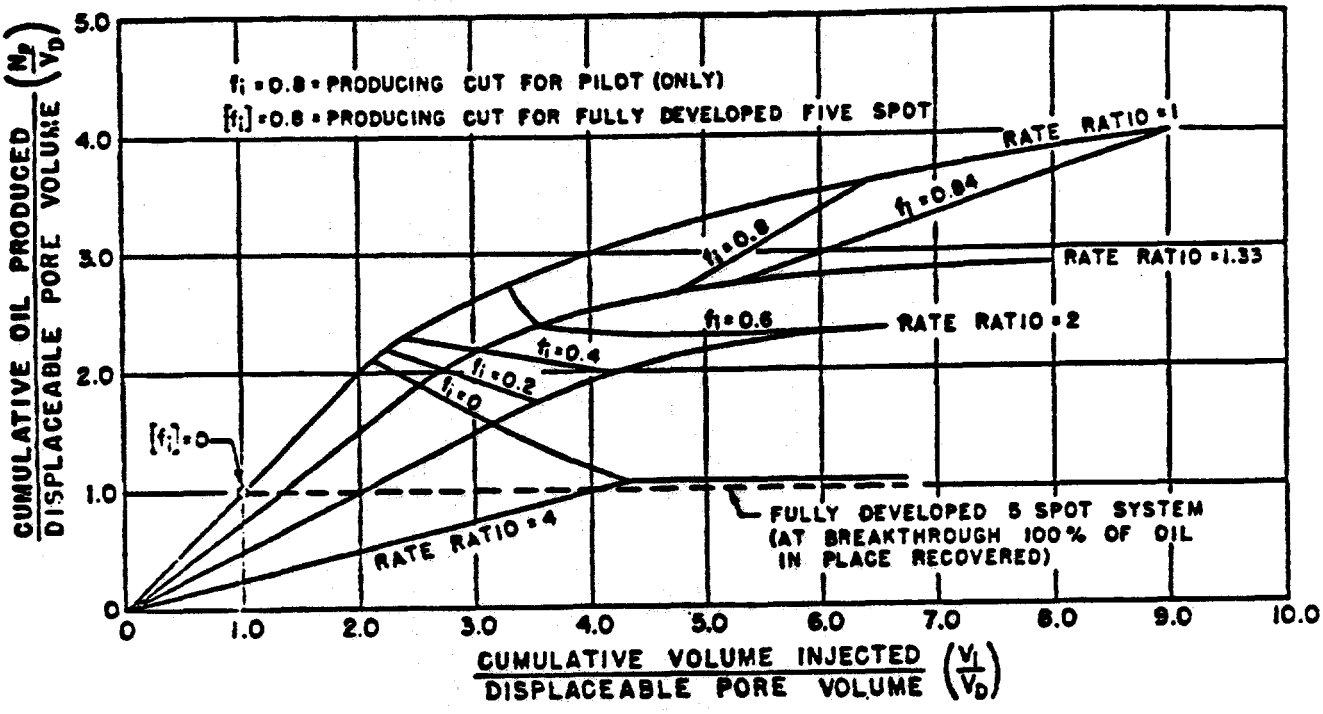

Fig. 6. Production histories of pilot floods at various rate ratios (q_i/q_D) and of a fully developed five-spot unit. Mobility ratio = 0.1. (Caudle and Loncaric,[2] Fig. 3)

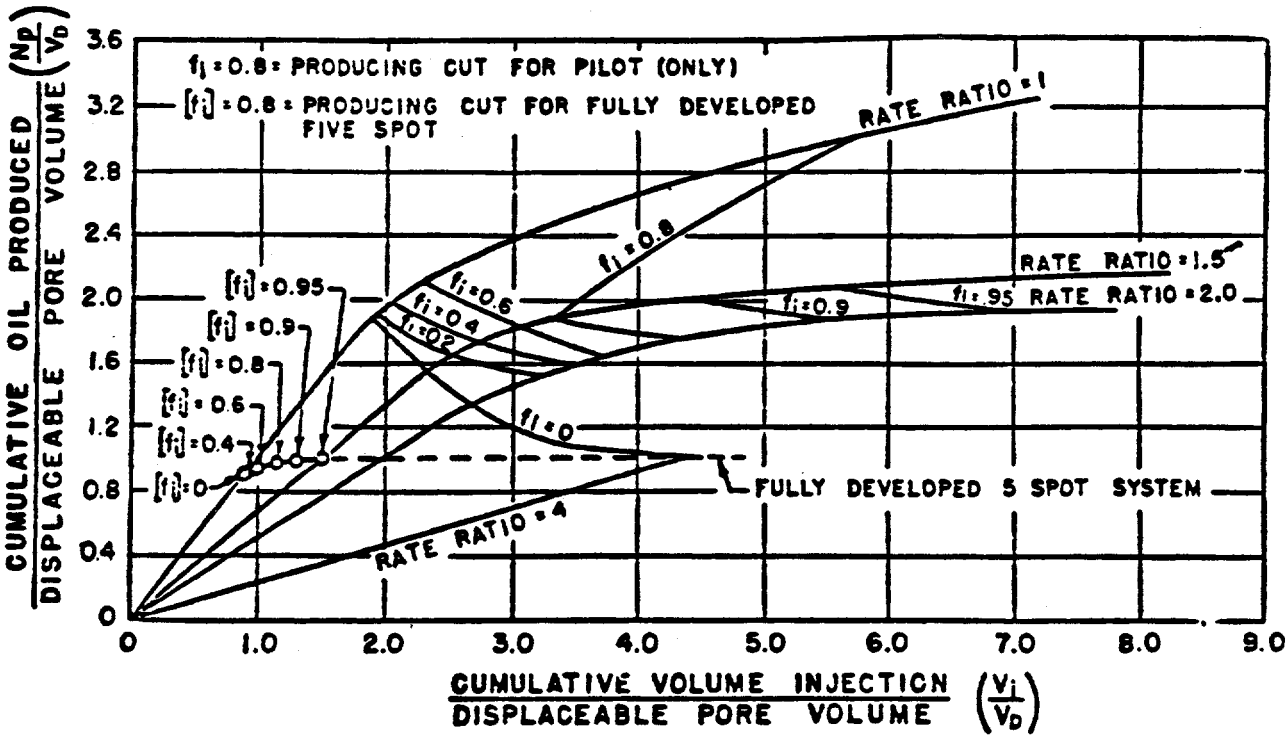

Fig. 7. Production histories of pilot floods at various rate ratios (q_i/q_p) and of a fully developed five-spot unit. Mobility ratio = 0.29. (Caudle and Loncaric,[2] Fig. 4)

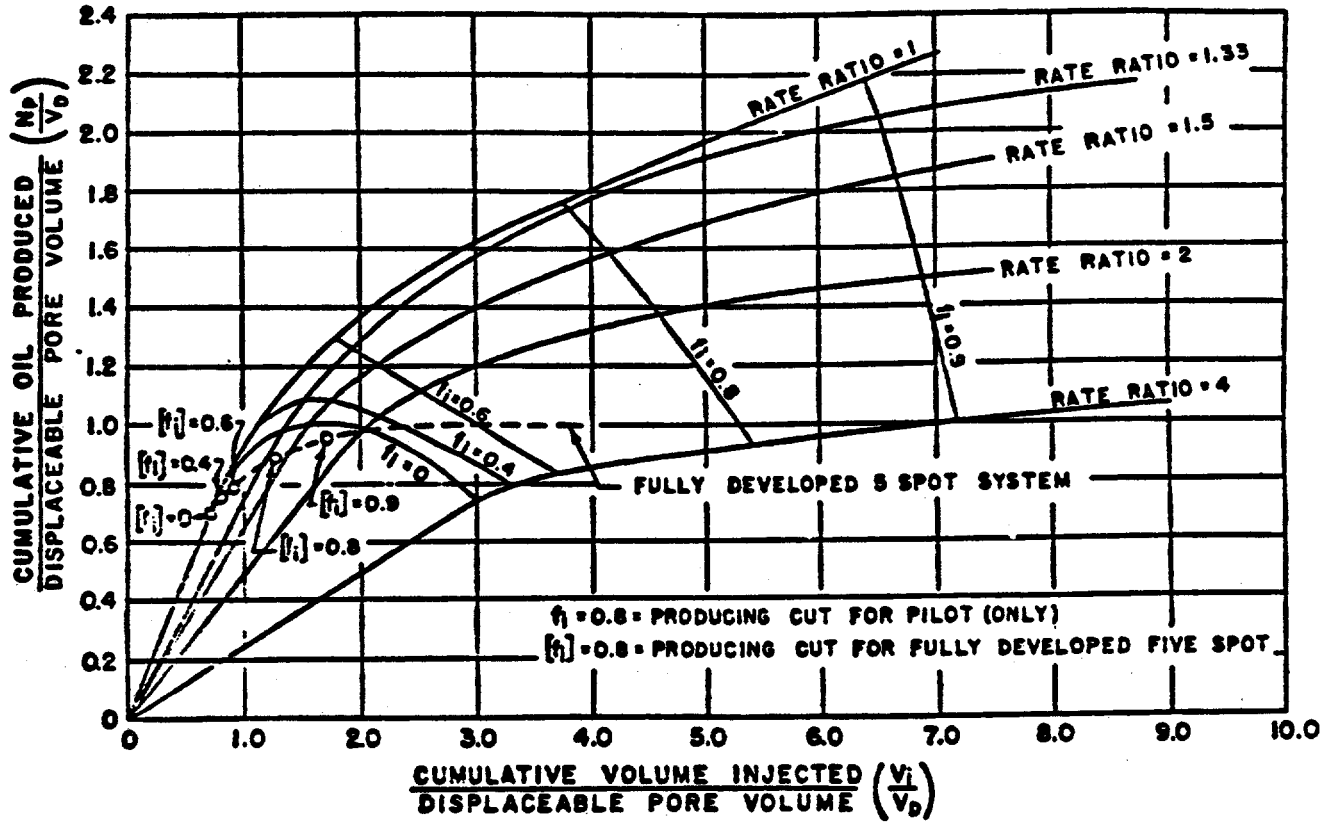

Fig. 8. Production histories of pilot floods at various rate ratios (q_i/q_D) and of a fully developed five-spot unit. Mobility ratio = 1. (Caudle and Loncaric,[2] Fig. 5)

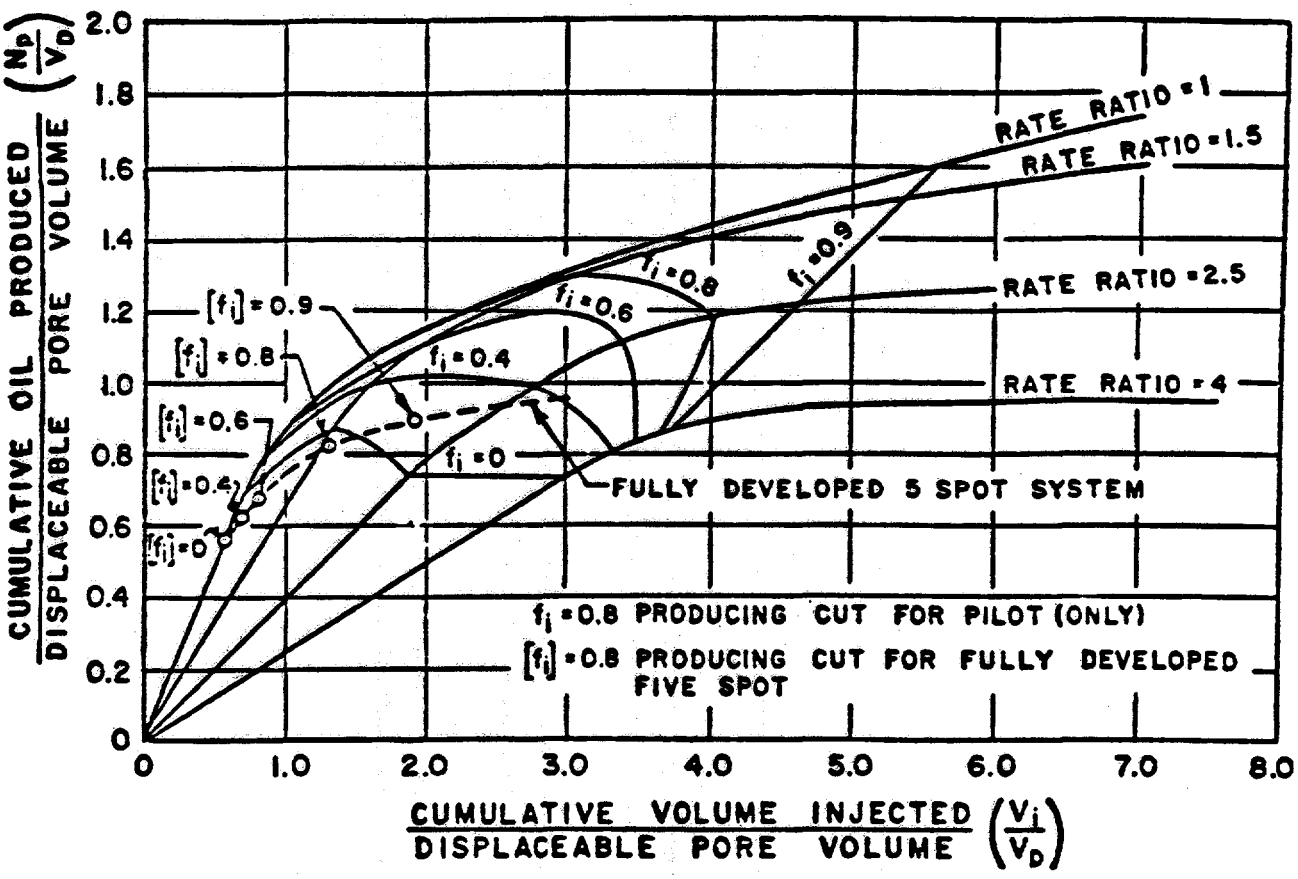

Fig. 9. Production histories of pilot floods at various rate ratios (q_i/q_D) and of a fully developed five-spot unit. Mobility ratio = 3.7. (Caudle and Loncaric,[2] Fig. 6)

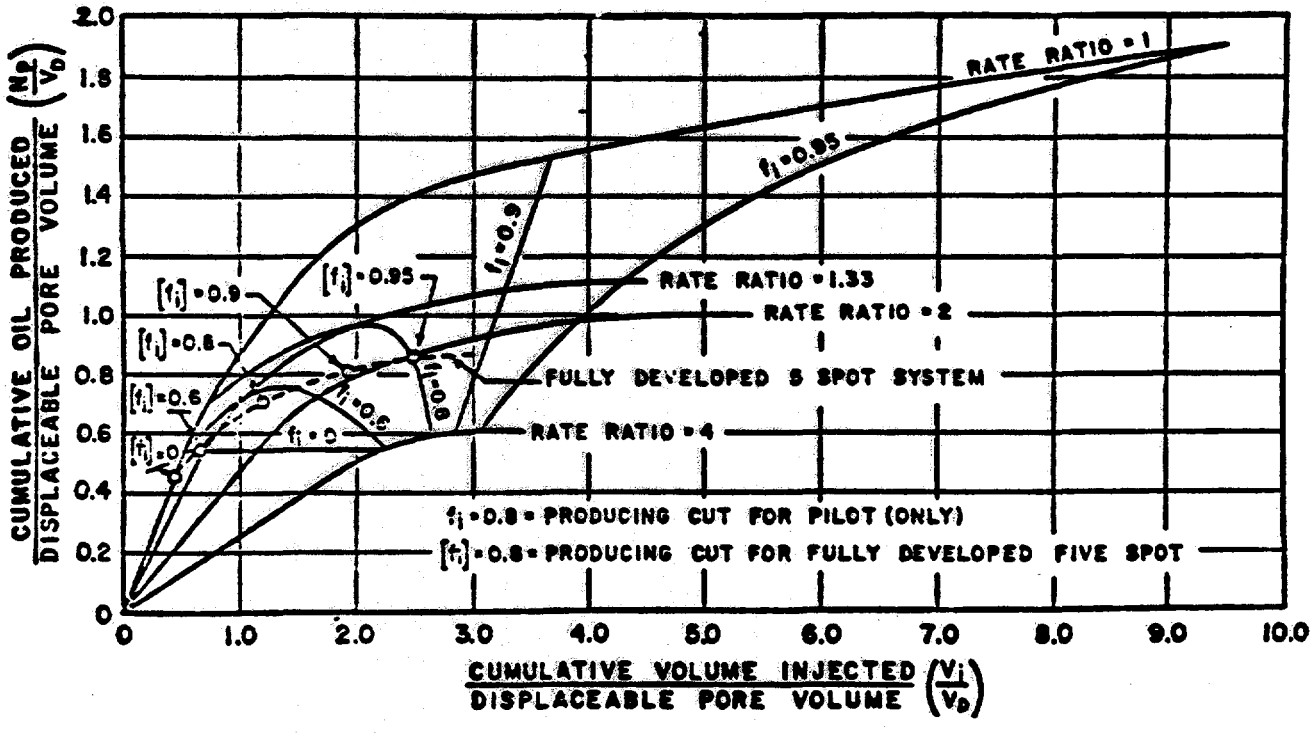

Fig. 10. Production histories of pilot floods at various rate ratios (q_i/q_D) and of a fully developed five-spot unit. Mobility ratio = 10. (Caudle and Loncaric,[2] Fig. 7)

At first glance these results are quite confusing, for there are many lines on each figure. The authors suggest ways to convert the actual pilot results to the equivalent field scale results shown as dashed lines in the figures. The authors seemed, however, to have missed the most important conclusion that can be reached from these data. Probably this was due to the coordinate system they used for graphing the data.

Consider the normal five-spot pilot which has four injectors for one producer. If we inject the same volume of fluid into each well that we produce from the center well, the rate ratio will be 4:1. Further the volume injected (graphed on the abcissa) will be four times the volume produced. If we take the curve at a rate ratio of 4:1 and ratio it back by a factor of four on the abcissa, we will have generated a graph of the oil produced at the center well (the ordinate) versus the total volume produced at that well (the adjusted abcissa). When we do this, we find that the curves for all five mobility ratios are virtually identical to the recovery curves for a fully developed pattern. This is a remarkable result!

The conclusion we reach from this exercise is that a normal five spot will give us good recovery data if the injection volume into each well is the same as the production volume from the center well. This conclusion is valid for a large range of mobility ratios, but is limited to a liquid filled system which has little production from outside wells near the pattern.

We next turn to work that includes initial gas saturations at the start of the pilot flood, and producing wells near the outside of the pattern.

CRAIG[3]

Craig performed a thorough study of both inverted and normal five-spot pilot patterns. In this work he studied varying amounts of gas saturation in the reservoir models, and he always included producing wells in the near area around the pilot pattern. Figures 11 and 12 show this clearly.

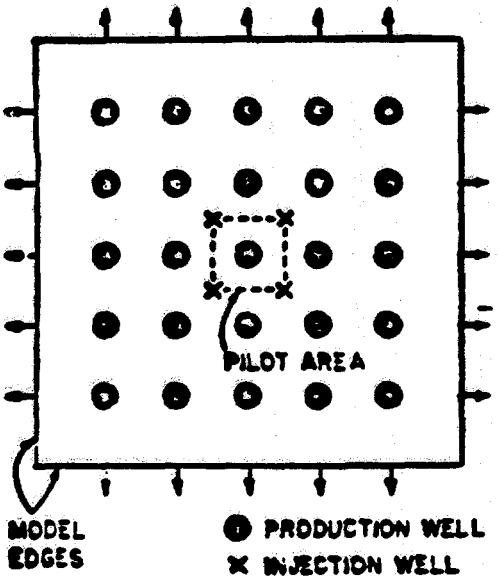

Fig. 11. Well arrangement for single five-spot pilot flood. (Craig,[3] Fig. 1)

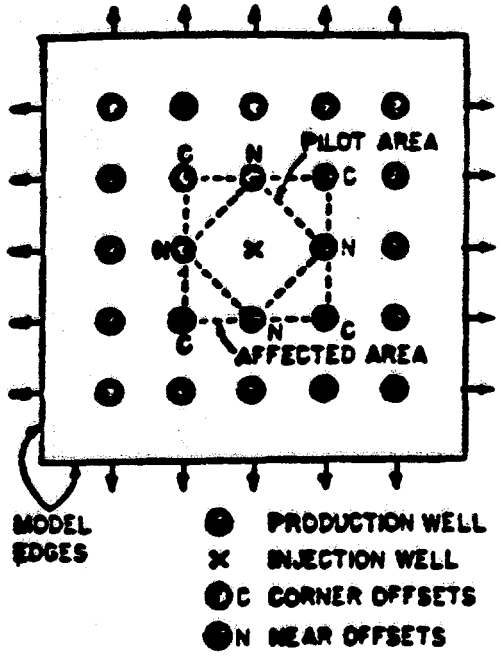

Fig. 12. Well arrangement for single well pilot flood (Craig,[3] Fig. 3)

His water to oil mobility ratios were all favorable, ranging from 0.20 to 0.94 in his tests. He concluded (correctly) that the inverted pattern gave results that were of little use. This was especially a problem if there was any gas saturation in this reservoir model, for the oil bank tended to flow by the producers without being captured. Notice that this confirms the results of Dalton *et al.*[1] which were for different outer boundary conditions. Generally the inverted five-spot pattern is not good to use.

His conclusions regarding the normal five-spot pilot are summarized in Fig. 13 below.

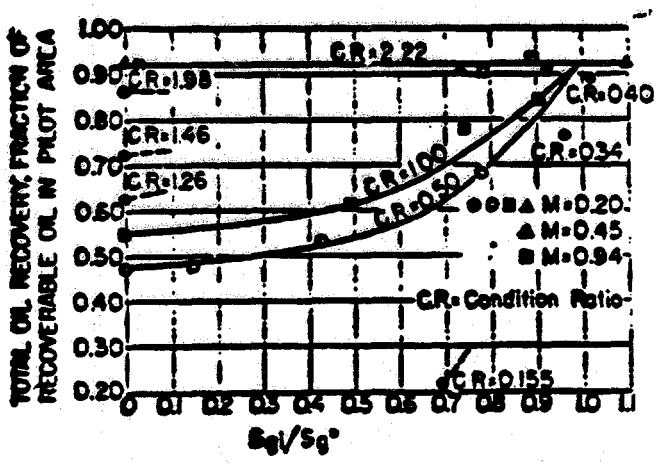

Fig. 13. Effect of producing well condition ratio and initial gas saturation on oil recovery of a single five-spot pilot waterflood (four injectors and one producer). (Craig,[3] Fig. 4)

Before discussing Fig. 13, it might be well to indicate the meaning of the abcissa in that figure. The term S_g* is the gas saturation that would allow the water invaded regions to interfere with each other before the oil bank reached the producing well. This is a very large gas saturation.

This figure indicates that if the gas saturation is this high (S_g*), then none of the pattern oil will escape no matter what the Condition Ratio of the center well; thus the recovery will be the same as it would be in a fully developed pattern. However, if the gas saturation is smaller than S_g*, then some oil may escape from the pattern and the recovery is likely to be reduced. Also, if the Condition Ratio of the center well is at least 2.22, then it makes no difference what the gas saturation is, the recovery will be the same as if would be in a developed pattern. This is the conclusion Craig reached, but this conclusion is misleading.

If we read the paper carefully we find that <u>all</u> the producers surrounding the pilot had a Condition Ratio of 2.22; thus we should change his conclusion to the following.

> As long as the pilot producer has a productivity index (Condition Ratio) at least as high as the surrounding producers, the recovery from a normal five-spot pilot can be extrapolated directly to field scale.

This conclusion is for a system with a favorable mobility ratio, up to $M = 1$. Notice that when these results are coupled with the results discussed previously, we see that the boundary conditions outside the pilot pattern have very little effect on the flood results if the pilot is operated logically.

These results, and the previous ones were stipulated to be for waterfloods. But suppose, instead, we were to look at a tertiary flood after waterflooding. In this case, the reservoir flow ahead of the flood is almost entirely water at a mobility near the irreducible oil saturation. A tertiary flood following this will build up an oil displacement bank, which will be at a lower mobility than the water ahead of it, and the following flushing fluid must also have a lower mobility if the flood is to be effective. So the sequence of fluids flowing is similar to the sequence for a waterflood, in that the mobility ahead of the displacement is much higher than that behind it. Thus the conclusions about recovery from the patterns should still be similar in nature. We turn now to more complex pilots.

BERNARD AND CAUDLE[4]

We turn now to the work of Bernard and Caudle[4] who looked at an array of pilot floods of varying complexity, for a range of mobility ratios and at various simulated gas saturations. I say "simulated gas saturations" because they used a fixed oil bank volume to define their system; while a true gas saturated system would have an ever-increasing oil bank volume.

The geometry of their various patterns is shown in Fig. 14:

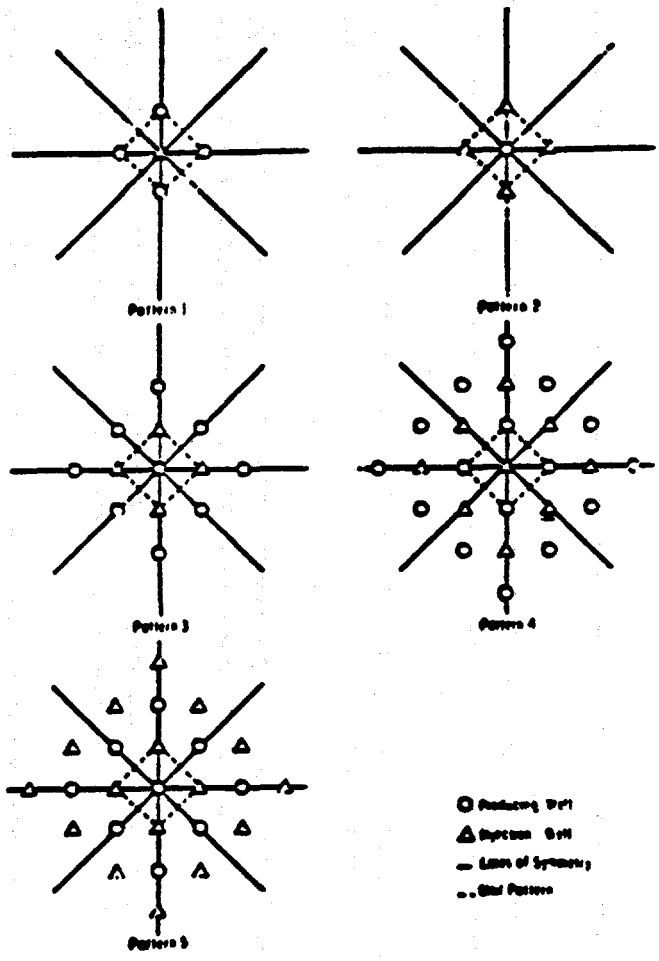

Fig. 14. Five-spot pilot patterns. (Bernard and Caudle,[4] Fig. 2)

Their simplest case is the inverted five-spot pattern, Pattern 1. They tested under what conditions various patterns would produce correct information from the innermost producing well(s). As we might expect from the previous pilot test studies, the inverted five-spot never gave a proper answer.

We might also predict that a system with a higher mobility ratio would require a more complex pattern. Last we might predict that a liquid-filled system would require a more complex pattern than one where there is some gas present (this is because the

water bank helps to contain the oil within the pattern as Craig[3] found). These suppositions were also found to be true. Figure 15 summarizes their results.

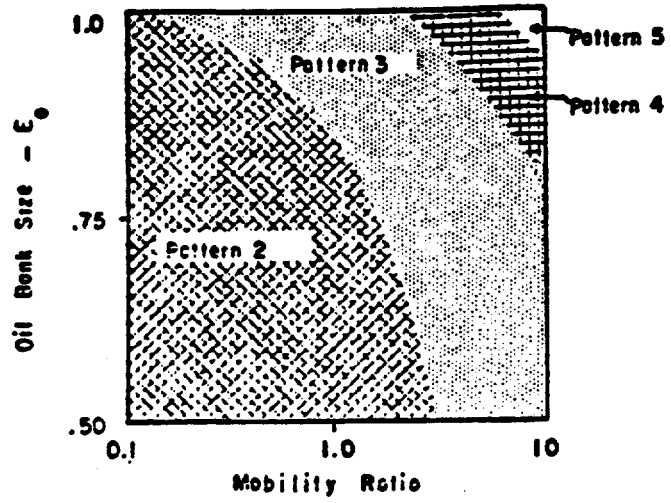

Fig. 15. Simplest five-spot pilot required. (Bernard and Caudle,[4] Fig. 16)

The areas in the figure define the simplest pattern which can be used to get reliable results. The ordinate in the figure, E_o, is a measure of the gas saturation; the largest E_o of 1.0 indicates zero gas saturation. As we speculated above, with a smaller gas saturation or with a higher mobility ratio, a more complex pilot pattern is needed before we can rely on the results.

Again we can directly relate these results to a tertiary flood after waterflooding. This figure is particularly useful, for one can relate the anticipated results to the tertiary oil bank size. We should expect the other parameters in the figure to act in the same way to define how well a tertiary flood will perform.

ADDITIONAL COMMENTS

In general it was seen that, in pilot floods, balanced enclosed patterns produce useful production histories from the interior wells. The studies were targeted toward evaluating waterflood pilots, but the fluid mobilities controlling the results make it clear that the general results are also valid for tertiary pilots.

Unbalanced Patterns

One important point was made in Craig's paper concerning an unbalanced pilot pattern. He ran one case where one of the injection wells was shut in, so only three of the injectors were active outside the center producer. The results were disasterous! Less than half the recoverable oil was produced, and this was only after five pore volumes of water injection.

Craig recognized that this was an extreme case, but pointed out that these data prove how important it is to balance injection rates with the actual thickness of the quadrant of the reservoir associated with each injector.

Field pilots are never uniform, they vary both in thickness (ϕh) and permeability (kh). Thus an injection imbalance is far more common than we would like to believe. It is for this reason that I always strongly stress the need for good pressure interference test data prior to running a pilot flood, and for well-to-well tracer tests before and during a pilot flood. These are the best ways to predict, and correct for, the natural tendency for imbalance in field pilots.

Thermal Recovery Pilots

All of the pilot tests cited here were dominated by fluid mechanics mechanisms. Thermal recovery pilots are strongly influenced by heat transfer mechanisms. This change in mechanism causes changes in the conclusions we reach concerning pilot flood behavior.

Clearly, from the results presented earlier in this paper, an inverted five-spot pilot can be disastrous, because fluids can either leave the pilot without being produced, or can be drawn into the pilot causing unrealistically high recovery. But a thermal recovery pilot is not bothered by this problem to nearly as great an extent. The reason is that, outside the pilot's affected area, the oil is not hot and is relatively immobile; while it is hot and mobile inside the pilot. Thus the recovery history will tend to be more realistic, for the fluid flow rates are largely controlled by the heat flow mechanisms.

At first glance, this result suggests that there is no problem with thermal recovery pilots. Not true! Due to the lower density of the injected fluids (air or steam), gravity override is always important in thermal recovery pilots. High temperature gravity tongues can and do flow toward the producers, thus affecting pilot recovery. This will always happen, and thankfully so; for, if it didn't, the producing wells would not

become hot, which they must for production rates to increase. So the thermal pilot operator must recognize that gravity override will take place, and he must account for it when designing and operating the pilot.

In general, these remarks concerning thermal recovery pilots are equally valid for in-situ combustion, steam flooding and even for steam flooding with foaming agents to improved sweep efficiency.

CONCLUSIONS

From the results discussed in this paper, the general conclusions we can draw are as follows:

1. An inverted five-spot pattern is generally useless. There is one exception to this rule. For in-situ combustion, steam and steam with foaming additives, the inverted five-spot is acceptable.
2. The normal five-spot pattern, or an enclosed pattern of any type, will generally produce reliable recovery results if the pattern is balanced, and if the injection volume into each exterior well is at least as high as the production volume in the center well. This is generally true for any system of external boundary conditions. However, whenever the initial gas saturation is very small and the mobility ratio is well above one, a more complex pattern will be necessary.
3. If a pattern is not balanced, the recovery results can be far lower than the optimum. For this reason it is mandatory that a thorough testing program be included in the pilot process. This should include well-to-well interference tests and well-to-well tracer tests to define values for kh, ϕh, anisotropy and heterogeneities.
4. Since the total volume injected in a pilot must be considerably greater than the volume produced (See Conclusion 2 above), and since the fluids injected in exotic EOR projects are quite espensive, we need to recognize that a well-designed pilot EOR project will almost always require a large expenditure of money with little hope of economic payout.

This last conclusion was not discussed in the text, but it becomes obvious once one realizes the importance of the interplay between pilot test recoveries and volumes injected.

REFERENCES

1. Dalton, R.L., Jr., Rapaport, L.A. and Carpenter, CW., Jr., "Laboratory Studies of Pilot Water Floods," *Trans. AIME 219* (1960) pp. 24-30.
2. Caudle, B.H. and Loncaric, I.G.: Oil Recovery in Five-Spot Pilot Floods," *Trans. AIME 219 (1960) pp. 132-136.*
3. Craig, F.F., Jr. "Laboratory Model Study of Single Five-Spot and Single Injection," *Trans. AIME 234* (1965) pp. 1454-1460.
4. Bernard, W.J. and Caudle, B.H.: "Model Studies of Pilot Waterfloods," *Trans AIME* (1967) pp. 404-410.

APPENDIX

Both Craig[3] and Bernard and Caudle[4] looked at waterflooding behavior when there was some gas saturation in the reservoir at the start of the flood. Craig chose to look at his results based on the ratio S_g/S_g^*, where S_g^* was defined as the gas saturation required to allow water bank interference at the time of liquid fillup of a 5-spot pattern. He showed the equation to be,

$$S_g^* = \frac{\pi}{4}(1 - S_{wc} - S_{or}) \tag{A.1}$$

This equation assumes that the oil saturation behind the waterfront is S_{or}. It is seldom this low, but in general, the equation can be corrected to read,

$$S_g^* = \frac{\pi}{4}(\bar{S}_w - S_{wc}) \tag{A.2}$$

where $\bar{S}_w$ is the average water saturation behind a Buckley-Leverett front. If S_g is less than S_g^*, then the oil ahead of the water bank is free to move either into or out of the pattern before the water banks meet each other at the periphery of the 5-spot pattern.

Bernard and Caudle looked at this idea in a somewhat different way. They defined a term, E_o, which is the oil bank volume ahead of the water bank at the time of liquid fillup of the pattern. If the flood starts at a liquid filled condition, E_o = 1.0. Any initial gas saturation reduces the value of E_o.

Suppose that the gas saturation was exactly S_g^*. In this case, at fillup, the water bank volume fraction would be $\pi/4$ as indicated by Eq. A.2, thus the term, E_o, would be,

$$E_o = 1 - \frac{\pi}{4} = 0.2146 \tag{A.3}$$

Notice that the value of E_o to meet Craig's criterion is far smaller than the smallest value of E_o (0.50) studied by Bernard and Caudle. In general, by material balance, the equation relating Craig's ratio to Bernard's is as follows:

$$E_o = 1 - \frac{\pi}{4}\frac{S_g}{S_g^*} \tag{A.4}$$

The smallest value of E_o studied by Bernard gives a Craig S_g/S_g^* ratio of 0.637. Under this condition, Craig shows that the outer boundary conditions can have an effect on the results if the relative production rates are not properly balanced.

5.4 USE OF THERMAL SIMULATORS TO MODEL STEAM INJECTION PROJECTS IN HEAVY OIL RESERVOIRS OF THE TYPE FOUND

(Jill Marcelle-DeSilva)

5.4.1 ABSTRACT

In Trinidad, there are several thermal projects. In the past, the production performance of these projects were estimated using simple analytical models. In partial fulfilment of the requirements for the Engineer degree in Petroleum Engineering at Stanford University, a numerical simulation study of the wells in one inverted 5-spot pattern in one of these projects, i.e. the Point Fortin Steam Project, was conducted.

The Point Fortin SteamProject, which started in 1986, consists of five (5) inverted 5-spot patterns and two (2) irregular 6-spot patterns. The wells in the project have undergone up to 4 cycles of steam injection and the project is currently on the steam drive phase. The sands in the project area are interpreted to be lenticular deltaic sediments, and in the pattern area, occur at depth of approximately 1335 ft. The sands contain 17^{o} API crude and viscosity ranges from 100 to 300 cp at the reservoir temperature of 115^{o}F. In the pattern area, net oil sand thicknesses average 128 ft. Reservoir dip averages 12^{o} to the north-northeast.

A numerical simulation sensitivity study was carried out, followed by the history matching of the production performance of the wells in the pattern. The commercially available thermal simulator, STARS, was used. This simulator was developed by the Computer Modelling Group (CMG) of Canada. The results from the simulation study were compared with those obtained using an analytical model developed to model cyclic steam injection in low gravity, pressure depleted reservoirs.

Sensitivity studies conducted using both the numerical and analytical models, indicated that several parameters significantly affected production performance.

Using the numerical model, a good match was obtained of the production performance of the initial 7.5 years in the life of the wells. The analytical model gave a better match of the production performance
of the initial 2.5 years in the life of these wells, when they were undergoing cyclic steam injection.

Based on this study, it is recommended that analytical models be used to provide initial estimates of the production forecast for thermal projects. Later in the life of the projects, as initial production data and more information on the properties of the reservoir rocks and fluids become available, the numerical simulator should be used to history match the initial production performance, make production forecasts, and optimize future production.

For the numerical simulation studies, additional data need to be collated. These data should include the spatial distribution of porosity, relative and absolute permeabilities, average reservoir pressure and bottomhole flowing pressures, bottomhole flowing temperatures and properties of the reservoir crude oil and gas. The properties of the reservoir crude oil and gas should include measured values of molecular weight, specific gravity, and normal boiling point of individual fractions.

It is also recommended that the analytical model used in this study be modified to take into account an initial gas saturation. This would make the model more general purpose.

REFERENCES

1. Arihara, N.: "A Study of Nonisothermal Single and Two-Phase Flow through Consolidated Sandstones," Ph.D. Dissertation, Stanford University (November 1974).

2. Baena C.J., Castanier L.M., and Brigham W.E.: "Effect of Metallic Additives on In-situ Combustion of Huntington Beach Crude Oil" SUPRI TR 78, Stanford University (June 1990).

3. Babadagli, T.: "Injection Rate Controlled Capillary Imbibition Transfer in Fractured Systems," SPE 28640, paper presented at the SPE Annual Technical Conference and Exhibition, New Orleans (September 25-28, 1994).

4. Bernard, G.G., Holm, L.W., and Jacobs, W.I.: "Effect of Foam on Trapped Gas Saturation and on Permeability of Porous Media to Water," SPEJ (Dec. 1965) 295-300; *Trans.*. AIME, 234.

5. Bond, D. C. and Holbrook, O. C.: "Gas Drive Oil Recovery Process," US Patent No. 2,866.507 (1958).

6. Bousaid, I.S. and Ramey, H.J. Jr.: "Oxidation of Crude Oil in Porous Media," *SPEJ* (June 1968) 137-48; also *Trans.* AIME 243.

7. Burger, J.G. and Sahuquet, B.C.: "Chemical Aspects of In-situ Combustion" *SPEJ* (October 1972) 410-420.

8. Brigham, W.E. and Castanier, L.M.: "SUPRI Heavy Oil Research," Seventeenth Annual Report, SUPRI TR 98, Stanford University (February 1994).

9. Brigham, W.E., Ramey, H.J., and Castanier, L.M.: "SUPRI Heavy Oil Research," SUPRI TR 92, Stanford University (February 1993).

10. Castanier, L.M. and Brigham, W.E.: "Selecting Foaming Agents for Steam Injection Improvement", *Chemical Engineering Progress* 81, No. 6 (June 1985).

11. Chambers, K. T., and Radke, C. J. : "Capillary Phenomena in Foam Flow Through Porous Media," Interfacial Phenomena in Petroleum Recovery, Morrow, N. R. Ed., Marcel Dekker Inc., New York (1991) Ch.6 191-255

12. Chen, H. K.,: "Measurement of Water Content in Porous Media under Geothermal Fluid Flow Conditions," Ph.D. Dissertation, Stanford University (November 1976).

13. Closmann, P. J., And Vinegar, H. J.: "Relative Permeabilities to Steam and Water at Residual Oil in natural Cores: CT Scan Saturations," SPE 17449, paper presented at the California Regional Meeting, Long Beach (March 23-1988).

14. Counsil, J. R.: "Steam-Water Relative Permeability," Ph.D. Dissertation, Stanford University (May 1979).

15. Dabbous, M.K. and Fulton, P.F.: "Low-Temperature-oxidation Reaction Kinetics and Effects on the In-Situ Combustion Process," *SPEJ* (June 1974) 253-62.

16. David, A. and Marsden, S.S.: "The Rheology of Foam," SPE 2544, paper presented at the SPE/AIME 44th Annual Fall Meeting, Denver (October 1969).

17. Demiral, B.M.R., Pettit, A.P., Castaniar, M.L., and Brigham, W.E.: "A Three-Dimensional Laboratory Steam Injection Model Allowing Insitu Saturation Measurements," SUPRI TR 83, Stanford University (August 1992).

18. Fassihi, M.R. and Brigham, W.E.: "Analysis of Fuel Oxidation in In-situ Combustion Oil Recovery," SUPRI TR-26, Stanford University (June 1981).

19. Fried, A. N.: "The Foam Drive Process for Increasing the Recovery of Oil," RI 5866, USBM, Washington, DC (1961).

20. Grant, M. A.,: "Permeability Reduction Factors at Wairakei," AIChE-ASME Heat Transfer Conference, Salt Lake City (August 15-17, 1977).

21. Guzman, R. and Aziz, K.: "Design and Construction of an Experiment for Two-Phase Flow in Fractured Porous Media", SUPRI TR 95, Stanford University (June 1993).

22. Hanssen, T. M., and Jakobsen, K. R.: "Interaction of Gas-Blocking Foam with Oil in Model Porous Media," Progress in Colloid and Polymer Science 81 (1990).

23. Haraski, G. T., and Lawson, J. B.: "Mechanism of Foam Flow in Porous Media - Apparent Viscosity in Smooth Capillaries," SPE 12129, paper presented at the 57th Annual Technical Conference and Exhibition, San Francisco (1983).

24. Haunsfield, G.N.: "A Method Of and Apparatus For Examination of a Body by Radiation Such as X- or Gamma- Radiation," British Patent No. 1,283,915, London (1972).

25. Holm, L.W.: "The Mechanism of Gas and Liquid Flow Through Porous Media in the Presence of Foam," SPEJ (Dec. 1968) 359-69; *Trans.* AIME 243.

26. Holt, R.J.: "In-Situ Combustion with Metallic Additives," Stanford University SUPRI TR-87, Stanford (July 1992).

27. Hornbrook, J. W., Castanier, L.M.and Pettit, P.A.: "Observation of Foam/Oil Interactions in a New High Resolution Micromodel," SPE 22631, Paper presented at the 66th Annual Technical Conference and Exhibition, Dallas (October 6-9, 1991).

28. Hornbrook, J.W., Castanier, L.M., and Pettit, P.A.: "Visualization of Foam/Oil in a New, High Resolution, Sandstone Replica Micromodel", SUPRI TR 86, Stanford University (August 1992).

29. Horne, R. N., and Ramey, H. J., Jr.: "Steam/Water Relative Permeabilities from Production Data," Proc., 1978 Geothermal Resources Council Annual Meeting, Hilo (July 25-27, 1978).

30. Huh, D. G., Cochrane, T. D. and Kovarik, F. S. : "The Effect of Microscopic Heterogeneity on CO_2/Foam Mobility: Part 1-A Mechanistic Study, SPE 17359, paper presented at the SPE/DOE EOR Symposium, Tulsa (April 1988).

31. Jimenez, A. I. and Radke, C. J. : "Dynamic Stability of Foam Lamellae Flowing Through a Periodically Constricted Pore," *Oilfield Chemistry*, Enhanced Recov. and Prod. Stimulation, 195th Amer. Chem. Soc. Nat. Mtg. Symp. , Toronto (1989).

32. Johns, R.A, Stude J., Castanier L.M. and Roberts P.V: "Nondestructive measurements of Fracture Aperture in Crystalline Rock Cores Using X-Ray Computer Tomography,"*Jour. of Geophysical Res.* 8 (1993) 1889-1900.

33. Kanda, M. and Schechter, R. S.: "On the Mechanism of Foam Formation in Porous Media," paper presented at the 51st Annual Technical Conference and Exhibition, New Orleans (1976).

34. Khatib, Z. I., Hiraski, G. J., and Falls, A. H.: "Effects of Capillary Pressure on Coalescence and Phase Mobilities in Foams Flowing Through Porous Media," SPE 15442, paper presented at the 61st Ann. Tech. Conf. and Exhitbition, New Orleans (1986).

35. Kazemi, H., and Merrill, L.: "Numerical Simulation of Water Imbibition in Fractured Cores", *SPEJ* (June 1979) 175-182.

36. Kleppe, J. and Morse, R.: "Oil Production from Fractured Reservoirs by Water Displacement", SPE 4102, paper presented at the SPE-AIME 49th Annual Fall Meeting (1974).

37. Kolb, G.E.: "Several Factors Affecting the Foam-Drive Process for the Removal of Water from Consolidated Porous Media," MS thesis, Penn. State U. (1964).

38. Kuhlman, M. I. : "Visualizing the Effect of Light Oil on CO_2 Foams," *JPT* (July 1990) 902-908.

39.. Lake, L.W.: Enhanced Oil Recovery, Prentice-Hall, Englewood Cliffs (1989).

40. Lau, H. C. and O"Brien, S. M. : "Effects of Spreading and Nonspreading Oils on Foam Propagation Through Porous Media," SPE Res. Eng. (August 1988).

41. Mamora, D.D., Ramey, H.J., Jr., Brigham, W.E., and Castanier L.M.: "Kinetics of In-Situ Combustion," SUPRI TR 91, Stanford University (May 1993).

42. Mahmood, S. M. and Brigham, W. E.: "Two Dimensional Displacement of Oil by Gas and Surfactant Solution under Foaming Conditions," SUPRI TR-58, Stanford U. (July 1987).

43. Manlowe, J. D., and Radke, C. J. :"A Pore-Level Investigation of Foam/Oil Interactions in Porous Media," SPE Res. Eng. (Nov. 1990).

44. Marsden, S.S.: "Foams in Porous Media", SUPRI TR-37, Stanford University (1986).

45. Marsden, S. S. Jr. and Khan, S. A.: "The Flow of Foam through Short Porous Media and Apparent Viscosity Measurements (1966).

46. Mast, R. F.: " Microscopic Behavior of Foam in Porous Media", SPE 3997, paper presented at SPE Annual Fall Meeting, San Antonio (October 8-11, 1972).

47. Mattax, C. and Kyte, J.: "Imbibition Oil Recovery from Fractured Water-Drive Reservoir", *SPEJ* (June 1962) 177-184.

48. Monsalve, Armando, Schechter, R. S., and Wade, W. H.: "Relative Permeabilities of Surfactant/Steam/Water Systems," SPE 12661, paper presented at the Fourth Symposium on Enhanced Oil Recovery, Tulsa (April 15-18, 1984).

49. Nahid, B.H.: "Non-Darcy Flow of Gas Through Porous Media in the Presence of Surface Active Agents," PhD dissertation, U. of Southern California (1971).

50. Nikolov, A. D., Wasan, D. T., Huang, D.W., and Edwards, D. A.: "The Effect of Oil on Foam Stability, Mechanisms and Implications for Oil Displacement by Foam in Porous Media," SPE paper 15443 pres. at the 61st Ann. Tech. Conf. and Ex., New Orleans (1986).

51. Oak, M. J., Baker, L. E., and Thomas, D. C.: "Three-Phase Relative Permeability of Berea Sandstone," *J. Pet. Tech.* (August 1990) 1054-1061.

52. Owete, O.S. and Brigham, W.E.: "Flow of Foam Through Porous Media," SUPRI TR-37 Stanford University (July 1984).

53. Parlar, M., and Yortsos, Y. C.: "Percolation Theory of Steam/Water Relative Permeability," SPE 16969, paper presented at the 62nd Annual Technical Conference and Exhibition, Dallas (September 27-30, 1987).

54. Persoff, P., Radke, C. J., Pruess, K. Bension, S.M., and Witherspoon, P. A.: "A Laboratory Investigation of Foam Flow in Sandstone at Elevated Pressure," *SPE Res. Eng.* (Aug. 1991).

55. Qadeer, S.: "Techniques to Handle Limitations in Dynamic Relative Permeability Measurements," Report in progress, Stanford University (1995).

56. Radke, C. J. and Ransohoff, T, C.: "Mechanisms of Foam Generation in Glass Bead Packs," SPE 15441, paper presented at the 61st Ann. Tech. Conf. and Exhibition, New Orleans (1986).

57. Racz, D.: "Development and Application of a Thermocatalytic In-Situ Combustion Process in Hungry" Proceedings, European Meeting on Improved Oil Recovery, Rome (April 16-18, 1985).

58. Raza, S.H. and Marsden, S.S.: "The Streaming Potential and Rheology of Foam," SPEJ (December 1967) 359-68; *Trans.* AIME 240.

59. Sanchez, J.M., and Hazlett, R.D.: "Foam Flow Through an Oil-Wet Porous Medium: A Laboratory Study",SPE 19687, paper presented at the SPE Annual Technical Conference and Exhibition, San Antonio (October 8-11, 1989).

60. Sanchez, J. M. and Schechter, R. S.: "The Effect of Trace Quantities of Surfactant on Nitrogen/Water Relative Permeabilities," SPE 15446, paper presented at the 61st Ann. Tech. Conf. and Exhibition, New Orleans (1986).

61. Sanchez, J. M., and Schechter, R. S.,: "A Comparison of the Two-Phase Flow of Steam/Water and Nitrogen/Water through an Unconsolidated Permeable Medium," SPE 16967, paper presented at the 62nd Annual Technical Conference and Exhibition, Dallas (September 27-30, 1987).

62. Sarathi, P.: "Using Micromodels to Study Steam Displacement Processes in Porous Media," NIPER-180 (1968).

63. Schramm, L.L., Turta, A. T., and Novosad, J.J.: "Micovisual and Coreflood Studies of Foam Interactions With a Light Crude Oil," *SPE Res. Eng.* (August 1993) 201-206

64. Schramm, L. L., and Novosad, J. J.: "Microvisualization of Foam Interactions with a Crude Oil," Proc. SPE/DOE 7th Symp. on EOR, Tulsa (1990).

65. Sedgwick, G. E., and Miles-Dixon, E.: "Application of X-ray Imaging Techniques to Oil Sands Experiments," *J. Canad. Pet. Tech* . 27 (March-April 2, 1988) 104-110.

66. Shallcross D.C., DeLos Rios C.F., Castanier L.M., and Brigham, W.E.: "Modifying In-Situ Combustion Performance by the Use of water-soluble Additives" *SPERE* (August 1991) 287-293.

67. Shinohara, K.: "Calculation and Use of Steam/Water Relative Permeabilities in Geothermal Reservoirs," M.S. Report, Stanford University (June1978).

68. Stars User's Manual: Computer Modeling Group, Version 94 (1994).

69. Thomas, G.W., Buthod, A.P. and Allag, O.: "An Experimental Study of the Kinetics of Dry, Forward Combustion, - Final Report," Report No. BETZ-1820-1, DOE (February 1979).

70. Trimble, A. E., and Menzie, D. E.: "Steam Mobility in Porous Media," SPE Paper No. 5571, Paper presented at the 50th Annual Fall Meeting, Dallas, (September 28-Oct.1, 1975).

71. Vinsome, P.K.W. and Westerveld, J.: "A Simple Method for Predicting Cap and Base Rock Heat Losses in thermal Reservoir Simulators," *Jour. Can. Pet. Tech.* (July-September 1980) 87-90.

72. Vogel, J.V.: "Simplified Heat Calculations for Steamfloods," *JPT* (July 1984) 1127-36.

73. Weijdema, J.: "Determination of the Oxidation Kinetics of the In-Situ Combustion Process," Koninklijke/Shell E.&P. Laboratorium, Rijswijk, The Netherlands (1968).

☆U.S. GOVERNMENT PRINTING OFFICE: 1995 - 660-029/20042